

**RODRIGO NOGUEIRA MARTINS**

**MODELING OF COFFEE RIPENESS AND BEVERAGE QUALITY USING  
PROXIMAL AND REMOTE SENSING**

Thesis submitted to the Agricultural Engineering  
Graduate Program of the Universidade Federal de  
Viçosa in partial fulfillment of the requirements for  
the degree of *Doctor Scientiae*.

Adviser: Francisco de Assis de Carvalho Pinto

Co-advisers: Daniel Marçal de Queiroz

Domingos Sárvio Magalhães Valente

**VIÇOSA - MINAS GERAIS  
2022**

**Ficha catalográfica elaborada pela Biblioteca Central da Universidade  
Federal de Viçosa - Campus Viçosa**

T

M386m  
2022  
Martins, Rodrigo Nogueira, 1988-  
Modeling of coffee ripeness and beverage quality using  
proximal and remote sensing / Rodrigo Nogueira Martins. –  
Viçosa, MG, 2022.

1 tese eletrônica (104 f.): il. (algumas color.).

Inclui apêndice.

Orientador: Francisco de Assis de Carvalho Pinto.

Tese (doutorado) - Universidade Federal de Viçosa,  
Departamento de Engenharia Agrícola, 2022.

Inclui bibliografia.

DOI: <https://doi.org/10.47328/ufvbbt.2022.371>

Modo de acesso: World Wide Web.

1. Café - Maturação. 2. Café - Avaliação sensorial. 3. Café -  
Qualidade. 4. Agricultura - Sensoriamento remoto. 5. Drone.  
6. Espectroscopia de infravermelho próximo. I. Pinto, Francisco  
de Assis de Carvalho, 1964-. II. Universidade Federal de Viçosa.  
Departamento de Engenharia Agrícola. Programa de  
Pós-Graduação em Engenharia Agrícola. III. Título.

CDD 22. ed. 633.7467

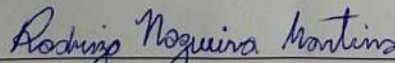
**RODRIGO NOGUEIRA MARTINS**

**MODELING OF COFFEE RIPENESS AND BEVERAGE QUALITY USING  
PROXIMAL AND REMOTE SENSING**

Thesis submitted to the Agricultural Engineering  
Graduate Program of the Universidade Federal de  
Viçosa in partial fulfillment of the requirements for  
the degree of *Doctor Scientiae*.

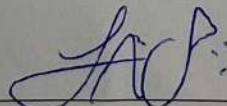
APPROVED: June 9, 2022.

Assent:



---

Rodrigo Nogueira Martins  
Author



---

Francisco de Assis de Carvalho Pinto  
Adviser

To my parents, Irene Aurora Martins (*in memoriam*) and Sebastião Martins (*in memoriam*), for their example of life, encouragement, love, and trust.

## ACKNOWLEDGMENTS

First, I would like to thank God for giving me the health, strength, and knowledge to overcome the difficulties along this journey.

To all my family, for their love, encouragement and support in every decision made.

To my beloved girlfriend Cleydiane, for all the support, love and encouragement.

To Professor Francisco de Assis de Carvalho Pinto, for his guidance, trust, friendship, and support throughout these years.

To the co-advisers professor Daniel Marçal and Domingos Sárvio, for their contributions and guidance, which were essential for the development of this thesis.

To Professor Elder Sanzio for his availability and help with the data collections.

To Mr. Edson “Alemão” and Afonso, I thank you both for making available the production areas for the accomplishment of this work.

To Jorge and Marcelo for their friendship, partnership in the work and availability to help whenever necessary.

To my colleagues from the agricultural mechanization laboratory (LMA) Lucas, Juliano, Flávio, Charles, Hugo, Poliana, Pedro, and Lucas Anício for their friendship, exchange of knowledge, help in the data collections, and valuable discussions that made me grow professionally and personally.

To all the other professors and staff who contributed to this achievement, especially professors Marconi, André Coelho, and Flora Villar for always being helpful when I needed it.

To the Universidade Federal de Viçosa and the Graduate Program in Agricultural Engineering, for the opportunity to complete de postgraduate course.

Thanks to everyone who, in some way, contributed to the realization of this project.

Thank you very much!

This study was financed in part by the Coordenação de Aperfeiçoamento de Pessoal de Nível Superior – Brasil (CAPES) – Finance Code 001.

To the Conselho Nacional de Desenvolvimento Científico e Tecnológico – Brasil (CNPQ) for granting the scholarship (Process 144740/2019-2).

*“O sucesso nasce do querer, da determinação e persistência em se chegar a um objetivo. Mesmo não atingindo o alvo, quem busca e vence obstáculos, no mínimo fará coisas admiráveis.”*

José de Alencar

## **BIOGRAPHY**

RODRIGO NOGUEIRA MARTINS, son of Irene Aurora Martins (*in memorian*) and Sebastião Martins (*in memorian*), was born in Janaúba, Minas Gerais, on June 24<sup>th</sup>, 1988.

In February of 2017, he concluded the Agricultural and Environmental Engineering undergraduate course at the Instituto Federal do Norte de Minas Gerais (IFNMG), Campus Januária.

In March of 2017 started his master's degree studies in the Postgraduate Program in Agricultural Engineering in the concentration area of Agricultural Mechanization, at the Universidade Federal de Viçosa, submitting his dissertation to defense in February 2019.

In March of 2019, he started his doctorate studies in the same Postgraduate Program and concentration area at the Universidade Federal de Viçosa and submitted his thesis to defense in June, 2022.

## ABSTRACT

MARTINS, Rodrigo Nogueira, D.Sc., Universidade Federal de Viçosa, June, 2022. **Modeling of coffee ripeness and beverage quality using proximal and remote sensing.** Adviser: Francisco de Assis de Carvalho Pinto. Co-advisers: Daniel Marçal de Queiroz and Domingos Sárvio Magalhães Valente.

Coffee is one of the most valuable agricultural commodities, whose price setting and export potential are defined according to its beverage quality. In turn, the beverage quality results from the interaction of different factors from the fruit ripeness degree at harvest to the post-harvest practices. Traditionally, the fruit ripeness is evaluated through manual samplings in the field, whereas the beverage quality is assessed through sensory analysis by trained tasters. These methods are time-consuming, not representative of the entire production area, and in the case of beverage quality assessment, they are subjective due to the personal influence of the taster. On the other hand, the advent of aerial remote sensing through the Unmanned Aerial Vehicles (UAV), as well as spectroscopy associated with chemometrics and statistical modeling techniques, are presented as a fast and accurate approach for monitoring the spatio-temporal variability of the fruit ripeness and predicting beverage quality. In this sense, the general objective of this thesis, structured in the form of chapters, including the introduction and general conclusions, consisted of modeling the fruit ripeness and beverage quality of Arabica coffee using proximal and remote sensing. In the second chapter, a vegetation index (VI) for monitoring the coffee ripeness using aerial images was developed. For doing that, an experiment was set up in five Arabica coffee fields in Paula Cândido, Minas Gerais state, Brazil. During the coffee ripeness stage in the 2018-2019 season, four flights were carried out to acquire spectral information on the crop canopy using two UAVs, one equipped with a five-band multispectral camera (RGB, RedEdge, and NIR) and another with an RGB camera. For validation purposes, manual counts of the percentage of unripe fruits were performed using irregular sampling grids on each data collection. After image processing, the coffee ripeness index (CRI) and five other VIs (MCARI1, NDVI, NDRE, GNDVI, and GRRI) were obtained. The CRI was developed by combining reflectance from the red band and from a ground-based red target placed on the study area. In general, the CRI showed a higher sensitivity to discriminate between coffee plants ready for harvest from not-ready for harvest regarding the fruit ripeness. Furthermore, the highest  $R^2$  and lowest RMSE values for estimating the coffee ripeness were also presented by the CRI ( $R^2$ : 0.70; 12.42%), whereas the other VIs showed  $R^2$  and RMSE values ranging from 0.22 to 0.67 and from 13.28 to 16.50%, respectively. In the



third chapter, two models for the prediction of fruit ripeness using spectral and textural variables were developed and the best variables for the development of spatio-temporal variability maps of fruit ripeness were determined. For that, the fruit ripeness data obtained from six coffee fields (including those described in the second chapter) in the 2018-2019 and 2020-2021 seasons and aerial images of seven flights performed in both seasons were used for data modeling. Through the images, 12 spectral and 64 textural variables composed of bands and VIs were obtained. The performance of the Random Forest algorithm using spectral and textural variables ( $R^2$ : 0.71 and RMSE: 11.47%) was higher than the model based solely on spectral variables ( $R^2$ : 0.67 and RMSE: 12.09%). Finally, in both scenarios, the most important variables in the prediction models were the VIs CRI and MCARI1 and the red and NIR bands. Lastly, in the fourth chapter, a method was developed for predicting the coffee beverage quality based on NIR spectroscopy of coffee samples, as well as for classifying the beverage final quality using different variables obtained from the UAV images. Initially, an experiment was set up in the 2020-2021 season in seven coffee fields in the municipalities of Paula Cândido and Araçuaia. During the harvesting, 13 flights were performed using a UAV equipped with an RGB camera. Then, different spectral, climatic, and terrain variables were obtained from the orthomosaics. For validation purposes, the harvested coffee was processed and subjected to sensory analysis. Next, NIR spectra (1000-2450 nm) were obtained from 180 samples of roasted and ground coffee. The prediction of the beverage quality attributes based on the NIR spectra was performed using Partial Least Squares (PLS) regression and the combination of PLS with the variable selection algorithm (OPS – Ordered Predictors Selection). Overall, the best predictions were obtained for the aftertaste, overall perception, body, and balance quality attributes using the PLS-OPS models, whose coefficient of correlation ( $r_p$ ) and the root-mean-square-error of the prediction ( $RMSEP$ ) ranged from 0.78 to 0.82 and from 0.15 to 0.13, respectively. In the second analysis, the variables extracted from the UAV images were used as input for developing classification models for the beverage final quality. The results were not satisfactory. Thus, the use of UAV images for beverage quality assessment still needs to be further explored in future studies.

**Keywords:** Digital agriculture. UAV. Coffee fruit ripeness. Sensory analysis. NIR spectroscopy.

## RESUMO

MARTINS, Rodrigo Nogueira, D.Sc., Universidade Federal de Viçosa, junho de 2022. **Modelagem da maturação e qualidade da bebida do café usando sensoriamento proximal e remoto.** Orientador: Francisco de Assis de Carvalho Pinto. Coorientadores: Daniel Marçal de Queiroz e Domingos Sárvio Magalhães Valente.

O café é uma das commodities agrícolas mais valiosas, cujo valor de mercado e potencial de exportação dependem da qualidade da bebida. Por sua vez, a qualidade da bebida resulta da interação de diferentes fatores desde a maturação dos frutos na colheita até as práticas pós-colheita. Tradicionalmente, a maturação dos frutos é avaliada por meio de amostragens manuais em campo, enquanto a qualidade da bebida é avaliada por meio de análise sensorial com provadores treinados. Esses métodos são demorados, não representativos de toda a área de cultivo e no caso da avaliação de qualidade são subjetivos devido a influência pessoal do provador. Por outro lado, o advento do sensoriamento remoto aéreo por meio dos Veículos Aéreos não Tripulados (VANT), bem como da espectroscopia associada a quimiometria e as técnicas de modelagem estatística apresentam-se como uma abordagem rápida e precisa para monitorar a variabilidade espaço-temporal da maturação e predizer a qualidade da bebida. Neste sentido, o objetivo geral dessa tese, estruturada na forma de capítulos, incluindo a introdução e conclusão geral, consistiu na modelagem da maturação e qualidade da bebida do café arábica usando sensoriamento remoto e proximal. No segundo capítulo, desenvolveu-se um índice de vegetação (IV) para monitoramento da maturação do café usando imagens aéreas. Para tal, foi montado um experimento em cinco talhões de café Arábica em Paula Cândido, Minas Gerais, Brasil. Durante a fase de maturação do café na safra 2018-2019, foram realizados quatro voos para aquisição de informações espectrais do dossel da lavoura utilizando dois VANTs, um equipado com uma câmera multiespectral de cinco bandas (RGB, RedEdge e NIR) e outro com câmera RGB. Para fins de validação, foram realizadas contagens manuais da porcentagem de frutos verdes usando grades de amostragem irregulares em cada coleta. Após o processamento das imagens, foram obtidos o índice de maturação do café (CRI – *Coffee Ripeness Index*) e outros cinco IVs (MCARI1, NDVI, NDRE, GNDVI e GRRI). O CRI foi desenvolvido combinando a refletância na banda do vermelho com a refletância dessa mesma banda extraída de um alvo vermelho incluído na área imageada. De maneira geral, o CRI mostrou maior sensibilidade em discriminar plantas de café aptas para colheita daquelas não aptas com relação a maturação. Além disso, os maiores valores de  $R^2$  e menor valor da raiz do erro quadrático médio (RMSE) para estimar a maturação do café também foram apresentados pelo CRI ( $R^2$ :

0,70; 12,42%), enquanto nos demais IVs os valores de  $R^2$  e RMSE variaram de 0,22 a 0,67 e de 13,28 a 16,50%, respectivamente. No terceiro capítulo, foram desenvolvidos dois modelos para a predição da maturação dos frutos usando variáveis espectrais e texturais e determinadas as melhores variáveis para o desenvolvimento de mapas de variabilidade espaço-temporal da maturação. Para tanto, dados de maturação obtidos de seis lavouras de café (incluindo aquelas descritas no segundo capítulo) nas safras 2018-2019 e 2020-2021 e imagens aéreas de sete voos realizados em ambas as safras foram utilizados para a modelagem. Por meio das imagens, foram obtidas 12 variáveis espectrais e 64 texturais compostas por bandas e IVs. O desempenho do algoritmo *Random Forest* utilizando variáveis espectrais e texturais ( $R^2$ : 0,71 e RMSE: 11,47%) foi superior ao modelo baseado apenas nas variáveis espectrais ( $R^2$ : 0,67 e RMSE: 12,09%). Por fim, em ambos os cenários, as variáveis que apresentaram maior importância nos modelos de predição foram os IVs CRI e MCARI1 e as bandas do vermelho e do NIR. Finalmente, no quarto capítulo, desenvolveu-se um método para predição da qualidade da bebida do café com base em espectroscopia do NIR de amostras de café, bem como para a classificação da qualidade final da bebida usando diferentes variáveis obtidas a partir de imagens de VANT. Inicialmente, foi montado um experimento na safra 2020-2021 em sete talhões de café nos municípios de Paula Cândido e Araçuaia. Durante a colheita do café foram realizados 13 voos usando um VANT equipado com uma câmera RGB. Em seguida, diferentes variáveis espectrais, climáticas e de terreno foram obtidas a partir dos ortomosaicos. Para fins de validação, o café colhido foi processado e submetido à análise sensorial. Na sequência, foram obtidos espectros do NIR (1000-2450 nm) de 180 amostras de café torrado e moído. A predição dos atributos de qualidade baseada nos espectros do NIR foi realizada usando regressão de mínimos quadrados parcial (PLS – *Partial Least Squares*) e a combinação do PLS com o algoritmo de seleção de variáveis (OPS – *Ordered Predictors Selection*). Em geral, as melhores predições foram obtidas para a finalização, percepção geral, corpo e equilíbrio usando o PLS-OPS, cujo coeficiente de correlação de predição ( $r_p$ ) e RMSE da predição ( $RMSE_p$ ) variaram de 0,78 a 0,82 e de 0,15 a 0,13, respectivamente. Na segunda análise, as variáveis extraídas das imagens foram usadas no desenvolvimento de modelos de classificação da qualidade da bebida. Os resultados não foram satisfatórios. Assim, o uso de imagens obtidas por VANT para classificação da qualidade da bebida ainda precisa ser mais bem explorado em estudos futuros.

**Palavras-chave:** Agricultura digital. VANT. Maturação dos frutos de café. Análise sensorial, Espectroscopia do NIR.

## SUMMARY

1	General Introduction .....	12
1.1	THESIS STRUCTURE .....	15
1.2	REFERENCES.....	15
2	A novel vegetation index for coffee ripeness monitoring using aerial imagery .....	19
2.1	INTRODUCTION .....	19
2.2	MATERIAL AND METHODS.....	22
2.3	RESULTS .....	27
2.4	DISCUSSION .....	36
2.5	CONCLUSION .....	39
2.6	REFERENCES.....	40
3	Digital mapping of coffee ripeness using UAV-based multispectral imagery .....	46
3.1	INTRODUCTION .....	46
3.2	MATERIAL AND METHODS.....	48
3.3	RESULTS .....	59
3.4	DISCUSSION .....	67
3.5	CONCLUSION .....	70
3.6	REFERENCES.....	70
4	Assessment of coffee cup quality using NIR spectroscopy and aerial remote sensing .....	76
4.1	INTRODUCTION .....	76
4.2	MATERIAL AND METHODS.....	78
4.3	RESULTS .....	86
4.4	DISCUSSION .....	92
4.5	CONCLUSION .....	96
4.6	REFERENCES.....	96
5	General Conclusions .....	103
	Appendix .....	104
	APPENDIX A .....	104

## 1 General Introduction

Coffee is recognized as the second most traded commodity globally. With a productive area of 1.8 million hectares and a production of 47.72 million bags in the 2020/21 season, Brazil is by far the world's largest coffee producer and exporter. In the 2020/21 season, the Brazilian foreign exchange revenue was US\$ 6.24 billion, with the Arabica variety (*Coffea arabica* L.) accounting for 71.1% of the exported volume (CONAB, 2022; USDA, 2022). Such facts consolidate the expressive economic and social importance of this crop for Brazil. However, the growing global demand for coffees with better sensory characteristics makes it necessary to develop production and marketing strategies to differentiate the Brazilian product.

Coffee is a product whose selling price depends on the beverage quality, which in turn is influenced by the fruit ripeness degree at harvest (MARTINEZ et al., 2013; SILVA et al., 2010; SILVA et al., 2014). In addition, factors such as altitude, plant nutrition, occurrence of multiple coffee blooms, variation in exposure to solar radiation, cultivation practices, soluble solids content (Brix degree), and post-harvesting practices also influence the coffee beverage quality (APARECIDO et al., 2017; CASSIA et al., 2013; CORREA et al., 2017; TOLESSA et al., 2018).

The uneven fruit ripeness directly influences the quality and final price of coffee (ANGÉLICO et al., 2011). This occurs because the beverage quality is higher when obtained from ripe fruits (cherry), as opposed to unripe and dry fruits, which deteriorate the sensory quality of the beverages, as well as the aesthetics of the grains (FAGAN et al. 2011; MARTINEZ et al. 2013; SILVA et al., 2014). In this case, the fruits harvested green become defective, acquire dark tones when processed, and make the beverage bitter (APARECIDO et al., 2017). On the other hand, the cherry coffee fruits, which have a higher brix degree, aggregate the most important chemical precursors for generating better quality beverages after roasting (ARRUDA et al., 2011).

Given the importance of the fruit ripeness degree at harvest for the production of higher quality coffee. The fruit ripeness prediction can be a useful tool for site-specific management of coffee plants with distinct qualities and for defining the moment of starting the harvest. Currently, the fruit ripeness is monitored through manual sampling for counting the percentage of unripe fruits. This method is labor-intensive and is limited to a few plants within the field, which may not be representative. An alternative would be monitoring via remote sensing.

In the context of crop monitoring, remote sensing (RS) has been highlighted by the possibility of non-destructive sampling throughout the area of interest and the diversity of

information use. In the coffee crop, the RS applications range from disease monitoring (CHEMURA et al., 2017; MARIN et al., 2019) to obtaining biophysical parameters that influence crop productivity (BERNARDES et al., 2012; NOGUEIRA et al., 2018; PETERSEN, 2018). However, limitations to this type of analysis still exist, especially when using data from orbital platforms, whose availability, the spatial and temporal resolution of images with good quality is low, which makes it unfeasible to carry out studies that require rapid decision-making.

On the other hand, with the advent of Unmanned Aerial Vehicles (UAV), these difficulties have been overcome, since these devices have a relatively low acquisition cost when compared to other platforms (LELONG et al., 2008). In addition, the UAVs allow high flexibility in image acquisition, performing autonomous work, and obtaining images without clouds and with high spatial (~1 cm) and temporal resolution. Furthermore, recent technological advances have enabled the development of cameras capable of recording the reflected energy in different spectral bands according to the detection objective.

In the coffee crop, the use of multispectral cameras onboard UAVs has enabled the monitoring of nutritional status (MARIN et al., 2021a; PARREIRAS et al., 2020), the determination of biophysical parameters (CUNHA et al., 2019; SANTOS et al., 2020), disease detection (MARIN et al., 2021b), yield estimation (BARBOSA et al., 2021), as well as the fruit ripeness monitoring (JOHNSON et al., 2004; HERWITZ et al., 2004). Most of these studies have used an approach based on vegetation indices such as NDVI (Normalized Difference Vegetation Index) and NDRE (Normalized Difference RedEdge Index), which provide information about variations in the photosynthetic activity of plants (FITZGERALD et al., 2006; ROUSE et al., 1973).

Besides the vegetation indices, other variables such as altitude, temperature, solar radiation, hydric condition, and soil fertility have been used to estimate biophysical parameters, yield, fruit ripeness, and the coffee beverage quality (APARECIDO et al., 2017; BARBOSA et al., 2012; FERREIRA et al., 2016; NOGUEIRA et al., 2018; RAMIREZ et al., 2010; SILVA et al., 2014). Thus, many of these studies have presented results that clarify important points about the influence of each variable on the coffee fruit ripeness and beverage quality. However, despite recent advances in remote monitoring and in the identification of attributes of the coffee crop, the beverage quality assessment, an essential parameter in the definition of the final price of the product, is still carried out through sensory analysis based on the evaluation of Q-Graders (DI DONFRANCESCO et al., 2014).

This methodology is quite subjective, expensive, time-consuming, and requires trained tasters, which hinders the efficient implementation of routine analysis (CRAIG et al., 2018;

FERIA-MORALES, 2002). Such limitations encourage the use of faster and more reliable methodologies as an alternative to evaluating the beverage quality and, eventually, other attributes present in the coffee beans. As an alternative, studies on this topic have been based on the use of proximal sensing through spectroscopy methods in the visible (Vis) and near (NIR), and mid-infrared ranges. In general, these methods are fast, reliable, chemical-free, and low-cost (BARBIN et al., 2014). The most common applications include, but are not limited to, the predicting coffee sensory attributes (BAQUETA et al., 2019; TOLESSA et al., 2016), adulteration detection (EBRAHIMI-NAJAFABADI et al., 2012), prediction of roasting degree (ALESSANDRINI et al., 2008), and evaluation of the presence of defects (CRAIG et al., 2015).

Generally, the beverage quality analyzes are carried out in the laboratory after harvesting and processing the coffee fruits. However, the information inherent to the production areas (*e.g.*, terrain attributes, climate variables, and the crop spectral response) that make it possible to infer the beverage quality are not considered or remains little explored as observed in previous studies (FERREIRA et al., 2014; LOUZADA PEREIRA et al., 2018; TOLESSA et al., 2017). Many of these attributes can be obtained through the UAV images and its byproducts, such as the digital elevation model of the production areas. In this sense, the integration of aerial and proximal remote sensing via Vis-NIR spectroscopy proves to be an advantageous approach, not only to monitor the fruit ripeness but to predict coffee beverage quality quickly and reliably, as well as to identify areas with potential for producing specialty quality coffees.

Thus, the general objective of this thesis consisted of modeling the fruit ripeness and beverage quality of Arabica coffee using proximal and remote sensing. The specific objectives were: (1) to develop a vegetation index for coffee ripeness monitoring using aerial images; (2) to predict the fruit ripeness using spectral and textural variables; and to determine the best variables for developing spatio-temporal variability maps of the fruit ripeness; and (3) to predict the coffee beverage quality based on NIR spectra of roasted coffee; and to classify the beverage quality using spectral, climate, and terrain variables obtained from UAV imagery.

## 1.1 Thesis Structure

This thesis was structured in the form of chapters, including the introduction and general conclusion. Initially, a general introduction is presented, justifying the development of the research. Next, the second, third, and fourth chapters referring to the three specific objectives are presented. Lastly, the final considerations of the thesis are presented.

## 1.2 References

ALESSANDRINI, L. et al. Near infrared spectroscopy: An analytical tool to predict coffee roasting degree. **Analytica Chimica Acta**, v. 625, n. 1, p. 95-102, 2008.

ANGÉLICO, C. L. et al. Diferentes estágios de maturação e tempo de ensacamento sobre a qualidade do café. **Coffee Science**, v. 6, n. 1, p. 8-19. 2011.

APARECIDO, L. E. O. et al. Maturation periods for *Coffea arabica* cultivars and their implications for yield and quality in Brazil. **Journal of the Science of Food and Agriculture**, v. 98, n. 10, p. 3880-3891. 2017.

ARRUDA, N. P. et al. Discriminação entre estádios de maturação e tipos de processamento de pós-colheita de cafés arábica por microextração em fase sólida e análise de componentes principais. **Química Nova**, v. 34, n. 5, p. 819-824, 2011.

BARBIN, D. F. et al. Application of infrared spectral techniques on quality and compositional attributes of coffee: An overview. **Food Research International**. v. 61, p. 23–32, 2014.

BAQUETA, M. R.; COQUEIRO, A.; VALDERRAMA, P. Brazilian Coffee Blends: A simple and fast method by near-infrared spectroscopy for the determination of the sensory attributes elicited in professional coffee cupping. **Journal of Food Science**, v. 84, p. 1247–1255, 2019.

BARBOSA, B. D. S. et al. UAV-based coffee yield prediction utilizing feature selection and deep learning. **Smart Agricultural Technology**, v. 1, p. 1-10, 2021.

BARBOSA, J. N. et al. Coffee quality and its interactions with environmental factors in Minas Gerais, Brazil. **Journal of Agricultural Science**, v. 4, n. 5, p. 181-190. 2012.

BERNARDES, T. et al. Monitoring biennial bearing effect on coffee yield using MODIS remote sensing imagery. **Remote Sensing**, n. 4, p. 2492–2509, 2012.

CASSIA, M. T. et al. Quality of mechanized coffee harvesting in circular planting system. **Ciência Rural**, v. 43, n. 1, p. 28-34. 2013.



CHEMURA, A.; MUTANGA, O.; DUBE, T. Separability of coffee leaf rust infection levels with machine learning methods at Sentinel-2 MSI spectral resolutions. **Precision Agriculture**, v. 18, n. 5, p. 859-881. 2017.

CONAB. Companhia Nacional de Abastecimento. **Acompanhamento da safra brasileira de café: Primeiro levantamento. Janeiro 2022. v. 9, safra 2020/21, n. 1.** Disponível em: <<https://www.conab.gov.br/info-agro/safra/cafe>> Acesso em: 01/02/2022.

CORREA, J. M. et al. Controlled water stress in uniformity of maturity and productivity of conilon coffee. **African Journal of Agricultural Research**, v. 12, n. 3, p. 192-199. 2017.

CRAIG, A. P. et al. Mid infrared spectroscopy and chemometrics as tools for the classification of roasted coffees by cup quality. **Food Chemistry**, v. 245, p. 1052–1061, 2018.

CRAIG, A. P. et al. Fourier transform infrared spectroscopy and near infrared spectroscopy for the quantification of defects in roasted coffees. **Talanta**, v. 134, p. 379–386, 2015.

CUNHA, J. P. et al. Estimating vegetation volume of coffee crops using images from unmanned aerial vehicles. **Engenharia Agrícola**, v. 39, p. 41-47. 2019.

DI DONFRANCESCO, B.; GUTIERREZ GUZMAN, N.; CHAMBERS, E. Comparison of results from cupping and descriptive sensory analysis of Colombian brewed coffee. **Journal of Sensory Studies**, v. 29, p. 301–311, 2014.

EBRAHIMI-NAJAFABADI, H. et al. Detection of addition of barley to coffee using near infrared spectroscopy and chemometric techniques. **Talanta**, v. 99, p. 175–179, 2012.

FAGAN, E. B. et al. Efeito do tempo de formação do grão de café (*Coffea sp.*) na qualidade da bebida. **Bioscience Journal**, v. 27, n. 5, p. 729-738, 2011.

FERIA-MORALES, A. M. Examining the case of green coffee to illustrate the limitations of grading systems/expert tasters in sensory evaluation for quality control. **Food Quality and Preference**, v. 13, p. 355–367, 2002.

FERREIRA, W. P. M. et al. Effects of the Orientation of the Mountainside, Altitude and Varieties on the Quality of the Coffee Beverage from the “Matas de Minas” Region, Brazilian Southeast. **American Journal of Plant Sciences**, v. 7, p. 1291-1303. 2016.

FERREIRA, W. P. M. et al. Influence of relief and global radiation on the quality of the coffee beverage. *In: American Society of Agricultural and Biological Engineers Annual International Meeting. ASABE. Annals [...]*, 2014, p. 1-10. Available online: <

<https://elibrary.asabe.org/abstract.asp?aid=44604>>. Accessed on: 10/06/2021.

FITZGERALD, G. J. et al. Spectral and thermal sensing for nitrogen and water status in rainfed and irrigated wheat environments. **Precision Agriculture**, v. 7, p. 233–248. 2006.

HERWITZ, S. et al. Imaging from an unmanned aerial vehicle: Agricultural surveillance and decision support. **Computers and Electronics in Agriculture**, v. 44, p. 49–61, 2004.

JOHNSON, L. F. et al. Feasibility of monitoring coffee field ripeness with airborne multispectral imagery. **Applied Engineering in Agriculture**, v. 20, p. 845–849, 2004.

LELONG, C. C. D. et al. Assessment of Unmanned Aerial Vehicles Imagery for Quantitative Monitoring of Wheat Crop in Small Plots. **Sensors**, v. 8, n. 5, p. 3557–85. 2008.

LOUZADA PEREIRA, L. et al. Influence of solar radiation and wet processing on the final quality of arabica coffee. **Journal of Food Quality**, v. 2018, p. 1–9, 2018.

MARIN, D. B. et al. Multispectral radiometric monitoring of bacterial blight of coffee. **Precision Agriculture**, v. 20, n. 5, p. 959-982, 2019.

MARIN, D. B. et al. Remotely Piloted Aircraft and Random Forest in the Evaluation of the Spatial Variability of Foliar Nitrogen in Coffee Crop. **Remote Sensing**, v. 13, n. 8, p. 1471-1486, 2021a.

MARIN, D. B. et al. Detecting coffee leaf rust with UAV-based vegetation indices and decision tree machine learning models. **Computers and Electronics in Agriculture**, v. 190, p. 1-10, 2021b.

MARTINEZ, H. E. P. et al. Zinc supplementation, production and quality of coffee beans. **Revista Ceres**, v. 60, n. 2, p. 293–299. 2013.

NOGUEIRA, S. M. C.; MOREIRA, M. A.; VOLPATO, M. M. L. Relationship between coffee crop productivity and vegetation indexes derived from Oli/Landsat-8 sensor data with and without topographic correction. **Engenharia Agrícola**, v. 38, n. 3, p. 387-394, 2018.

PARREIRAS, T. C. et al. Using unmanned aerial vehicle and machine learning algorithm to monitor leaf nitrogen in coffee. **Coffee Science**, v. 15, p. 1-9, 2020.

PETERSEN, L. K. Real-time prediction of crop yields from MODIS relative vegetation health: A Continent-wide analysis of Africa. **Remote Sensing**, v. 10, p. 1726-1755. 2018.

RAMIREZ, G. A.; ZULO JÚNIOR, J. Estimativa de parâmetros biofísicos de plantas de café a partir de imagens orbitais de alta resolução espacial. **Engenharia Agrícola**, v. 30, p. 231- 238, 2010.

ROUSE, J. W. et al. Monitoring vegetation systems in the Great Plains with ERTS (Earth Resources Technology Satellite). *In*: III Earth Resources Technology Satellite-1 Symposium; 1973, NASA. Washington, DC, USA. **Annals [...]**, 1973, p. 301-317.

SANTOS, L. M. et al. Determining the leaf area index and percentage of area covered by coffee crops using UAV RGB images. **IEEE Journal of Selected Topics in Applied Earth Observations and Remote Sensing**, v. 13, p. 6401-6409, 2020.

SILVA, S A.; LIMA, J. S. S.; ALVES, A. I. Spatial study of grain yield and percentage of bark of two varieties of *Coffea arabica* L. to the production of quality coffee. **Bioscience Journal**, v. 1, v. 26, n. 4, p. 558–565. 2010.

SILVA, A. S. et al. Coffee quality and its relationship with Brix degree and colorimetric information of coffee cherries. **Precision Agriculture**, v. 15, p. 543-554. 2014.

TOLESSA, K. et al. Influence of growing altitude, shade and harvest period on quality and biochemical composition of Ethiopian specialty coffee. **Journal of the Science of Food and Agriculture**, v. 97, p. 2849–2857, 2017.

TOLESSA, K. et al. Prediction of specialty coffee cup quality based on near infrared spectra of green coffee beans. **Talanta**, v. 150, p. 367–374, 2016.

TOLESSA, K.; DUCHATEAU, L.; BOECKX, P. Analysis of coffee quality along the coffee value chain in Jimma zone, Ethiopia. **African Journal of Agricultural Research**, v. 13, n. 29, p. 1468-1475, 2018.

USDA. United States Department of Agriculture. **Coffee: Market and Trade Data**. Disponível em: <<https://apps.fas.usda.gov/psdonline/app/index.html#/app/downloads>>: Acesso em: 01/02/2022.

## 2 A novel vegetation index for coffee ripeness monitoring using aerial imagery <sup>1</sup>

### Abstract

Coffee ripeness monitoring is a key indicator for defining the moment of starting the harvest, especially because the coffee quality is related to the fruit ripeness degree. The most used method to define the start of harvesting is by visual inspection, which is time-consuming, labor-intensive, and does not provide information on the entire area. There is a lack of new techniques or alternative methodologies to provide faster measurements that can support harvest planning. Based on that, this study aimed at developing a vegetation index (VI) for coffee ripeness monitoring using aerial imagery. For this, an experiment was set up in five arabica coffee fields in Minas Gerais State, Brazil. During the coffee ripeness stage, four flights were carried out to acquire spectral information on the crop canopy using two quadcopters, one equipped with a five-band multispectral camera and another with an RGB (Red, Green, Blue) camera. Prior to the flights, manual counts of the percentage of unripe fruits were carried out using irregular sampling grids on each day for validation purposes. After image acquisition, the coffee ripeness index (CRI) and other five VIs were obtained. The CRI was developed combining reflectance from the red band and from a ground-based red target placed on the study area. The effectiveness of the CRI was compared under different analyses with traditional VIs. The CRI showed a higher sensitivity to discriminate coffee plants ready for harvest from not-ready for harvest in all coffee fields. Furthermore, the highest  $R^2$  and lowest RMSE values for estimating the coffee ripeness were also presented by the CRI ( $R^2$ : 0.70; 12.42%), whereas the other VIs showed  $R^2$  and RMSE values ranging from 0.22 to 0.67 and from 13.28 to 16.50, respectively. Finally, the study demonstrated that the time-consuming fieldwork can be replaced by the methodology based on VIs.

**Keywords:** *Coffea arabica* L., coffee fruit ripeness, unmanned aerial vehicle, remote sensing

### 2.1 Introduction

Coffee is the second most traded commodity worldwide, playing an important role in the economy of several Latin American, African, and Asian countries (ICO, 2020). Brazil is by far the world's largest producer and exporter of coffee beans, accounting for 35% of the global

---

<sup>1</sup> This chapter refers to the original version of the manuscript "A novel vegetation index for coffee ripeness monitoring using aerial imagery" published in the Journal *Remote Sensing*, volume 13, p. 1-16, 2021.

production in the 2019/2020 season (USDA, 2020). About 70% of the Brazilian production is arabica type (*Coffea arabica* L.), and Minas Gerais State is the state with the largest production. Such facts consolidate the expressive economic and social importance of this crop for Brazil.

The growing global demand for specialty coffee, makes it necessary to develop productive strategies to differentiate the Brazilian product. Coffee is a product whose price depends on the beverage quality, which in turn is influenced by the level of fruit ripeness at harvest and, among other things, by environmental and soil conditions, and crop management and post-harvesting practices (MARTINEZ et al., 2013; SILVA et al., 2014; SILVA et al., 2010). The beverage quality is higher when obtained from ripe fruits (cherry), in contrast to unripe and overripe fruits that deteriorate its beverage quality, as well as the color and size uniformity of the grains (FAGAN et al., 2011; MARTINEZ et al., 2013; SILVA et al., 2014). Therefore, knowing the when the fruit is ripe is crucial so that farmers can carry out the planning of their crop harvesting.

Ripeness is the stage where coffee fruits are fully formed and undergo changes in color and chemical and enzymatic composition (APARECIDO et al., 2018; CASTRO; MARRACCINI, 2006). At present, coffee ripeness monitoring relies on repeated manual fruit counts made on a few sampled branches within fields. Then, farmers attempt to harvest those fields with the greatest percentage of ripe fruits. This method is time-consuming and labor-intensive, demanding alternative methodologies to provide faster measurements that can support harvest planning. Besides that, a major source of error is associated with the lack of sufficient data to represent the spatial and temporal variability of fruit ripeness (FURFARO et al., 2007; HERWITZ et al., 2004). Punctuality is also an issue because manual monitoring of multiple fields may become subjective and overly prolonged. Together, these errors may reduce the accuracy of ripeness monitoring, which can affect harvest planning, mainly in mountainous areas where the harvest is carried out manually due to the absence of agricultural mechanization.

Remote sensing (RS) has been used to obtain information on crops in a dynamic, non-destructive, and rapid manner and has been applied in numerous subjects (REN et al., 2020). The use of RS has been explored in the last years using satellite imagery for a variety of applications in the coffee crop. Studies were carried out to assess the crop biomass and carbon stocks (COLTRI et al., 2013), the biennial effect on yield (BERNARDES et al., 2013), crop yield (NOGUEIRA et al., 2018), and other characteristics (MIRANDA et al., 2020; RAMIREZ et al., 2010; TSAI; CHEN, 2017). However, the use of satellite imagery can be complex because it depends on spectral, temporal, and spatial resolutions from the sensor used (BERNARDES

et al., 2013). Furthermore, most satellites with data freely available lack good spatial and temporal resolutions, which are essential for crop monitoring. Additionally, for those with high resolution, imagery is usually costly and cannot be afforded by small farmers.

On the other hand, the development of Unmanned Aerial Vehicles (UAV) and modern Red, Green, Blue (RGB) and multispectral sensors has enabled the acquisition of imagery with a higher spatial, and temporal resolution at a lower cost, as well as providing detailed information on crop spectral patterns. The effectiveness of the UAV imagery on the coffee crop has been demonstrated on a few studies, including fruit detection (CARRIJO et al., 2017), estimation of biophysical parameters (CUNHA et al., 2019; SANTOS et al., 2020a), crop coefficient (Kc) prediction (SANTOS et al., 2020b), leaf nitrogen monitoring (PARREIRAS et al., 2020), and also for fruit ripeness monitoring (FURFARO et al., 2007; HERWITZ et al., 2004; JOHNSON et al., 2004).

Most studies related to the use of satellite and UAV imagery uses vegetation indices (VIs) to assess the spectral response of the vegetation. Several VIs were proposed throughout the years for different reasons, and the most commonly used and studied VIs are the Normalized Difference Vegetation Index (NDVI) (ROUSE et al., 1973), and the Soil Adjusted Vegetation Index (SAVI) (HUETE et al., 1988). Commonly, these VIs can highlight plant intrinsic characteristics that are well related to crop greenness and vigor. In addition, each VI has its specific expression which can represent vegetation properties better than using individual bands (BALOLOY et al., 2020). However, most of these known VIs are not specific for a single crop (*e.g.*, coffee) and cannot alone discriminate specific crop parameters.

The spectral response of the coffee crop varies depending on several factors such as planting density, crop management, crop age, and others (MOREIRA et al., 2004). In addition, as arabica coffee blossoms do not appear and develop uniformly throughout the field, unequal fruit ripening is practically inevitable (DAMATTA et al., 2007). This leads to spatial and temporal variability among trees as well as within a single tree. It is known that during the coffee ripeness, the fruit color changes from green to red or yellow depending on the plant cultivar. Based on that, it has been hypothesized that as plants with ripe fruits reflect more radiation in the red band than plants with unripe fruits, a VI using only the red band can be more efficient for coffee ripeness monitoring than conventional VIs, which uses more than one spectral band. In this sense, a VI considering the amount of red in the field can provide a better assessment of the fruit ripeness, being useful for harvest planning. Therefore, the aim of this study was to develop a vegetation index for coffee ripeness monitoring using aerial imagery.

## 2.2 Material and Methods

### 2.2.1 Study area

This study was carried out in five fields of arabica coffee (*Coffea arabica* L.) located in the Jatobá farm, municipality of Paula Cândido, Minas Gerais State, Brazil (42°55'11.906" W; 20°49'26.158" S and 42°55'1.076" W; 20°49'39.997" S, and 753 m above sea level) (Figure 1). The relief in the area is mountainous (slope varies from 0 to 45%), and the climate is classified as “CWA”, (humid subtropical with dry winter and hot summer) according to the Köppen-Geiger climate classification (ALVARES et al., 2013).

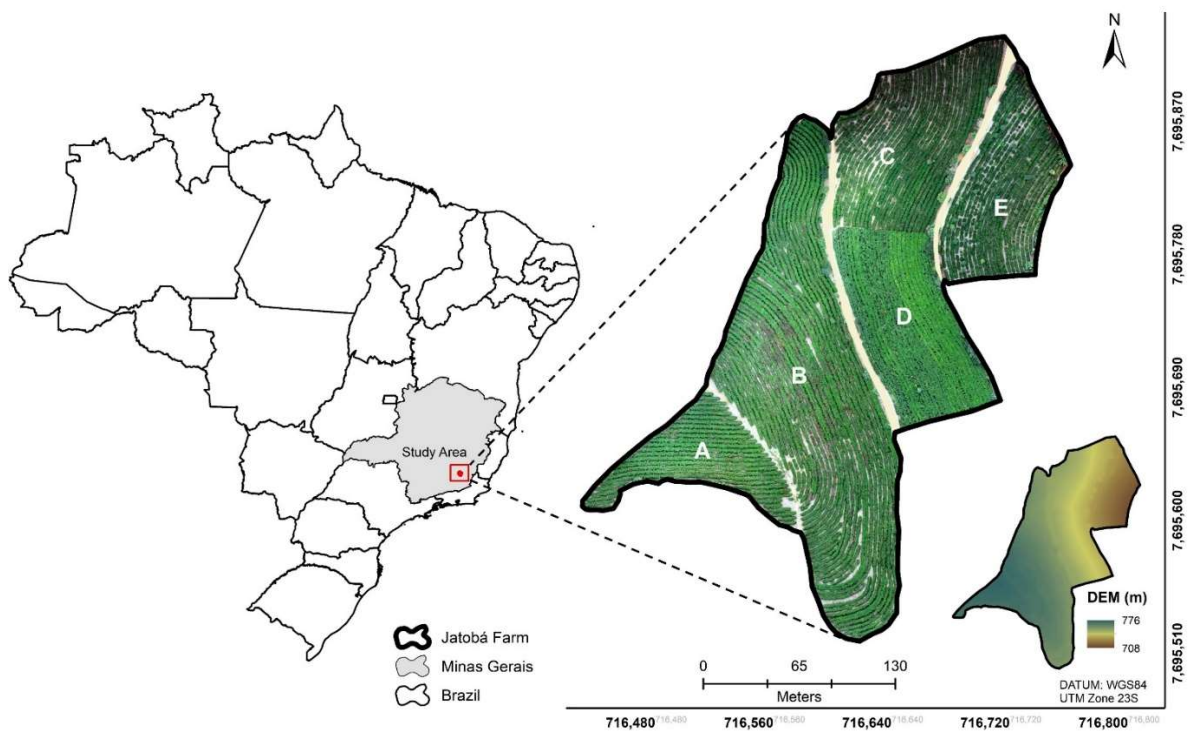


**Figure 1.** Location of the study area in Minas Gerais State, Southeastern Brazil.

### 2.2.2 UAV platform and imagery acquisition

Two models of quadcopters were used for this study. First, the DJI Matrice 100 (DJI Innovations, Shenzhen, China) was equipped with the multispectral camera MicaSense RedEdge MX (MicaSense, Seattle, WA, USA). This camera is composed of five complementary metal oxide semiconductor (CMOS) sensors that simultaneously captures five bands: 475 nm  $\pm$  20 nm (Blue), 560 nm  $\pm$  20 nm (Green), 668 nm  $\pm$  10 nm (Red), 840 nm  $\pm$  40 nm (NIR), and 717 nm  $\pm$  10 nm (RedEdge) (DADRASJAVAN et al., 2019). The second UAV was the DJI Phantom 4 Pro, equipped with its RGB camera, which registers information in the

following bandwidth: 450 nm  $\pm$  16 nm (Blue), 560 nm  $\pm$  16 nm (Green), and 650 nm  $\pm$  16 nm (Red). The technical characteristics of both cameras are presented in Table 1.

**Table 1.** Technical characteristics of the MicaSense RedEdge MX, and the Phantom 4 Pro Red, Green, Blue (RGB) camera.

Camera	RedEdge MX	Phantom 4 RGB
Acquisition	RGB-RE-NIR	R-G-B
Sensor size (mm)	4.8 $\times$ 3.6	4.7 $\times$ 6.3
Sensor size (px)	1280 $\times$ 960	5472 $\times$ 3648
Focal length (mm)	5.4	8.8
Field of View (FOV)	47.2°	84°
Output format	RAW, TIF image	RAW, JPG image

R, Red; G, Green; B, Blue; RE, RedEdge; and NIR, Near-infrared.

The UAVs campaigns were carried out under clear-sky conditions between 11:00 and 13:00 h local time using a flight plan, previously defined with the DroneDeploy software (DroneDeploy Inc., San Francisco, CA, USA). Before the UAV flights, 20 ground control points (GCP) were distributed around the study area for further geometric correction of the orthomosaic map. Then, the GCPs coordinates were obtained using a topographic GNSS (Global Navigation Satellite System) receiver, model Trimble ProXT (Trimble Inc., Sunnyvale, CA, USA). Data collection timeline and flight specifications of both UAV platforms are summarized in Table 2.

**Table 2.** Unmanned Aerial Vehicles (UAV) data collection timeline and flight specifications.

Date	AGL (m) <sup>1</sup>	Overlap (%) <sup>2</sup>	Spatial Resolution (cm)
29/04/2019	60	<sup>3</sup> -/75	-/2.3
07/05/2019	60	-/75	-/2.3
13/05/2019	60	80/75	5.0/2.3
27/05/2019	60	80/75	5.0/2.3

<sup>1</sup> Above ground level; <sup>2</sup> Lateral and longitudinal overlap; <sup>3</sup> The RedEdge MX was available only for the last two flights.

Before and after each flight, images of the reflectance target provided by the Micasense were taken at 1 m height to perform the radiometric calibration of the images during postprocessing. On the other hand, the RGB camera onboard of the Phantom 4 does not have a



specific calibration target or system. Therefore, for this study, four grayscale reflectance targets (85, 27, 12, and 7%) made of plywood and covered with synthetic nappa leather of polyvinyl chloride (PVC) were placed in the field during all flight campaigns and used for calibration of the RGB bands (Figure 2). Additionally, a red target made of the same material with dimensions of  $0.5 \times 0.5$  m was used to obtain the coffee ripeness index. The reflectance of all targets was obtained using a portable spectroradiometer ASD Handheld 2 (Analytical Spectral Devices, Inc., Boulder, CO, USA), which operates in the wavelength range from 325 nm to 1075 nm with resolution of  $\pm 1$  nm. A spectralon plate was used as white reference for spectroradiometer calibration.

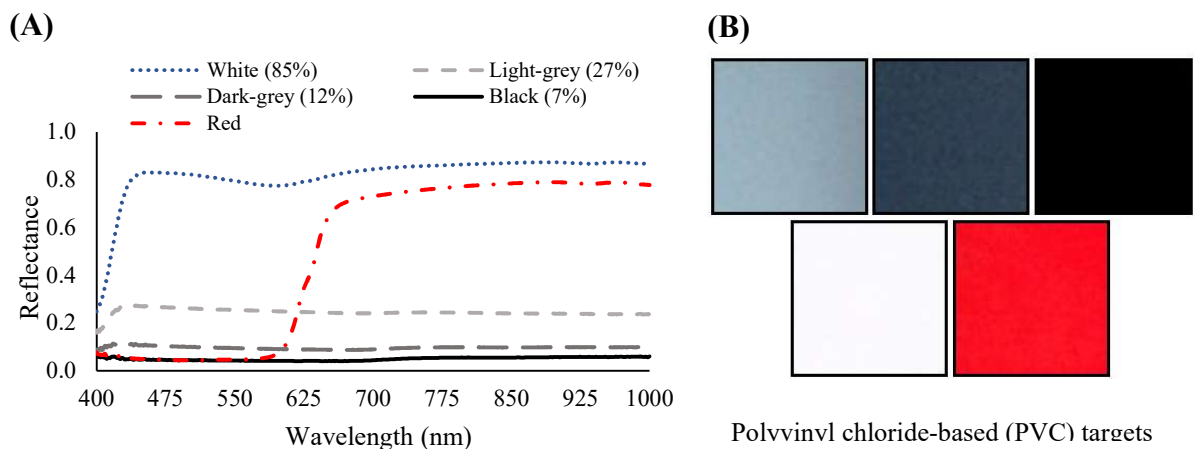


**Figure 2.** Spectral response curves (A) of the polyvinyl chloride-based (PVC) and (B) calibration targets used during the flight campaigns.

### 2.2.3 UAV imagery pre-processing

All images were recorded in RAW format and after processing converted to the Tagged Image File Format (TIFF). The images were processed in the Agisoft<sup>TM</sup> MetaShape software, version 1.5.3 (Agisoft LLC, St. Petersburg, Russia). The RedEdge MX images were radiometrically calibrated using the correction factors of the Micasense's calibration target, and the RGB camera images were calibrated using the vicarious method (DEL POZO et al., 2014; ROSAS et al., 2020; WANG; MYINT, 2015). For that, the pixels of the four PVC targets were manually clipped. Then, linear regression models for each three-band were adjusted using the average pixel digital number (DN) and reflectance values of the targets obtained with the spectroradiometer. The DN values in the whole images were converted to reflectance based on the regression equations.

Subsequently, all images were processed to create the orthomosaics. Firstly, all five bands from the RedEdge MX needed to be aligned since the sensor acquires one image per

channel. Thus, the five bands were aligned and grouped in a single file for each multispectral image. Then, the orthomosaics of both cameras were created performing the following steps: (1) image alignment using the UAV's GPS unit; (2) construction of a three-dimensional point cloud using the Structure from Motion (SfM) technique (BRENNER et al., 2018; ZARCO-TEJADA et al., 2014); (3 and 4) creation of the dense point cloud, which served as the basis for creating the Digital Surface Model (DSM); (5) the DSM was used to project every image pixel to generate the orthomosaics (ASHAPURE et al., 2019; WIJESINGHA et al., 2020); and finally, (6), using the QGIS, version 3.2 (QGIS DEVELOPMENT TEAM, 2020), all orthomosaics were georeferenced using the GCP coordinates (Figure 3).

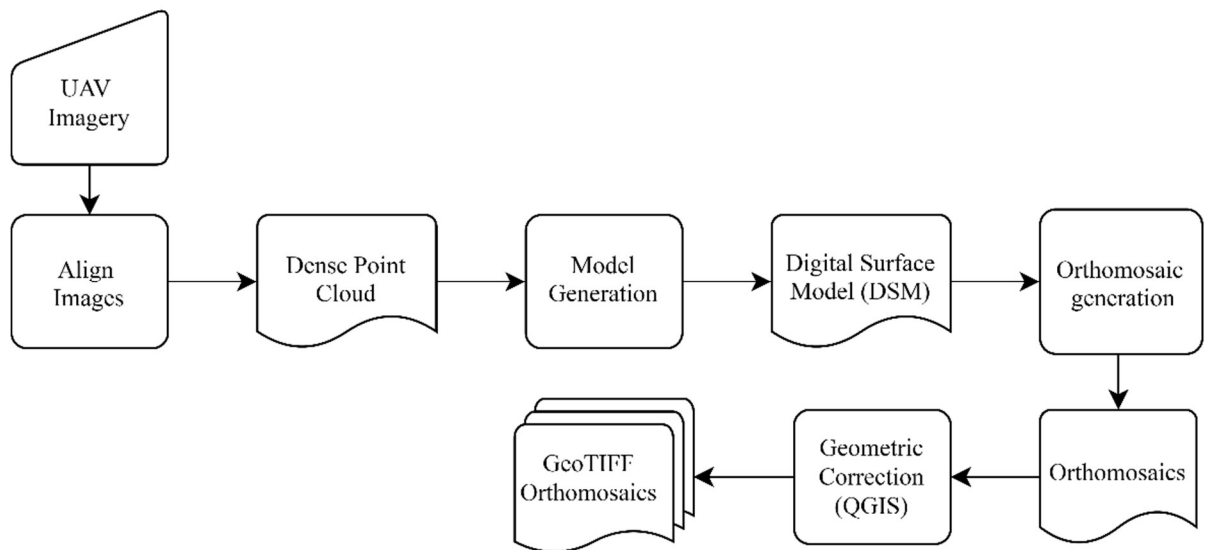


**Figure 3.** Workflow developed for processing the UAV images to obtain the georeferenced orthomosaics.

#### *2.2.4 Laboratory experiment for coffee fruit ripeness spectra characterization*

Spectral reflectance patterns of the coffee fruits are useful to understand the main differences and challenges of monitoring their ripeness at the field level from that observed in the UAV images. Based on that, a laboratory reflectance spectroscopy experiment was performed to characterize the spectral pattern of the fruit ripeness. Five samples of coffee fruits (500 fruits per sample) with different percentages of unripe and ripe fruits (ranging from 100% to 0%) were conditioned in a flat surface with a single layer of fruits, 8 cm from the spectroradiometer and 80 cm from two halogen lamps (300 W) (Figure 4). Five measurements per sample were performed using the spectroradiometer.

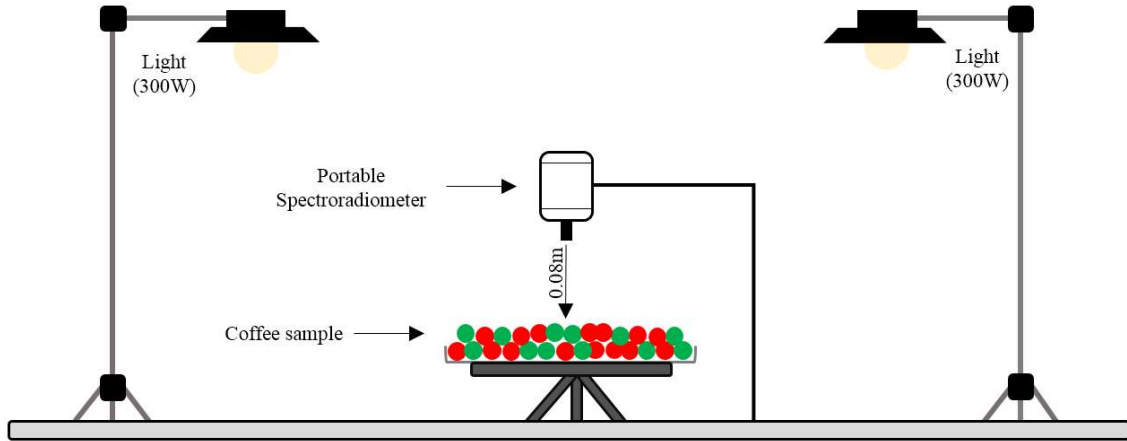


**Figure 4.** Laboratory experiment set up used to characterize the spectra of the coffee fruit ripeness.

### 2.2.5 Extraction of the vegetation indices and fruit ripeness assessments

From the GeoTIFF orthomosaics, the following VIs were obtained for the study area: the Coffee Ripeness Index (CRI); the Green-red Ratio Ripeness Index (GRRI); the Modified Chlorophyll Absorption in Reflectance Index 1 (MCARI1); the Normalized Difference Vegetation Index (NDVI); the Normalized Difference RedEdge Index (NDRE); and the Green Normalized Difference Vegetation Index (GNDVI) (Table 3). The GRRI was selected because it was previously created to assess the coffee ripeness using UAV imagery, whereas the MCARI1, NDVI, NDRE, and GNDVI were selected due to their good relationship with vegetation pigments, as well as to their extensive use in crop monitoring studies. Those five VIs were chosen for comparison purposes with the CRI.

**Table 3.** References and equations of the spectral vegetation indices evaluated in this study.

Vegetation Index	Equation	Reference
CRI	$(R/R_{\text{target}})100$	Proposed VI
GRRI	$(G/R)$	Johnson et al. (2004)
MCARI1	$1.2[2.5(\text{NIR} - R) - 1.3(\text{NIR} - G)]$	Haboudane et al. (2004)
NDVI	$(N - R)/(N + R)$	Rouse et al. (1973)
NDRE	$(N - \text{RE})/(N + \text{RE})$	Fitzgerald et al. (2006)
GNDVI	$(N - G)/(N + G)$	Gitelson et al. (1996)

N, Near-infrared; R, Red; G, Green; RE, RedEdge; and  $R_{\text{Target}}$ , Average reflectance value of the red target in the red band.

The VIs were obtained at the sampling point level, which was defined considering three plants in the same cultivation row. After calculating the IVs, polygonal masks were manually created for each sampling point using the QGIS software. Then, the average values of the polygon pixels were extracted using the zonal statistics tool.

For the validation of the VIs, manual measurements of the coffee ripeness (percentage of unripe fruits) were carried out on the same dates of image acquisition (Table 2). An irregular grid with 20 samples per hectare was set up on each measurement day for the fields A, C, D, and E. For field B, only 10 samples per hectare were considered due to its lower fruit load. Furthermore, on each plant, four plagiotropic branches were randomly chosen in the plant's middle third, considering one branch per quadrant. After that, the unripe fruits, and the total of fruits on the branches of each plant were counted and the percentage of unripe fruits was used to represent the fruit ripeness at each sampling point. Finally, using the percentage of unripe fruits, the sampling points were classified into two ripeness class: not ready for harvest with more than 30% of unripe fruits; and ready for harvest with the percentage of unripe fruits with less than 30%. This proportion has been used by the farmers in the region to begin the harvest.

### *2.2.6 Statistical analysis*

Initially, an analysis of variance (ANOVA) was carried out between the ripeness classes to evaluate the potential of the six VI to discriminate plants that were ready to harvest from not-ready in the field. First, this analysis was performed for each coffee field, and then, all data were grouped into a single dataset to evaluate the influence of the different cultivars, crop canopy and yield on the VIs performance.

Next, linear regression ( $Y = \beta_0 + \beta_1 X$ ) was used to model the relationship between the VIs and the coffee fruit ripeness. In addition, the significance of the regression coefficients was evaluated using the t-test at 1% probability ( $p < 0.01$ ). Finally, to infer about which VI presented better adjustment to the coffee ripeness, the following statistical metrics were calculated: Coefficient of determination ( $R^2$ ), and Root mean square error (RMSE). All statistical analyses were performed using the R software, version 3.6.1 (R CORE TEAM, 2019).

## **2.3 Results**

### *2.3.1 Spectral characterization of coffee fruits ripeness*

Measurements done in laboratory showed that the coffee fruits spectra are highly variable according to the fruit ripeness degree (Figure 5). As expected, unripe fruits presented

a reflectance peak in the green band ( $560 \text{ nm} \pm 20 \text{ nm}$ ), whereas in the red band ( $650 \pm 30 \text{ nm}$ ) it showed an absorption peak, possibly related to the higher amount of chlorophyll in this region (CASTRO; MARRACCINI, 2006). Then, the reflectance increased up to 900 nm in the NIR region. Conversely, after reducing the percentage of unripe fruits (Figure 5A–E), the samples tended to present a flat spectral behavior up to the red band, where it presented a reflectance peak, which is related to the reduction of chlorophyll pigments and accumulation of anthocyanins (CASTRO; MARRACCINI, 2006). After that, there was an increase in reflectance as observed in the sample with 0% of unripe fruits (Figure 5E).

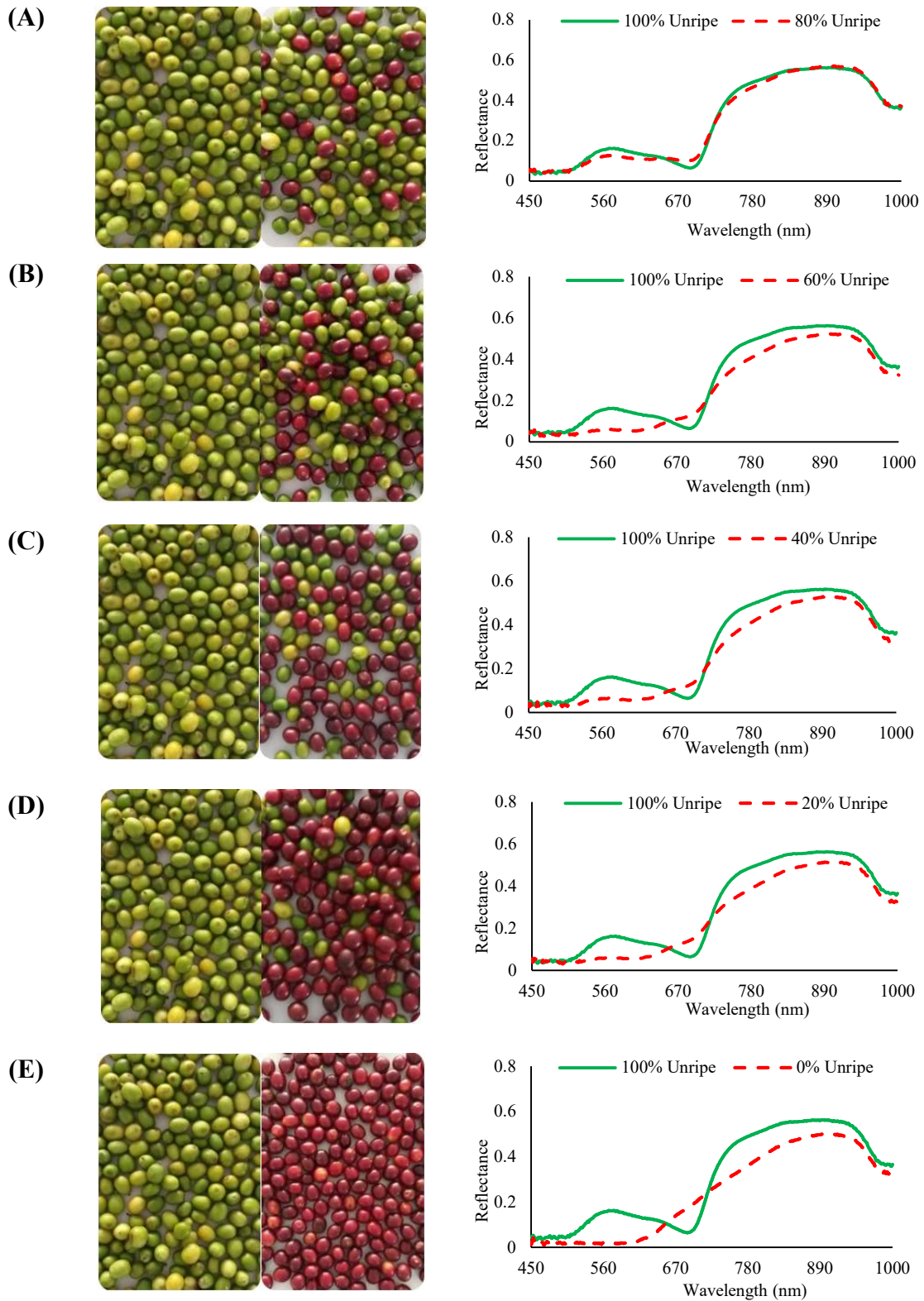


**Figure 5.** Spectral reflectance patterns for different ripeness percentages of coffee fruits (A) 100% and 80% of unripe; (B) 100% and 60% of unripe; (C) 100% and 40% of unripe; (D) 100% and 20% of unripe; and (E) 100% of unripe and 100% of ripe fruits.

In addition, the results also showed that the R, G and NIR bands presented better discrimination of unripe and ripe coffee fruits, while in the RedEdge band ( $717 \text{ nm} \pm 10 \text{ nm}$ ), the spectra from both classes tended to overlap around  $720 \text{ nm}$ . These bands are important to discriminate plants with unripe from those with ripe fruits, in which the differences can be detected using the VIs. Besides that, if we consider the application of the method in field conditions, the R band should be highlighted over the G and NIR bands since the coffee crop reflects a higher proportion of the G and NIR radiation. This characteristic can make it difficult to differentiate coffee fruits from leaves at  $60 \text{ m}$  height (UAV imagery). Thus, the R band is better since a subtle increase in its reflectance (*i.e.*, increase of fruit ripeness) can be easier to detect than when using the G and NIR bands, in which a reduction of their reflectance cannot discriminate the fruit ripeness due to the spectral confusion among leaves and unripe fruits.

### 2.3.2 Potential of VIs for discrimination of coffee ripeness classes

The characterization of the arabica coffee fields used in this study is shown in Table 4. The study area is represented by different coffee cultivars and each coffee field presented different canopy volumes, density of plants, and crop yield. Additionally, the terrain of the region is mountainous, and the slope varied throughout the coffee fields. Regarding the crop yield, the field B that had the highest cultivation area, showed, on the other hand, the lowest yield among all fields. This lower yield is a result of the biennial yield effect, a peculiar characteristic of this crop which exhibits high and low yield values in alternated years.

**Table 4.** Characteristics of the five arabica coffee fields used in this study.

Field	Area (ha)	Cultivar	Canopy Volume ( $\text{m}^3$ )	Density (Plants $\text{ha}^{-1}$ )	Average Slope (%)	Yield ( $\text{kg ha}^{-1}$ )
A	0.54	Red Catuai	$2.91 \pm 0.19$	4000	7.66	1220
B	2.1	Red Catuai	$1.87 \pm 0.14$	4000	14.39	480
C	1.01	MG H 419-1	$0.62 \pm 0.04$	8000	16.24	3750
D	0.77	Red Bourbon	$0.70 \pm 0.06$	13333	23.76	2500
E	0.65	Icatu	$1.77 \pm 0.10$	2222	20.79	2220

OBS: Coffee fruits from fields C and E present a yellow color when ripe.

Results of the ANOVA showed that only the CRI (both cameras), GRII (RGB camera), and the MCARI1 were able to discriminate the coffee plants ready for harvest from not-ready for harvest (*i.e.*, plants with unripe fruits from plants with ripe fruits), for all coffee fields (Table

5). Conversely, the GRRl when obtained from the RedEdge MX showed significant differences only in the fields A, B, and E. This result can be associated with different factors, such as the size of the dataset among cameras, temporal variability of the VI, and especially the specific characteristics of each coffee field.



**Table 5.** Comparison of average values of the vegetation indices from plants with unripe (G) and ripe (R) coffee fruits per field.

MicaSense RedEdge MX										
Field	<i>n</i>	Class	CRI	<i>p</i> -Value	GRI	<i>p</i> -Value	MCARI1	<i>p</i> -Value	NDVI	<i>p</i> -Value
A	13	G ± SD	5.680 ± 0.867	0.000 ***	3.213 ± 0.529	0.011 *	0.450 ± 0.069	0.000 ***	0.823 ± 0.014	0.772 <sup>ns</sup>
	07	R ± SD	8.746 ± 0.774		2.621 ± 0.200		0.613 ± 0.038		0.821 ± 0.018	
B	27	G ± SD	6.509 ± 1.193	0.000 ***	3.246 ± 0.255	0.000 ***	0.480 ± 0.044	0.000 ***	0.821 ± 0.017	0.067 <sup>ns</sup>
	15	R ± SD	8.353 ± 1.519		2.924 ± 0.159		0.579 ± 0.057		0.810 ± 0.018	
C	25	G ± SD	6.740 ± 0.922	0.000 ***	3.034 ± 0.295	0.257 <sup>ns</sup>	0.493 ± 0.075	0.000 ***	0.812 ± 0.022	0.891 <sup>ns</sup>
	12	R ± SD	9.174 ± 0.834		2.912 ± 0.310		0.609 ± 0.029		0.811 ± 0.201	
D	18	G ± SD	6.354 ± 1.343	0.000 ***	3.178 ± 0.311	0.121 <sup>ns</sup>	0.474 ± 0.139	0.000 ***	0.847 ± 0.011	0.017 *
	12	R ± SD	9.727 ± 0.468		2.988 ± 0.202		0.725 ± 0.064		0.835 ± 0.010	
E	20	G ± SD	5.910 ± 0.931	0.000 ***	3.006 ± 0.254	0.005 **	0.396 ± 0.069	0.000 ***	0.803 ± 0.010	0.016 *
	08	R ± SD	9.094 ± 0.544		2.723 ± 0.111		0.521 ± 0.067		0.792 ± 0.009	
Phantom 4 Pro RGB camera										
Field	<i>n</i>	Class	CRI	<i>p</i> -value	GRI	<i>p</i> -value	NDRE	<i>p</i> -value	GNDVI	<i>p</i> -value
A	26	G ± SD	7.090 ± 1.535	0.000 ***	1.332 ± 0.227	0.019 *	0.556 ± 0.020	0.000 ***	0.847 ± 0.005	0.069 <sup>ns</sup>
	11	R ± SD	9.880 ± 1.292		1.132 ± 0.048		0.513 ± 0.021		0.841 ± 0.006	
B	61	G ± SD	7.118 ± 1.450	0.001 **	1.284 ± 0.193	0.005 **	0.549 ± 0.023	0.002 **	0.843 ± 0.011	0.041 *
	19	R ± SD	8.460 ± 1.006		1.140 ± 0.047		0.520 ± 0.030		0.835 ± 0.010	
C	48	G ± SD	6.075 ± 1.392	0.000 ***	1.255 ± 0.221	0.014 *	0.555 ± 0.022	0.097 <sup>ns</sup>	0.845 ± 0.014	0.097 <sup>ns</sup>
	16	R ± SD	8.190 ± 0.926		1.084 ± 0.046		0.541 ± 0.026		0.837 ± 0.008	
D	45	G ± SD	6.998 ± 1.613	0.004 **	1.202 ± 0.215	0.000 ***	0.547 ± 0.010	0.000 ***	0.848 ± 0.007	0.053 <sup>ns</sup>
	11	R ± SD	8.744 ± 0.632		0.915 ± 0.074		0.530 ± 0.006		0.839 ± 0.012	
E	44	G ± SD	6.831 ± 0.958	0.000 ***	1.184 ± 0.134	0.001 **	0.526 ± 0.028	0.022 *	0.832 ± 0.010	0.165 <sup>ns</sup>
	08	R ± SD	8.171 ± 0.257		1.007 ± 0.135		0.501 ± 0.015		0.826 ± 0.011	

G, Average values of the vegetation indices from plants with unripe coffee fruits; R, Average values of the vegetation indices from plants with ripe coffee fruits; and SD, Standard deviation; <sup>ns</sup>, Not significant; *p*-values followed by \*\*\*, \*\*, and \* are significant at 0.1, 1, and 5% probability ( $p < 0.001$ ;  $p < 0.01$ ;  $p < 0.05$ ).

Regarding the other VIs, the NDRE presented the best results for discriminating the coffee ripeness, in which only the field C presented no significant differences between the ripeness classes. Conversely, the NDVI showed significant differences only for field D and E, whereas the GNDVI was only significant in field 2. Moreover, those coffee fields where the ripeness classes were not discriminated by the VIs, presented either higher canopy volumes or higher plant density (Table 4).

A second ANOVA was performed considering the data from all coffee fields as a single dataset. This analysis aimed to evaluate the influence of the different crop characteristics on the VIs performance. Results showed that only the CRI, GRRI, MCARI1, and NDRE presented significant ( $p < 0.001$ ) differences between the ripeness classes. Furthermore, the information presented in Figure 6, especially the two circles, reinforces the information that pixels of the VIs on the crop canopy could effectively discriminate plants with unripe fruits from those with ripe fruits. In addition, the boxplots make clear that the CRI and MCARI1 presented the higher threshold among the ripeness classes, whereas, for the GRRI and NDRE there was some overlapping between classes.

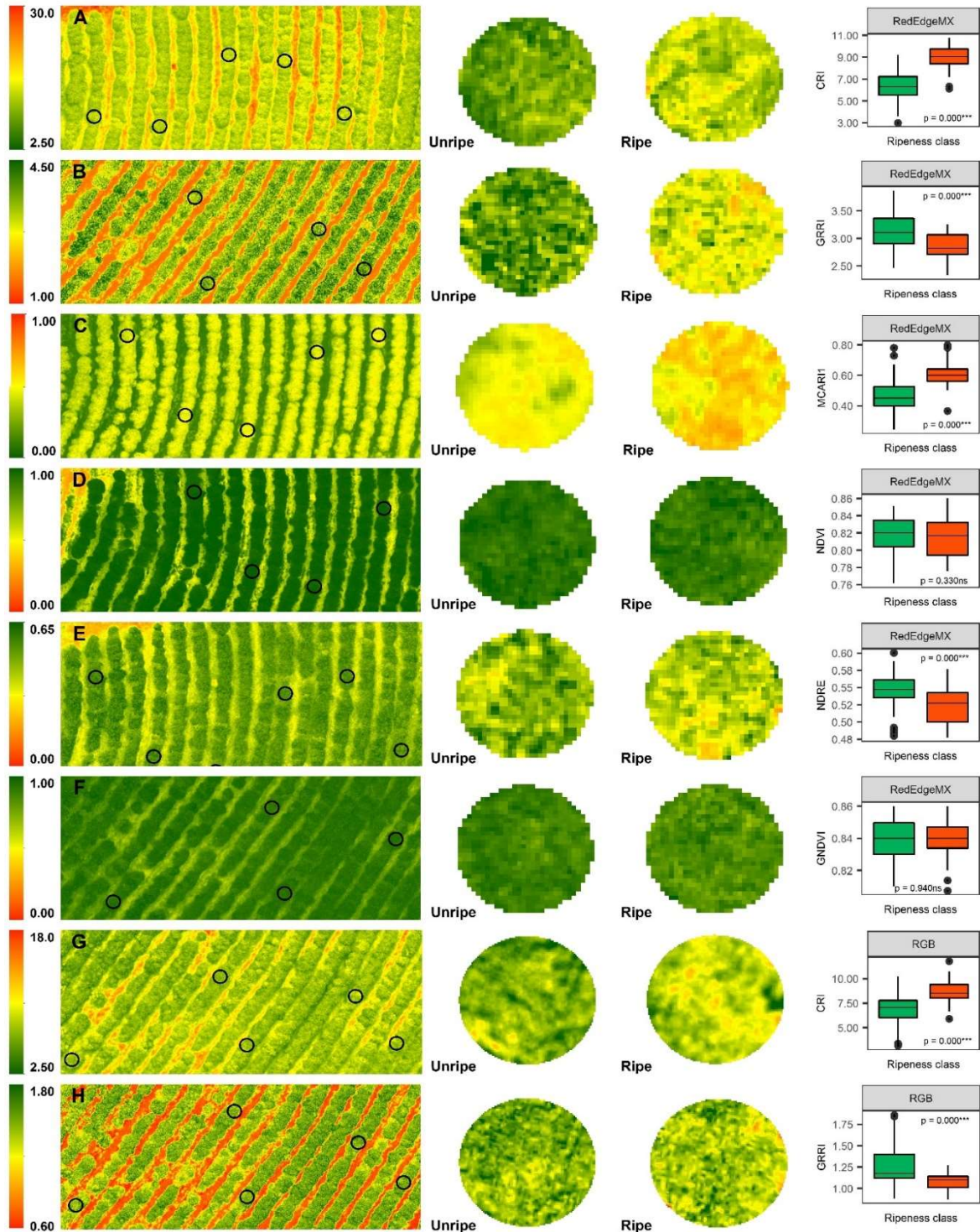


**Figure 6.** Comparison of average values of the vegetation indices from plants with unripe (G) and ripe (R) coffee fruits in all fields. From right to the left: the rectangular boxes (A–H) represent parts of the vegetation indices maps and the two central circles are examples of plant canopy under different ripeness classes. The boxplot presents the variation of the canopy spectral response from plants with unripe and ripe coffee fruits.  $p$ -values followed by \*\*\* are significant at 0.1% probability ( $p < 0.001$ ); and <sup>ns</sup>, Not significant.

### 2.3.3 Relationship between VIs and coffee ripeness

Results of the statistical metrics obtained with the five VIs for estimation of the coffee ripeness are presented in Figure 7. From a general point of view, it can be observed that the linear models used for estimation of the coffee ripeness showed satisfactory adjustments (*i.e.*,  $R^2$  and RMSE) considering the characteristics of the fields. Overall, the highest  $R^2$  and lowest RMSE values were obtained in field C ( $R^2$ : 0.70; RMSE: 12.42%) and A ( $R^2$ : 0.68; RMSE: 12.86%) by the CRI using the RedEdge MX, followed by the MCARI1 (Field A and C,  $R^2$ : 0.66 and 0.67; RMSE: 13.77 and 13.28%) and the CRI from the RGB camera (Field A and C,  $R^2$ : 0.62 and 0.62; RMSE: 15.43 and 14.35%).

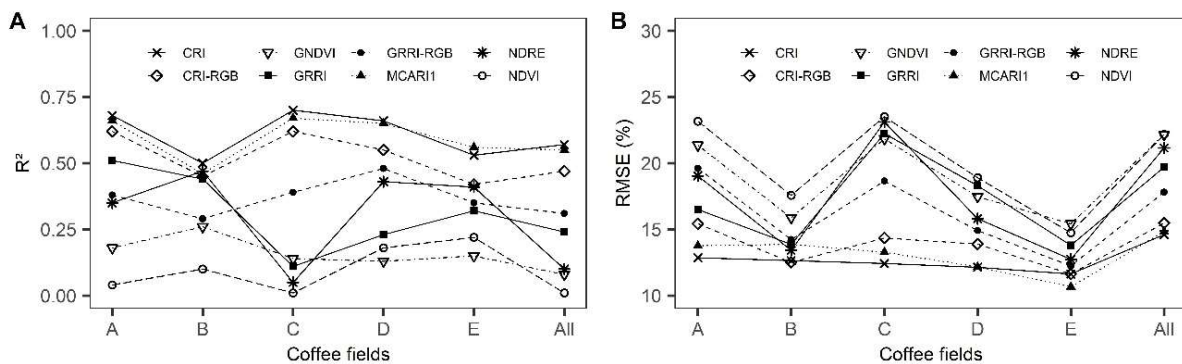


**Figure 7.** Statistical metrics of the linear models for coffee ripeness estimation: (A) determination coefficient ( $R^2$ ); and (B) root mean square error (RMSE).

Regarding the other VIs, they presented on the best-case scenarios  $R^2$  values of 0.51 (Field A), 0.48 (Field D), 0.47 (Field B), 0.22 (Field E), and 0.26 (Field B) and RMSE values of 16.50, 14.92, 13.42, 14.74, and 15.88%, respectively for the GRRi (RedEdge MX and RGB camera), NDRE, NDVI, and the GNDVI. Besides that, when considering all coffee fields as a single dataset, the linear models from all VIs presented lower performances. Moreover, it is worth mentioning that the differences in the statistical metrics between fields are related to the specific characteristics and dataset size of each coffee field.

Due to the large amount of data, only the linear models that ranked best on the  $R^2$  and RMSE metrics are presented in Figure 8. Overall, the CRI (RedEdge MX) performed best in all fields, except to field E, where the MCARI1 was better fit to the data. In addition, the version derived from the RedEdge MX presented higher performance than its version from the RGB camera in all coffee fields. Despite that, these VIs showed good results considering the

variability between fields and the non-uniform fruit ripeness presented by the crop, which makes it harder to develop a universal model for coffee ripeness estimation.

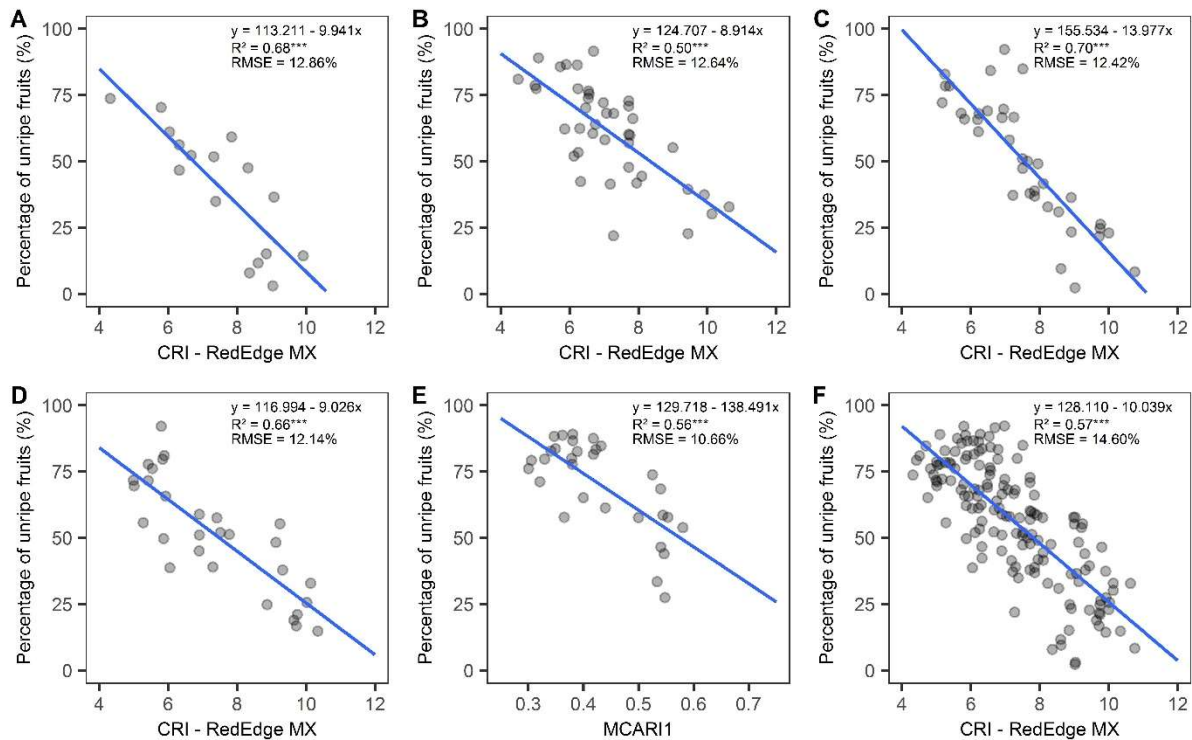


**Figure 8.** Best ranked models adjusted to the coffee ripeness using the vegetation indices. (A) Field A; (B) Field B; (C) Field C; (D) Field D; (E) Field E; (F) All coffee fields; CRI, Coffee ripeness index using the RedEdge MX camera; MCARI1, Modified Chlorophyll Absorption in Reflectance Index 1;  $R^2$  values followed by \*\*\* are significant at 0.1 probability ( $p < 0.001$ ).

## 2.4 Discussion

Coffee fruit ripeness monitoring is a crucial indicator for defining the optimal harvest time, especially because unlike unripe and overripe fruits, the ripe fruits (cherries) tend to produce beverages with higher quality (SILVA et al., 2014). Remote sensing is an effective approach that has been widely used to investigate crop parameters, in which some studies resulted in the development of several vegetation indices (BALOLOY et al., 2020; HE et al., 2019; MAIMAITIJIANG et al., 2019; REN et al., 2020). In this study, a simple and effective VI based on a single spectral band was developed using UAV imagery for coffee fruit ripeness monitoring.

The CRI outperformed traditional VIs such as the MCARI1, NDVI, NDRE, GNDVI, and also the GRRI, which was previously developed for coffee ripeness monitoring (JOHNSON et al., 2004). However, the field characteristics such as plant density, canopy

volume and especially, the crop yield (fruit load) directly influenced the VIs performance. The spectral response of a crop canopy tend to be similar to that of a single leaf, but changeable by many factors such as plant tissue optical properties, canopy structure, plant physiology, and climatic conditions (HEDE et al., 2015; KOIDE et al., 2012; ZARCO-TEJADA et al., 2001). For the coffee crop, there is an additional factor, the unequal fruit ripening, which is practically inevitable under natural conditions because coffee blossoming in nonequatorial regions as in the southcentral Brazil occurs at different times in the same season (*e.g.*, from August to November) in most of the production areas (DAMATTA et al., 2007). These factors made it more challenging to differentiate coffee fruits (unripe and ripe) from leaves when the VIs were used.

As stated before, at the laboratory level, the spectra of unripe and ripe fruits can be easily differentiated as the percentage of unripe fruits reduces (Figure 5). However, it can be very difficult to differentiate them using aerial imagery, especially under highly dense crop canopies that can induce spectral confusion. For the initial analysis, the CRI, GRRI (RGB camera), and MCARI1 were the only VIs capable of discriminating the ripeness classes in all coffee fields. The GRRI (RedEdge MX) and NDRE presented satisfactory performances, yet they were still influenced by field characteristics. On the other hand, the worst performance was presented by the NDVI and GNDVI that saturated, especially in the fields with higher plant density and canopy volume (Table 4). This problem has been addressed in other studies, whose authors reported the influence of several factors related to crop species, leaf area, crop biomass, its foliage, and others (BERNARDES et al., 2012; CARNEIRO et al., 2019; HUNT et al., 2008; KROSS et al., 2015).

When the five fields dataset was grouped, only the CRI, GRRI, MCARI1, and NDRE showed significant differences between the ripeness classes. This result is related to the temporal fruit color change, which is caused by the disappearance of chlorophyll pigments and the accumulation of anthocyanins (CASTRO; MARRACCINI, 2006) that altered the crop canopy spectral response (Figure 6). Besides that, from the fruit filling to the ripeness stage, coffee plants present a high nutritional demand, especially for NPK, which leads to an increase in nutrient translocation from the leaves to the fruits (LAVIOLA et al., 2009). This can result in nutrient deficiency and also in changes of leaf reflectance in the visible (400–700 nm) and NIR (700–1100 nm) wavelengths (AYALA-SILVA; BEYL, 2005), which can be better-detected with VIs of higher sensitivity to chlorophyll pigments (HUANG et al., 2015; LIN et al., 2019; SONOBE et al., 2017). Together, these factors led these VIs, and especially the CRI

due to its higher sensitivity of changes in the red wavelength, to present better capability of discriminating plants with unripe fruits from those with ripe fruits.

For the regression analysis, the CRI outperformed the other VIs on most coffee fields, except to field 5 where the MCARI1 showed better performance (Figures 7 and 8). Compared to this study, Johnson et al. (2004) developed and evaluated the GRRI for ripeness monitoring in nine coffee fields and obtained a  $R^2$  of 0.43. On the other hand, Herwitz et al. (2004) using the same index reported a much better correlation ( $R^2$ : 0.81) for seven coffee fields. However, these authors presented the results at the field level, which does not entirely represent the spatial variability of the fruit ripeness. Moreover, all coffee fields presented high fruit display on the canopy exterior. Differently, in this study, the sampling points were defined at every three plants, which better represented the spatial variability of fruit ripeness. In addition, not all five coffee fields presented high yield, which as discussed before, played a key role on the VIs performance. In this sense, our results were more satisfactory than those presented above, especially due to the higher sensitivity shown by the CRI in detecting the fruit ripeness changes.

Regarding the results obtained with the CRI and GRRI from both cameras, the differences in the ANOVA and linear regression analysis are related to the radiometric calibration method and mainly to the dataset size of both cameras. The RedEdge MX besides presenting an individual CMOS for each band, it presents a more complex calibration system composed by its downwelling light sensor and the factory-calibrated reference target (For more details look at Mamaghani et al. (2019)). On the other hand, in the RGB camera due to the absence of a calibration system, we used low-cost targets and the vicarious calibration, a simple and effective method (IQBAL et al., 2018); but not as robust as the one presented by the RedEdge MX.

Apart from that, the dataset size was the main factor influencing the VIs results. The RGB camera was used in four weeks, whereas the RedEdge MX was used only in the third and fourth weeks due to availability (Table 2). During the two first weeks, there was a higher percentage of unripe fruits than in the last two weeks. This increased the temporal variability of the fruit ripeness and resulted in lower performance by the CRI from the RGB camera. Conversely, the version derived from the RedEdge MX presented a better result due to the higher percentage of ripe fruits in the last weeks, which could be detected from the crop canopy. Differently, the GRRI (RGB camera) was positively influenced by the higher number of samples, unlike its other version (Table 5 and Figure 7).

In addition, the magnitude of the CRI and GRRI values from the RGB camera was different than the ones derived from the RedEdge MX. This result is possibly associated with

the sensitivity of the CMOs that can be variable among different wavelengths (LULE et al., 2000). For the RGB camera, the same settings of ISO and shutter aperture are used since its single sensor is used to register the information from RGB bands. Conversely, the RedEdge MX does not present this limitation since there is one CMOs for each band, whose settings are individually adjusted according to the band's specifications. Regardless, both VIs obtained with the RGB camera presented satisfactory results, especially the CRI. In this sense, the RGB camera use can be a feasible alternative to monitor the coffee ripeness, especially in small farms due to its lower cost compared to the RedEdge MX.

Overall, our findings corroborate those stated by Herwitz et al. (2004) and Johnson et al. (2004), in which the use of RS in the coffee crop for fruit ripeness monitoring is still challenging due to the plant architecture and the high canopy volume presented by most cultivars. In addition, another characteristic that plays a significant role on the performance of RS-based methodologies in the coffee crop is the crop yield. Due to the biennial effect, the crop yield alternates between low and high yields every year (BERNARDES et al., 2012). This characteristic has a direct influence on the number of fruits displayed on the crop canopy, which end up affecting the performance of the VIs. Despite that, the study demonstrated that the time-consuming manual fruit counts made on a few plants can be replaced by remote sensing approaches. Furthermore, these results fill a gap in the literature of remote sensing studies related to the coffee fruit ripeness monitoring, which is a key factor for defining the beverage quality. Lastly, a recommendation for future studies would be the use of the CRI and other variables (*e.g.*, solar radiation, Brix degree, canopy temperature, etc.) for prediction of fruit ripeness and beverage quality using machine learning algorithms.

## 2.5 Conclusion

In this study, a simple and effective vegetation index (VI) was proposed for coffee ripeness estimation using aerial imagery. The Coffee ripeness index (CRI) was developed, combining reflectance from the red band and from a ground-based red target. The effectiveness of the CRI was compared in different analysis with traditional VIs such as the MCARI1, NDVI, NDRE, GNDVI, and the GRRI in five coffee fields under distinct cultivation characteristics.

The CRI showed a higher sensitivity to discriminate coffee plants ready for harvest from not-ready for harvest in all coffee fields. However, the field characteristics such as plant density, canopy volume and especially, the crop yield played a key role in the VIs performance.



Therefore, the methodology based on VIs, especially the CRI, can yield better results on coffee fields with higher fruit display on the canopy exterior.

Regarding the two cameras evaluated, both of them presented satisfactory results. However, the RGB camera use can be a feasible alternative to monitor the coffee ripeness, especially in small farms due to its lower cost compared to the RedEdge MX. Finally, the study demonstrated that the time-consuming fieldwork can be replaced by the methodology based on VIs.

## 2.6 References

ALVARES, C. A. et al. Köppen's climate classification map for Brazil. **Meteorologische Zeitschrift**, v. 22, p. 711–728, 2013.

APARECIDO, L. E. O. et al. Maturation periods for *Coffea arabica* cultivars and their implications for yield and quality in Brazil. **Journal of the Science of Food and Agriculture**, v. 98, n. 10, p. 3880-3891. 2017.

ASHAPURE, A. et al. A novel framework to detect conventional tillage and no-tillage cropping system effect on cotton growth and development using multi-temporal UAS data. **ISPRS Journal of Photogrammetry and Remote Sensing**, v. 152, 49–64, 2019.

AYALA-SILVA, T.; BEYL, C.A. Changes in spectral reflectance of wheat leaves in response to specific macronutrient deficiency. **Advances in Space Research**, v. 35, n. 2, p. 305–317, 2005.

BALOLOY, A. B. et al. Development and application of a new mangrove vegetation index (MVI) for rapid and accurate mangrove mapping. **ISPRS Journal of Photogrammetry and Remote Sensing**, v. 166, p. 95–117, 2020.

BERNARDES, T. et al. Monitoring biennial bearing effect on coffee yield using MODIS remote sensing imagery. **Remote Sensing**, v. 4, p. 2492–2509, 2012.

BRENNER, C. et al. Estimation of evapotranspiration of temperate grassland based on high-resolution thermal and visible range imagery from unmanned aerial systems. **International Journal of Remote Sensing**, v. 39, p. 5141–5174, 2018.

CARNEIRO, F. M. et al. Comparison between vegetation indices for detecting spatial and temporal variabilities in soybean crop using canopy sensors. **Precision Agriculture**, v. 21, p. 979–1007, 2019.

- CARRIJO, G. L. A. et al. Automatic detection of fruits in coffee crops from aerial images. *In: Proceedings of the 2017 Latin American Robotics Symposium (LARS) and 2017 Brazilian Symposium on Robotics (SBR)*, Curitiba, Brazil. **Annals [...]**, 2017, p. 1-6. Available online: <<https://ieeexplore.ieee.org/xpl/conhome/8168942/proceeding>>. Accessed on: 10/05/2020.
- CASTRO, R. D.; MARRACCINI, P. Cytology, biochemistry and molecular changes during coffee fruit development. **Brazilian Journal of Plant Physiology**, v. 18, n. 1, p. 175–199, 2006.
- COLTRI, P. P. et al. Coffee crop's biomass and carbon stock estimation with usage of high-resolution satellites images. **IEEE Journal of Selected Topics in Applied Earth Observations and Remote Sensing**, v. 6, p. 1786–1795, 2013.
- CUNHA, J. P. A. R.; NETO, M. A. S.; HURTADO, S. M. C. Estimating vegetation volume of coffee crops using images from unmanned aerial vehicles. **Engenharia Agrícola**, v. 39, p. 41–47, 2019.
- DAMATTA, F. M. et al. Ecophysiology of coffee growth and production. **Brazilian Journal of Plant Physiology**, v. 19, p. 485–510, 2007.
- DEL POZO, S. et al. Vicarious Radiometric Calibration of a Multispectral Camera on Board an Unmanned Aerial System. **Remote Sensing**, v. 6, p. 1918–1937, 2014.
- FAGAN, E. B. et al. Efeito do tempo de formação do grão de café (*Coffea sp.*) na qualidade da bebida. **Bioscience Journal**, v. 27, n. 5, p. 729–738. 2011.
- FITZGERALD, G. et al. Spectral and thermal sensing for nitrogen and water status in rainfed and irrigated wheat environments. **Precision Agriculture**, v. 7, p. 233–248, 2006.
- FURFARO, R. et al. Neural network algorithm for coffee ripeness evaluation using airborne images. **Applied Engineering in Agriculture**, v. 23, p. 79–387, 2007.
- GITELSON, A. A.; KAUFMAN, Y. J.; MERZLYAK, M. N. Use of a green channel in remote sensing of global vegetation from EOS-MODIS. **Remote Sensing of Environment**, v. 58, p. 289–298, 1996.
- HABOUDANE, D. et al. Hyperspectral vegetation indices and novel algorithms for predicting green LAI of crop canopies: Modeling and validation in the context of precision agriculture. **Remote Sensing of Environment**, v. 90, p. 337–352, 2004.

HE, J. et al. Estimating leaf area index with a new vegetation index considering the influence of rice panicles. **Remote Sensing**, v. 11, p. 1809-1833, 2019.

HEDE, A. N. H. et al. A new vegetation index for detecting vegetation anomalies due to mineral deposits with application to a tropical forest area. **Remote Sensing of Environment**, v. 171, p. 83–97, 2015.

HERWITZ, S. et al. Imaging from an unmanned aerial vehicle: Agricultural surveillance and decision support. **Computers and Electronics in Agriculture**, v. 44, p. 49–61, 2004.

HUANG, S. et al. Satellite Remote Sensing-Based In-Season Diagnosis of Rice Nitrogen Status in Northeast China. **Remote Sensing**, v. 7, p. 10646–10667, 2015.

HUETE, A. A soil-adjusted vegetation index (SAVI). **Remote Sensing of Environment**, v. 25, p. 295–309, 1988.

HUNT, E. R. et al. Remote sensing of crop leaf area index using unmanned airborne vehicles. *In: Proceedings of the Pecora*, 2008, Denver, USA. **Annals [...]**, 2008, v. 17. p. 18-20.

ICO. International Coffee Organization. **Historical data on the global coffee trade**; International Coffee Organization (ICO), London, England: 2020. Available online: <[https://www.ico.org/new\\_historical.asp](https://www.ico.org/new_historical.asp)>. Accessed on 10/09/2020.

IQBAL, F.; LUCIEER, A.; BARRY, K. Simplified radiometric calibration for UAS-mounted multispectral sensor. **European Journal of Remote Sensing**, v. 51, p. 301–313, 2018.

JAVAN, F. D. et al. UAV-based multispectral imagery for fast Citrus Greening detection. **Journal of Plant Diseases and Protection**, v. 126, p. 307–318, 2019.

JOHNSON, L. F. et al. Feasibility of monitoring coffee field ripeness with airborne multispectral imagery. **Applied Engineering in Agriculture**, v. 20, p. 845–849, 2004.

KOIDE, K.; KOIKE, K. Applying vegetation indices to detect high water table zones in humid warm-temperate regions using satellite remote sensing. **International Journal of Applied Earth Observation and Geoinformation**, v. 19, p. 88–103, 2012.

KROSS, A. et al. Assessment of RapidEye vegetation indices for estimation of leaf area index and biomass in corn and soybean crops. **International Journal of Applied Earth Observation and Geoinformation**, v. 34, p. 235–248, 2015.

LAVIOLA, B. G. et al. Macronutrient accumulation in coffee fruits at Brazilian Zona da Mata conditions. **Journal of Plant Nutrition**, v. 32, p. 980–995, 2009.

- LIN, S. et al. Evaluating the effectiveness of using vegetation indices based on red-edge reflectance from Sentinel-2 to estimate gross primary productivity. **Remote Sensing**, v. 11, p. 1303-1328, 2019.
- LULE, T. et al. Sensitivity of CMOS based imagers and scaling perspectives. **IEEE Transactions on Electron Devices**, v. 47, p. 2110–2122, 2000.
- MAIMAITIJIANG, M. et al. Vegetation index weighted canopy volume model (CVMVI) for soybean biomass estimation from unmanned aerial system-based RGB imagery. **ISPRS Journal of Photogrammetry and Remote Sensing**, v. 151, p. 27–41, 2019.
- MAMAGHANI, B.; SALVAGGIO, C. Multispectral sensor calibration and characterization for sUAS remote sensing. **Sensors**, v. 19, p. 4453-4482, 2019.
- MARTINEZ, H. E. P. et al. Zinc supplementation, production and quality of coffee beans. **Revista Ceres**, v. 60, n. 2, p. 293–299, 2013.
- MIRANDA, J. D. R. et al. Detection of coffee berry necrosis by digital image processing of Landsat 8 OLI satellite imagery. **International Journal of Applied Earth Observation and Geoinformation**, v. 85, p. 1-10, 2020.
- MOREIRA, M. A.; ADAMI, M.; THEODOR, F. Análise espectral e temporal da cultura do café em imagens Landsat Spectral and temporal behavior analysis of coffee crop in Landsat images. **Pesquisa Agropecuária Brasileira**, v. 39, n. 3, p. 223–231, 2004.
- NOGUEIRA, S. M. C.; MOREIRA, M. A.; VOLPATO, M. M. L. Relationship between coffee crop productivity and vegetation indexes derived from OLI/Landsat-8 sensor data with and without topographic correction. **Engenharia Agrícola**, v. 38, n. 3, p. 387–394, 2018.
- PARREIRAS, T. C. et al. Using unmanned aerial vehicle and machine learning algorithm to monitor leaf nitrogen in coffee. **Coffee Science**, v. 15, p. 1–9, 2020.
- QGIS Development Team. **QGIS Geographic Information System**. Open Source Geospatial. Foundation Project. 2016. Available online: <<http://qgis.osgeo.org>>.
- R CORE TEAM. **R: A language and environment for statistical computing**. R Foundation for Statistical Computing, Vienna, Austria. 2019. Available online: <<https://www.R-project.org/>>.
- RAMIREZ, G. M.; ZULLO, J. JR. Estimation of biophysical parameters of coffee fields based on high-resolution satellite images. **Engenharia Agrícola**, v. 30, n. 3, p. 468–479, 2010.

- REN, Y. et al. Novel vegetation indices for cotton boll opening status estimation using Sentinel-2 data. **Remote Sensing**, v. 12, p. 1712-1729, 2020.
- ROSAS, J. T. F. et al. A. Low-cost system for radiometric calibration of UAV-based multispectral imagery. **Journal of Spatial Science**, v. 1, p. 1–15, 2020.
- ROUSE, J. W. et al. Monitoring vegetation systems in the Great Plains with ERTS (Earth Resources Technology Satellite). *In: III Earth Resources Technology Satellite-1 Symposium; 1973, NASA. Washington, DC, USA. Annals [...]*, 1973, p. 301-317.
- SANTOS, L. M. et al. Biophysical parameters of coffee crop estimated by UAV RGB images. **Precision Agriculture**, v. 21, p. 1227–1241, 2020a.
- SANTOS, L. M. et al. Coffee crop coefficient prediction as a function of biophysical variables identified from RGB UAS images. **Agronomy Research**, v. 18, p. 1463–1471, 2020b.
- SILVA, S. D. A. et al. Coffee quality and its relationship with Brix degree and colorimetric information of coffee cherries. **Precision Agriculture**, v. 15, p. 543–554, 2014.
- SILVA, S. D. A.; DE SOUZA LIMA, J. S.; ALVES, A. I. Spatial study of grain yield and percentage of bark of two varieties of *Coffea arabica* L. to the production of quality coffee. **Bioscience Journal**, v. 26, n. 4, p. 558–565. 2010.
- SONOBE, R.; WANG, Q. Hyperspectral indices for quantifying leaf chlorophyll concentrations performed differently with different leaf types in deciduous forests. **Ecological Informatics**, v. 37, p. 1–9, 2017.
- TSAI, D. M.; CHEN, W. L. Coffee plantation area recognition in satellite images using Fourier transform. **Computers and electronics in agriculture**, v. 135, p. 115-127, 2017.
- USDA. United States Department of Agriculture. **Coffee: World Markets and Trade** (Issue June, 2020). Available online: <<http://apps.fas.usda.gov/psdonline/circulars/coffee.pdf>>. Accessed on 08/09/2020.
- WANG, C.; MYINT, S. W. A Simplified Empirical Line Method of Radiometric Calibration for Small Unmanned Aircraft Systems-Based Remote Sensing. **IEEE Journal of Selected Topics in Applied Earth Observations and Remote Sensing**, v. 8, p. 1876–1885, 2015.
- WIJESINGHA, J. et al. Predicting forage quality of grasslands using UAV-borne imaging spectroscopy. **Remote Sensing**, v. 12, p. 126-149, 2020.

ZARCO-TEJADA, P. J. et al. Tree height quantification using very high-resolution imagery acquired from an unmanned aerial vehicle (UAV) and automatic 3D photo-reconstruction methods. **European Journal of Agronomy**, v. 55, p. 89–99, 2014.

ZARCO-TEJADA, P. J. et al. Scaling-up and model inversion methods with narrowband optical indices for chlorophyll content estimation in closed forest canopies with hyperspectral data. **IEEE Transactions on Geoscience and Remote Sensing**, v. 39, p. 1491–1507, 2001.

### 3 Digital mapping of coffee ripeness using UAV-based multispectral imagery <sup>2</sup>

#### Abstract

Timely and accurate monitoring of coffee fruit ripeness is essential for harvest planning, especially in mountainous areas where the harvest is performed manually due to the limited use of agricultural mechanization. The increase of temporal and spatial resolutions of remote sensing based on low-altitude unmanned aerial vehicles (UAV) provides a feasible way to monitor the fruit ripeness variability. Due to these facts, the objectives of this study were: (1) to predict the fruit ripeness using spectral and textural variables; and (2) to determine the best variables for developing spatio-temporal variability maps of the fruit ripeness. To do so, an experiment with six arabica coffee fields was set up. During the coffee ripeness stage in the 2018-2019 and 2020-2021 seasons, seven flights were carried out using a quadcopter equipped with a five-band multispectral camera. After that, 12 spectral and 64 textural variables composed of bands and vegetation indices were obtained. For the same time, the percentage of unripe fruits (was used to evaluate the fruit ripeness) was determined using an irregular grid on each field. Then, the fruit ripeness was predicted and mapped using (1) the spectral variables and (2) the combination of spectral and textural variables. Results demonstrated that the accuracy of the random forest model using the spectral and textural variables ( $R^2$ : 0.71 and RMSE:11.47%) was higher than the model based solely on spectral variables ( $R^2$ : 0.67 and RMSE: 12.09%). Finally, this study demonstrated the feasibility of using spectral and textural variables derived from UAV imagery for mapping and monitoring the spatiotemporal changes in the fruit ripeness at a fine scale.

**Keywords:** Fruit ripeness; drone; digital agriculture; remote sensing; random forest

#### 3.1 Introduction

Coffee is one of the three major beverages consumed worldwide whose economic value is defined according to its quality, which in turn is affected by many characteristics (SILVA et al., 2014, 2017). One of the most important characteristics is the fruit ripeness at harvest. Ripen fruits provides a better coffee quality, while unripen and overripen fruits reduce its quality (MARTINEZ et al., 2013; SILVA et al., 2014). Because of that, the fruit ripeness is a key

---

<sup>2</sup> This chapter refers to the original version of the manuscript “Digital mapping of coffee ripeness using UAV-based multispectral imagery” submitted to the journal *Computers and Electronics in Agriculture*.

parameter for defining the moment of starting the harvest, especially for farmers that want to reach higher beverage quality.

Currently, the fruit ripeness monitoring is carried out periodically through repeated manual counts of ripe fruits made on a few plants within each field (NOGUEIRA MARTINS et al., 2021). To avoid the traditional field monitoring, which is time-consuming, labor-intensive, and not fully representative, a few studies were conducted throughout the years using vegetation indices (VI) derived from unmanned aerial vehicle (UAV) imagery (HERWITZ et al., 2004; JOHNSON et al., 2004; NOGUEIRA MARTINS et al., 2021; ROSAS et al., 2021).

The studies conducted by Herwitz et al. (2004) and Johnson et al. (2004) were pioneers in using aerial remote sensing for monitoring the coffee ripeness. By using UAV images, these authors found that the spectral response of the crop canopy was highly correlated ( $R^2$ : 0.81) with the fruit ripeness, especially in fields with high fruit display on the canopy. However, despite finding promising results, these studies were conducted determining the mean value of fruit ripeness of each field, which does not consider the spatial variability of the fruit ripeness. In addition, since arabica coffee blossoms do not appear and develop uniformly throughout the field, the spatial and temporal variability of fruit ripeness among trees as well as within a single tree is practically inevitable (DAMATTA et al., 2007).

To overcome the limitation of not analyzing the spatial variability of fruit ripeness, Rosas et al. (2021) used different VIs derived from a low-cost multispectral camera onboard a UAV for monitoring the fruit ripeness at the plant level. Results showed that the VIs were able to discriminate plants with unripe fruits from those with ripe fruits in most fields. However, their performance was mostly affected by the canopy volume and crop yield. Similarly, Nogueira Martins et al. (2021) used spectral information obtained from different cameras and developed a novel VI for monitoring the fruit ripeness. The coffee ripeness index (CRI) was validated under different analysis and presented superior performance over different VIs. However, there is still a gap in the literature of strategies for mapping the fruit ripeness spatial variability remotely, as well as to aid in the definition of the ideal harvest time.

Recent published works have concentrated only on the spectral information of UAV imagery, but the spatial information in the form of texture remains unexplored. Spectral variables represent the average tonal variations in various bands, whereas textural variables contain information about the spatial distribution of tonal variations of pixels within a defined area of an image (HARALICK et al., 1973; WANG et al., 2021; WOOD et al., 2012; ZHOU et al., 2021). In contrast, the use of textural variables derived from UAV images can enhance



the detection of finer vegetation structural features (DUBE; MUTANGA, 2015; SCHUMACHER et al., 2016). Therefore, the use of textural variables has potential for improving the fruit ripeness prediction and mapping.

Previous research works that compared the use of either spectral or textural variables alone to the combination of both variables have shown that the latter resulted in better performance for crop yield prediction (MAIMAITIJIANG et al., 2020; WANG et al., 2021), nitrogen status estimation (FU et al., 2020), and crop biomass and leaf area index predictions (DOS REIS et al., 2020; FU et al., 2021; LI et al., 2019; ZHENG et al., 2019). Thus, since UAV images present spatial resolution at centimeter-level and comprise rich spatial information of observed objects, the use of spectral information combined with textural information for improving fruit ripeness prediction and mapping becomes possible.

Based on that, it has been hypothesized that the use of spectral bands and VIs combined with textural variables derived from UAV imagery could potentially improve the performance of prediction models for coffee fruit ripeness mapping. Therefore, the objectives of this study were: (1) to predict the fruit ripeness using spectral and textural variables; and (2) to determine the best variables for developing spatio-temporal variability maps of the fruit ripeness.

## **3.2 Material and Methods**

### *3.2.1 Study site*

The study site (42°55'11.906" W; 20°49'26.158" S and 42°55'1.076" W; 20°49'39.997" S) is located in the municipality of Paula Candido, Minas Gerais State, Brazil (Figure 1). According to the Köppen-Geiger Climate Classification, the climate of the region is Cwa (humid subtropical), with a rainy season in the summer and dry winter (ALVARES et al., 2013).

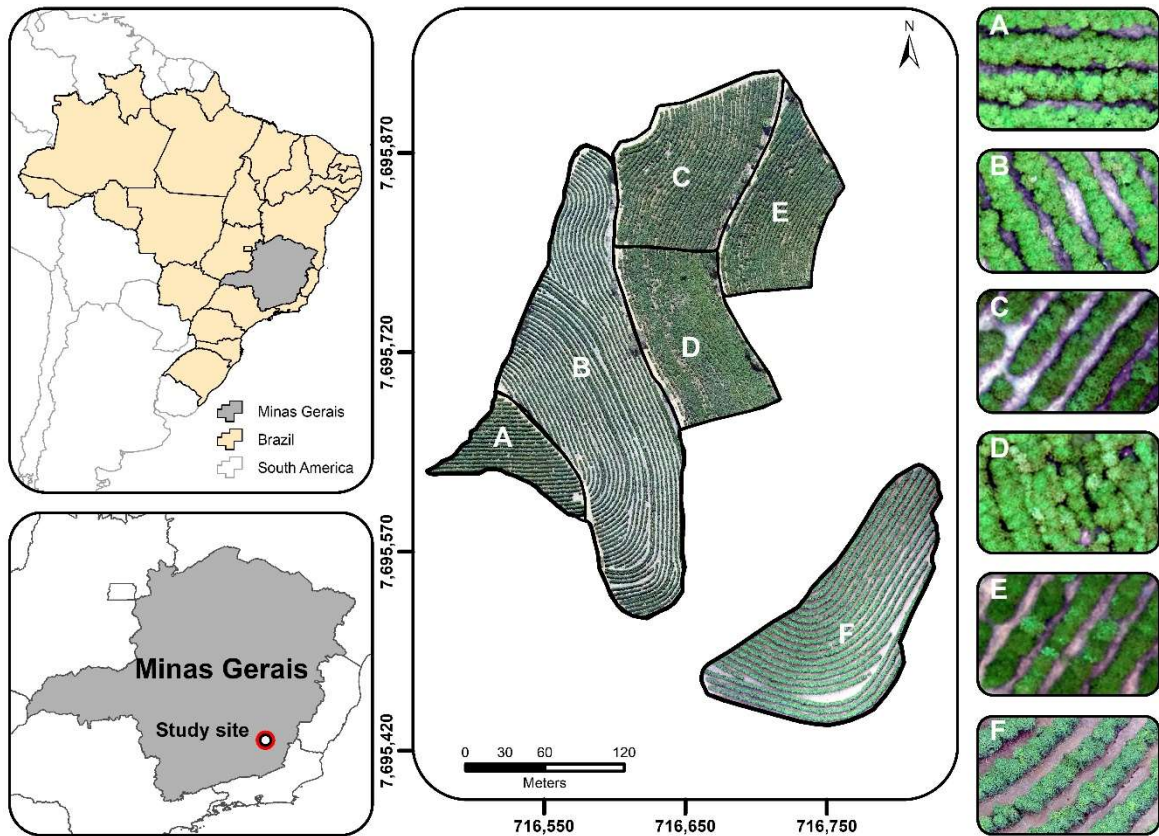


**Figure 1.** Location of the study site in the *Zona da Mata* region of Minas Gerais State, Southeastern Brazil. The rectangular boxes on the right side of the figure present an aerial view of each coffee field.

This study was conducted in six fields of arabica coffee (*Coffea arabica* L.) with a total area of 5.95 ha. These fields were represented by the following cultivars: Red Catuai (Fields A, B, and F), MGH 4191 (Field C), Red Bourbon (Field D), and Icatu (Field E). In addition, all fields presented distinct characteristics for the cropped area, fruit color, canopy volume, plant density, and yield (Figure 2).

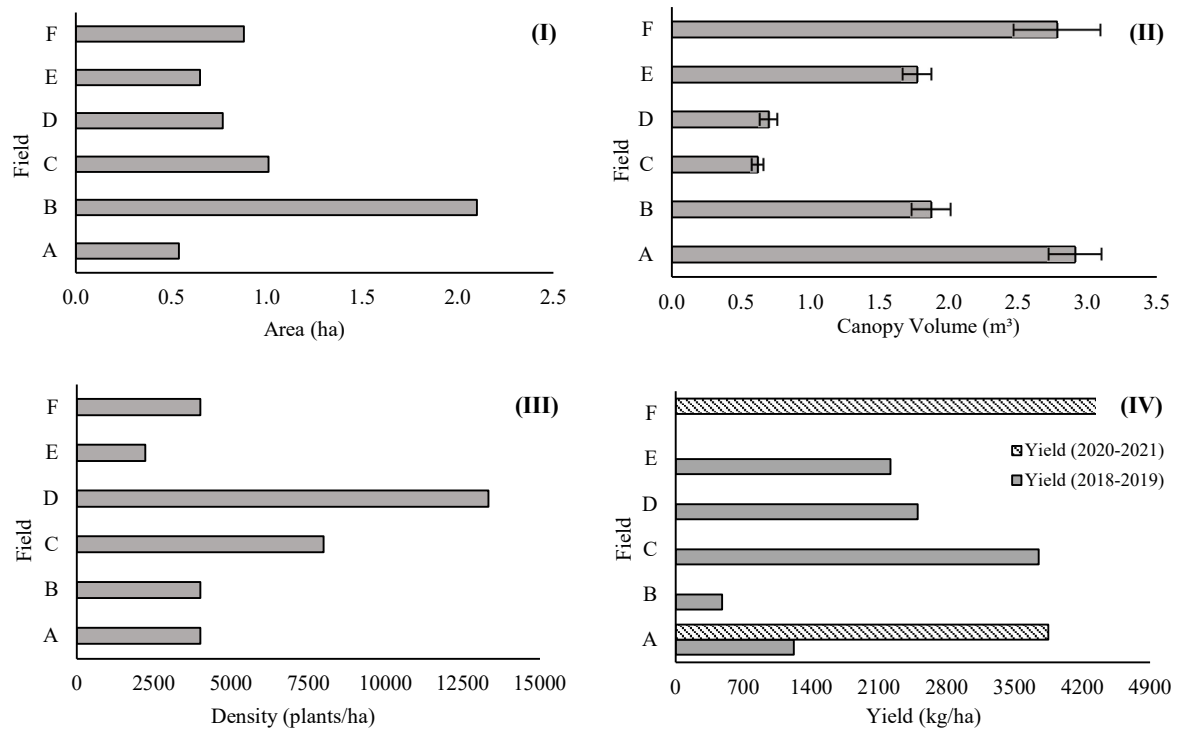


**Figure 2.** Cultivation area (I), canopy volume (II), density of plants (III), and yield (IV) of the coffee fields evaluated in this study. For fields A, B, D, and E the coffee fruits were red when ripe; conversely, in field C they were yellow when ripe. The crop yield refers to the 2018-2019 (Fields A, B, C, D, and E), and 2020-2021 seasons (Fields A and F).

### 3.2.2 UAV imagery acquisition and processing

Imagery acquisition in the study site was performed using a quadcopter (model: Matrice 100, DJI Innovations, Shenzhen, China) equipped with a multispectral camera (model: RedEdge MX, MicaSense, Seattle, USA). The RedEdge MX contains five CMOS (complementary metal oxide semiconductor) sensors, which captures five spectral bands in the following wavelengths: (1) Blue (455–495 nm); (2) Green (540–580 nm); (3) Red (658–678 nm); (4) Rededge (RE) (707–727 nm); and (5) Near-infrared (NIR) (800–880 nm) (DADRASJAVAN et al., 2019).

The UAV flights were conducted between 11:00 and 13:00 h local time under clear-sky conditions on seven dates within the 2018-2019 and 2020-2021 seasons (Table 1). For that, a flight plan previously defined in the DroneDeploy software (DroneDeploy Inc., San Francisco, CA, USA) was used. All flights were carried out at  $9.3 \text{ m s}^{-1}$  speed at 60 meters above ground level with 80% front overlap and 75% side overlap between images. In addition, before and after each flight, images of the reflectance calibration target provided by the

manufacturer were taken at 1.00 m height to perform the radiometric calibration in postprocessing.

**Table 1.** Unmanned Aerial Vehicles (UAV) imagery collection timeline and flight parameters.

Season	Field	Date	Overlap (%) <sup>1</sup>	AGL (m) <sup>2</sup>	GSD (m) <sup>3</sup>
2018-2019	A, B, C, D, and E	13/05/2019			
	A, B, C, D, and E	27/05/2019			
	A	04/05/2021			
	F	10/05/2021	80 / 75	60	0.05
2020-2021	A	18/05/2021			
	A and F	24/05/2021			
	F	31/05/2021			

<sup>1</sup>Lateral and longitudinal overlap; <sup>2</sup>AGL, Above ground level; and <sup>3</sup>GSD, Ground sampling distance.

After the flights, all images were stored in RAW format and after processing, they were converted to the Tagged Image File Format (TIFF). All images were processed using the Agisoft™ MetaShape software, version 1.5.3 (Agisoft LLC, St. Petersburg, Russia) following the same procedures from the image alignment to the creation, and georeferencing of the orthomosaics as detailed in Nogueira Martins et al. (2021). The georeferencing of the orthomosaics was conducted in the QGIS software, version 3.2 (QGIS Development Team, 2016) using the information from 20 ground control points (GCP), which were placed on the area before the flights. These GCPs were georeferenced using a topographic GNSS (Global Navigation Satellite System) receiver, model Trimble ProXT (Trimble Inc., Sunnyvale, CA, USA).

### 3.2.3 Spectral and Textural data extraction

In this study, the spectral bands Red, Green, Blue, RE, and NIR and the following VIs: Coffee Ripeness Index (CRI); Green-red Ratio Ripeness Index (GRRI); Modified Chlorophyll Absorption in Reflectance Index 1 (MCARI1); Plant Senescence Reflectance Index (PSRI); Normalized Difference RedEdge Index (NDRE); Normalized Green-red Difference Index (NGRDI); and Excess of Red (EXR) were obtained from the UAV images (Table 2). These VIs were chosen based on their sensitivity to changes in the canopy structure and fruit ripeness as well as to changes in pigment and plant nutritional status

**Table 2.** Summary of the vegetation indices used in this study.

Vegetation Index	Equation	Reference
CRI	$(R/R_{\text{target}})100$	Nogueira Martins et al. (2021)
GRRI	$(G/R)$	Johnson et al. (2004)
MCARI1	$1.2[2.5(\text{NIR} - R) - 1.3(\text{NIR} - G)]$	Haboudane et al. (2004)
PSRI	$(R - B)/N$	Merzlyak et al. (1999)
NDRE	$(N - \text{RE})/(N + \text{RE})$	Fitzgerald et al. (2006)
NGRDI	$(G - R)/(G + R)$	Zheng et al. (2018)
EXR	$1.4R - G$	Meyer and Hindman (1998)

R, Red; G, Green; B, Blue; RE, Rededge; N, Near-infrared; and  $R_{\text{Target}}$ , Average reflectance value of the red target in the red band.

In addition to the spectral bands and VIs, the grey level co-occurrence matrix (GLCM) was used to compute textural variables. The GLCM is a matrix where the number of rows and columns is equal to the number of gray levels in the image. Basically, the GLCM interprets the spatial distribution of pairs of pixel separated by a certain distance in a given direction (LIU et al., 2019). Eight textural variables proposed by Haralick et al. (1973), including mean (MEA), variance (VAR), homogeneity (HOM), dissimilarity (DIS), contrast (CON), entropy (ENT), second moment (SM), and correlation (COR) were obtained in this study (Table 3). The texture variables were obtained using the smallest moving window size ( $3 \times 3$  pixels) with an orientation of  $45^\circ$  (1,1) due to the UAV imagery spatial resolution (0.05 m), and to the absence of significant heterogeneity between other orientations (FU et al., 2021, 2020).

**Table 3.** Summary of the texture variables used in this study.

Textural Variables	Equation	Meaning
Mean (MEA)	$\sum_{i,j=0}^{N-1} i (P_{i,j})$	Gray level average in the GLCM window.
Variance (VAR)	$\sum_{i,j=0}^{N-1} i P_{i,j} (i - MEA)^2$	Gray level variance in the GLCM window.
Homogeneity (HOM)	$\sum_{i,j=0}^{N-1} i (P_{i,j}) / (1 + (i - j))^2$	A measure of homogenous pixel values across an image.
Dissimilarity (DIS)	$\sum_{i,j=0}^{N-1} i P_{i,j}  i - j $	Similar to contrast and inversely related to homogeneity.
Contrast (CON)	$\sum_{i,j=0}^{N-1} i P_{i,j} (i - j)^2$	Measures the local variations among neighboring pixels in the GLCM matrix.
Entropy (ENT)	$\sum_{i,j=0}^{N-1} i P_{i,j} (-\ln P_{i,j})$	Represents the degree of disorder present in the image. The value of entropy is the largest when all elements of the cooccurrence matrix are the same and small when elements are unequal
Second moment (SM)	$\sum_{i,j=0}^{N-1} i (P_{i,j})^2$	A measure of homogeneity of the image.
Correlation (COR)	$\sum_{i,j=0}^{N-1} i P_{i,j} \left[ \frac{(i - MEA)(j - MEA)}{\sqrt{VAR_i VAR_j}} \right]$	Measures the joint probability occurrence of the specified pixel pairs.

Notes:  $P_{i,j} = V_{i,j} / \sum_{i,j=0}^{N-1} V_{i,j}$  GLCM, is the grey level co-occurrence matrix;  $V_{i,j}$ , is the value in the cell  $i$ ,  $j$  (row  $i$  and column  $j$ ) of the moving window; and  $N$ , is the number of rows or columns. Adapted from Haralick et al. (1973), Lu and Batistella (2005), and Wang et al. (2021).

The textural analysis resulted in eight variables for each spectral band (RGB, RE, and NIR) (Figure 3). These variables were named using the first letter of the band's name in combination with the texture metric's name (*e.g.*, Rmean, Bmean, Gmean, Nmean, and REmean). This process was performed for all texture metrics. Further, a detailed description of the eight texture measurements used in this study is presented in the literature (Soares et al., 1997). All textural variables were obtained using the R software, version 3.5.1 through the GLCM package (R CORE TEAM, 2019; ZVOLEFF, 2020).

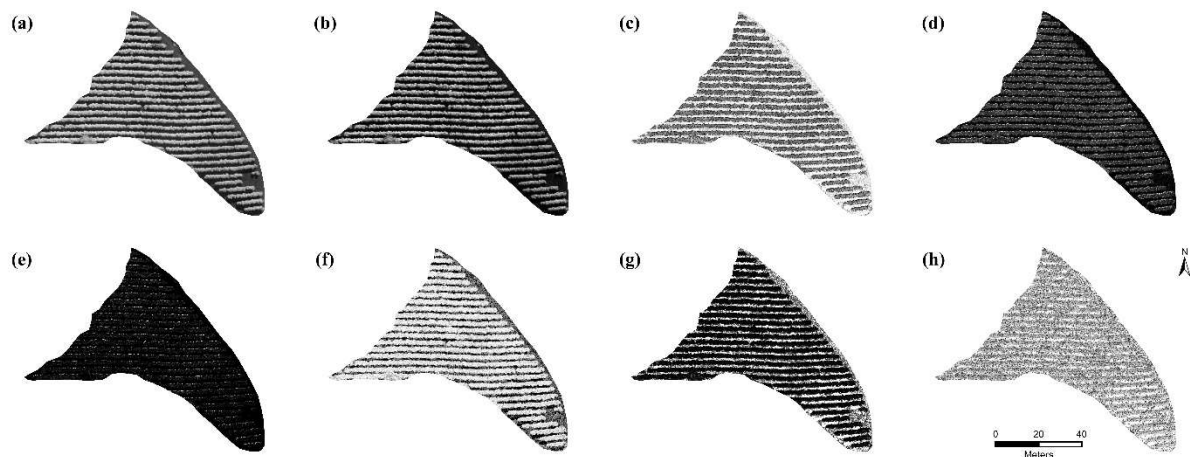


**Figure 3.** GLCM-based texture variables: mean (a), variance (b), homogeneity (c), dissimilarity (d), contrast (e), entropy (f), second moment (g), and correlation (h) obtained from the NIR band in 04/05/2021.

Since textural variables are single band parameters, they can be used to develop textural indexes. Thus, textural variables from different bands can formulate different indexes such as the spectral VIs used in this study. In this sense, the VIs NDVI (Normalized Difference Vegetation Index), GNDVI (Green Normalized Difference vegetation Index), and NDRE were used as references for calculating a normalized difference texture index (NDTI) (GITELSON et al., 1996; ROUSE et al., 1973; ZHENG et al., 2019). The NDTI was obtained using the two-band combinations from all textural variables (mean, variance, homogeneity, dissimilarity, contrast, entropy, second moment, and correlation) (Table 4). Then, all the NDTI-based VIs were named from NDTI1 to NDTI8 according to the eight texture metrics (*e.g.*, NDTI1 refers to the mean, NDTI2 refers to the variance, and so on). This process was repeated for the NDVI, GNDVI, and NDRE indices.

**Table 4.** Summary of the textural indices used in this study.

Vegetation Index	Reflectance-based Equation	Texture-based Equation
NDTI	-	$(T_{\lambda} - T_{\lambda}) / (T_{\lambda} + T_{\lambda})$
NDVI	$(R_N - R_R) / (R_N + R_R)$	$(T_N - T_R) / (T_N + T_R)$
GNDVI	$(R_N - R_G) / (R_N + R_G)$	$(T_N - T_G) / (T_N + T_G)$
NDRE	$(R_N - R_{RE}) / (R_N + R_{RE})$	$(T_N - T_{RE}) / (T_N + T_{RE})$

$R_R$ ,  $R_G$ ,  $R_N$ , and  $R_{RE}$  refer to the reflectance of the red, green, near-infrared, and reledge bands, respectively; and  $T_R$ ,  $T_G$ ,  $T_N$ , and  $T_{RE}$  refer to the texture variables derived from the red, green, near-infrared, and reledge spectral bands, respectively.

Finally, from the coordinates of the sampling grid, polygonal masks (region of interest) for each sampling point were created in the QGIS software. The polygons covered three plants in a row that were used to represent each point. Then, the average values of the 76 predictor variables (5 spectral bands, 7 vegetation indices, 40 texture bands, and 24 texture indices) within the polygons were extracted using the zonal statistics tool. The dataset obtained from the images was arranged in an X matrix (predictors) and the fruit ripeness (percentage of unripe fruits) measured on the field was arranged in the Y vector (response variable).

#### 3.2.4 Field data collection

Coffee fruit ripeness was measured manually on seven dates during the 2018-2019 crop season (May 13<sup>th</sup> and May 27<sup>th</sup>, 2019) for fields A, B, C, D, and E and in the 2020-2021 season for fields A (May 05<sup>th</sup>, 19<sup>th</sup>, and 25<sup>th</sup>, 2021), and F (May 11<sup>th</sup>, and 25<sup>th</sup>, and June 01<sup>st</sup>, 2021). For that, an irregular sampling grid with 20 sampling points per hectare was defined on each date for fields A, C, D, E, and F (Figure 4). For field B, only 10 points per hectare were collected due to its lower fruit load. The sampling points were represented by three plants located side by side in the same cultivation row. Then, four plagiotropic branches, one per plant quadrant were randomly chosen in the middle third of each plant. Finally, the average value of unripe fruits and the total of fruits were determined and used to represent each sampling point. From now on, the percentage of unripe fruits will be referred to as fruit ripeness.



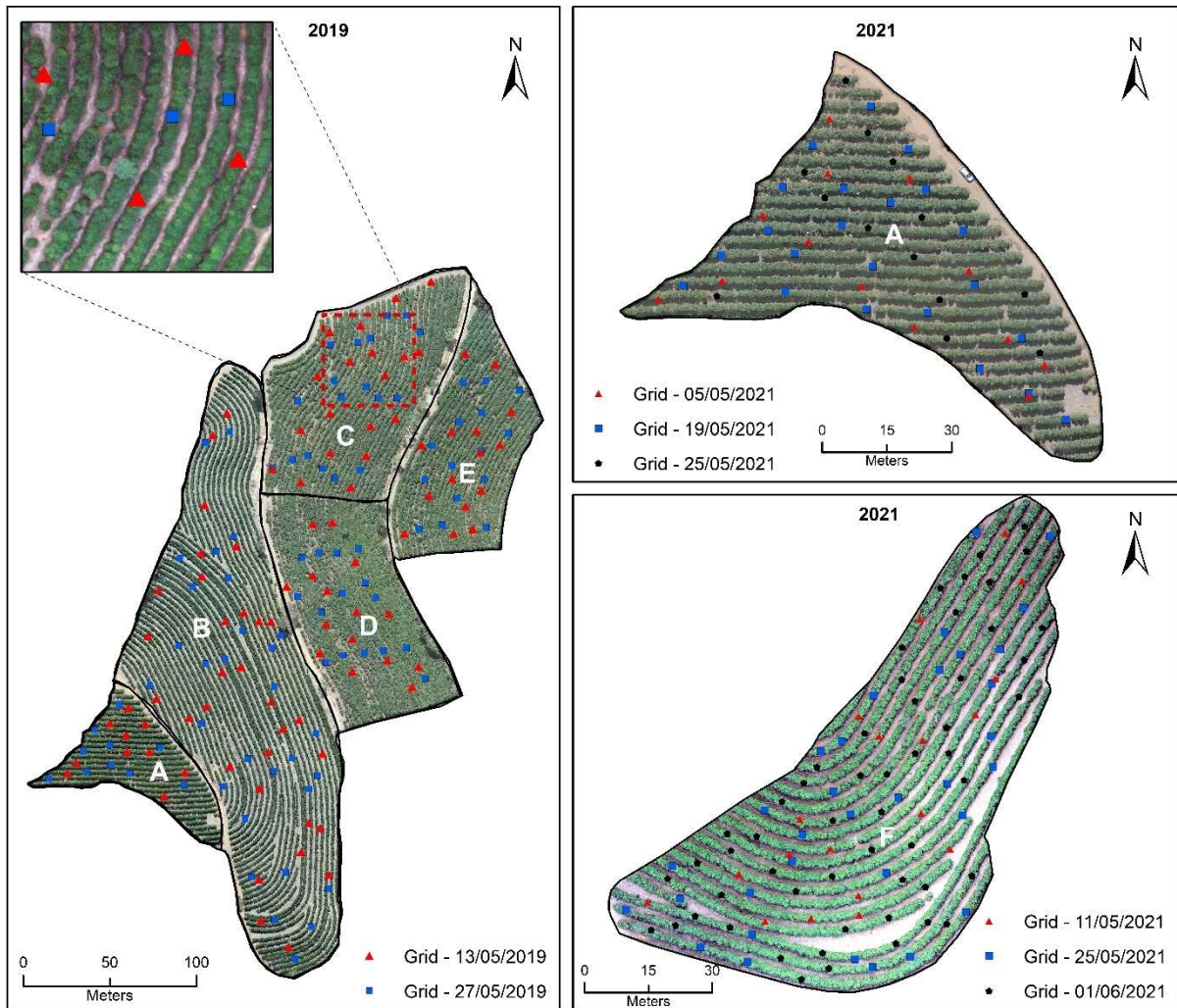


**Figure 4.** Spatial distribution of the sampling points used for field measurements of the coffee ripeness

### 3.2.5 Data modelling

To develop and validate the predictive models, the two-year experimental data were randomly split into training ( $n = 227$ , 70%) and testing ( $n = 96$ , 30%) datasets. The training dataset was used for preprocessing of data, selection of optimal variables, and optimization of hyperparameters, while the testing dataset was used to test the fruit ripeness prediction capability of the model. The random forest (RF) algorithm was used to develop the prediction models using the ‘*randomforest*’ package through the R software (BREIMAN, 2001; LIAW; WIENER, 2002).

Furthermore, to evaluate the potential influence of the texture variables to predict the fruit ripeness, two scenarios including as predictors only the spectral variables (bands and VIs) (1); and the combination of spectral and textural variables (2) were evaluated. Prior to training the RF models, the recursive feature elimination (RFE) method was used for variable selection,

removing the variables of minor importance based on the performance of the k-fold cross-validation (5 folds) with 10 repeated experiments. Then, a Pearson correlation analysis was carried out to assess the association of the selected variables with the fruit ripeness.

Next, the hyperparameters *mtry* (number of variables randomly sampled as candidates at each split) and *ntree* (number of trees) from both models were fine-tuned using the grid search method, and selected according to the accuracy estimation in the training dataset. These analyses were performed using the '*caret*' package (KUHN, 2008). In addition, to analyze the relative importance of the predictors in the RF models, the predictors were ranked based on the increase of the mean-square-error (IncMSE) when a variable was randomly permuted (BREIMAN, 2001). The performance of the RF models was evaluated using the coefficient of determination ( $R^2$ ), and the root-mean-square-error (RMSE) for the validation dataset. All modelling analyses and evaluations were performed using R the software. The flow chart of data processing and statistical analyses for prediction and mapping the fruit ripeness is presented in Figure 5.

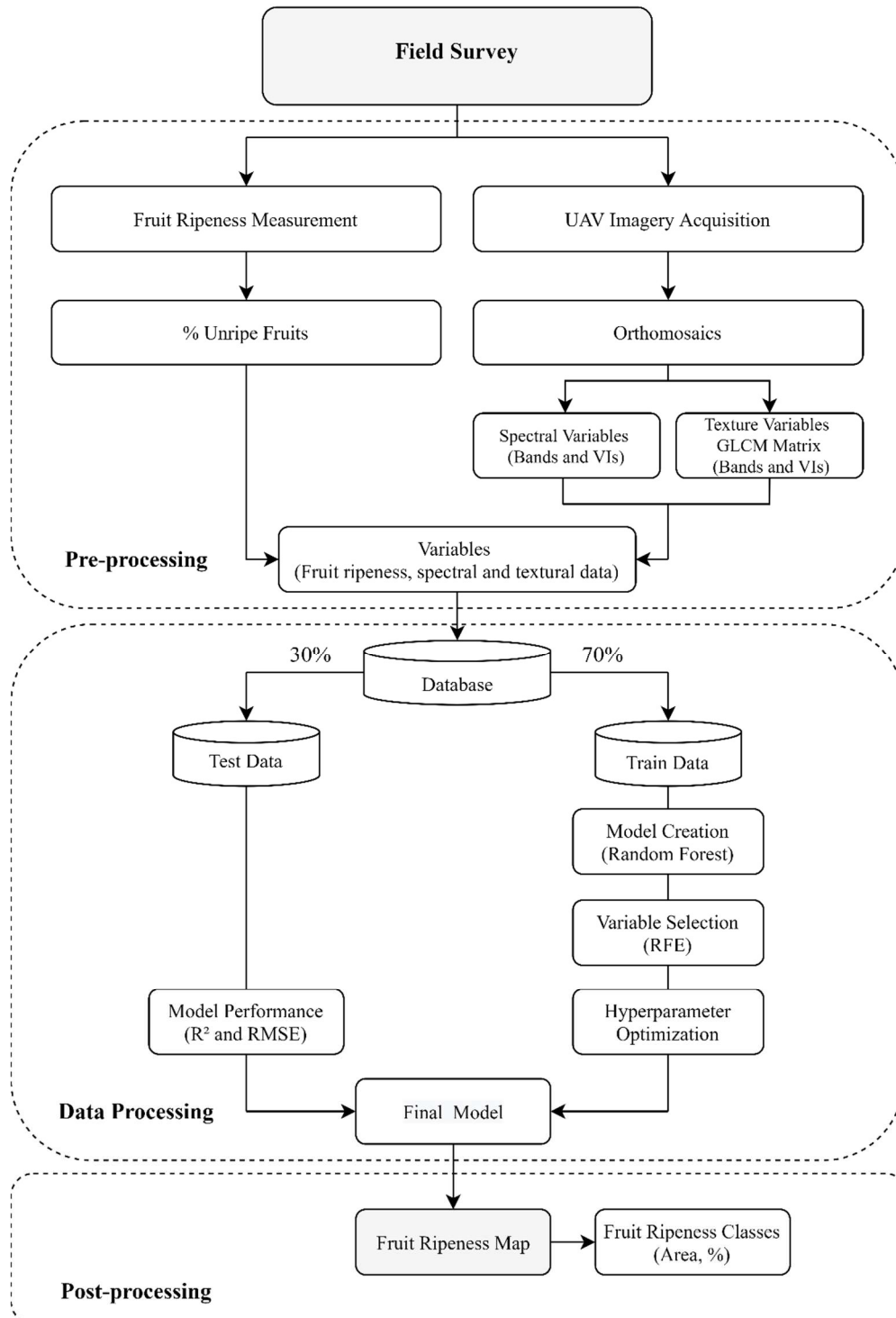


**Figure 5.** Flowchart of the fruit ripeness prediction and mapping.

After testing the RF models, the whole imagery dataset, including the spectral and textural variables, was used as input for mapping the spatial distribution of the fruit ripeness. This process was performed using the ‘raster’ package (HIJMANS et al., 2012) by combining the predictor variables (raster) into a single multi-layered (.tif) file, which was then used as input to predict each pixel through the RF models. Then, the fruit ripeness maps were arranged

in a layout with different classes, whose area (m<sup>2</sup> and %) were later obtained to assess the temporal evolution of the fruit ripeness.

### 3.3 Results

#### 3.3.1 Relationships between spectral and texture variables and the fruit ripeness

Among the 12 spectral (bands and VIs) and 64 textural variables (bands and textural indices) created for developing the prediction models, the variable selection using the RFE method resulted in 10 and 19 variables, respectively for scenarios 1 (only spectral variables) and 2 (spectral and textural variables). Then, a Pearson correlation analysis between the selected variables with the fruit ripeness was performed. Significant correlations ( $p < 0.05$ ) were found between the majority of the selected variables (Figure 6). Overall, the highest correlation ( $r$ ) values were presented by the spectral variables, which ranged from -0.7 (CRI) to 0.2 (EXR). Conversely, for the textural variables, when significant, the  $r$  values varied from -0.22 (Nvariance) to -0.12 (NDVI1).

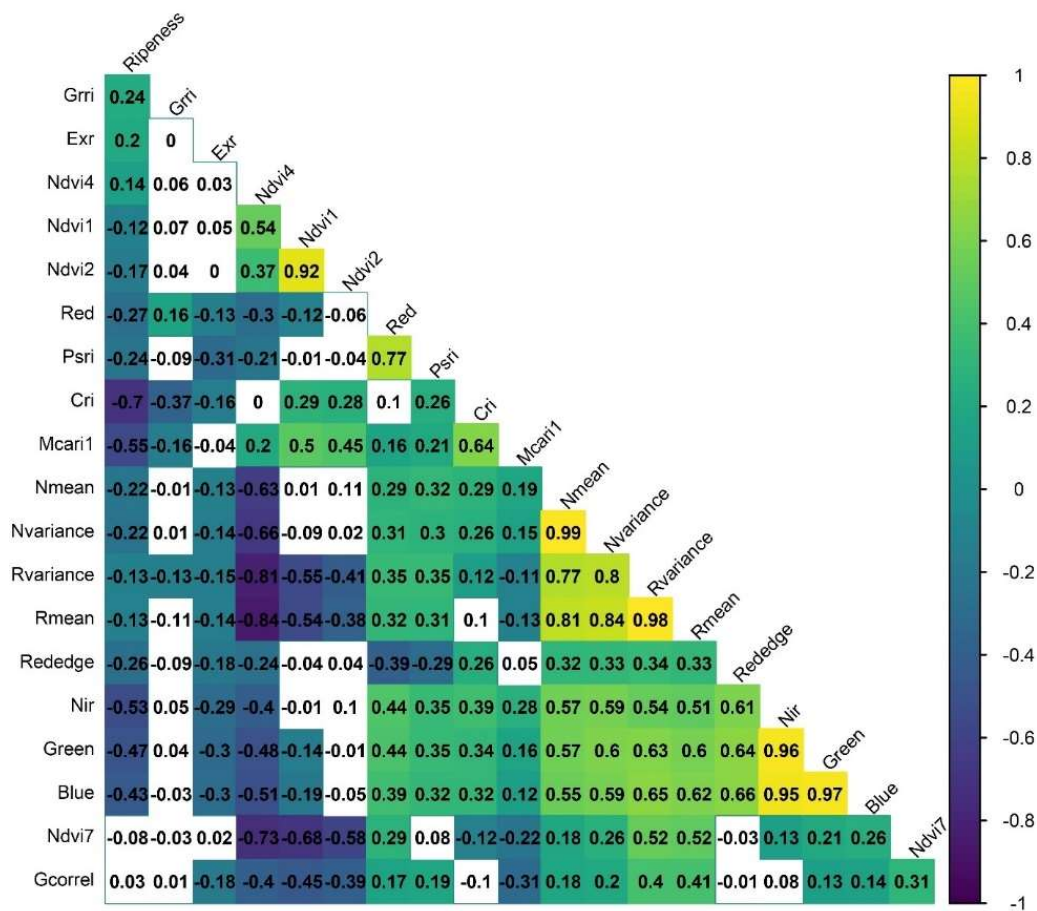


**Figure 6.** Pearson's correlation matrix between the fruit ripeness and the selected spectral and textural variables. Colored correlations are significant by test  $t$  ( $p < 0.05$ ).

### 3.3.2 Prediction of fruit ripeness with spectral and textural variables

The RF model (ntree: 200; mtry: 4) based solely on the selected spectral variables (spectral bands and VIs) demonstrated moderated accuracy in the fruit ripeness prediction; however, lower than the second model (ntree: 850; mtry: 10), which used as predictors the combination of spectral and textural variables (Figure 7). Together these variables improved the accuracy of the RF model, in which the  $R^2$  value for the test dataset increased 5.97%, while the RMSE decreased 5.62% when compared to the RF model developed with the spectral variables.

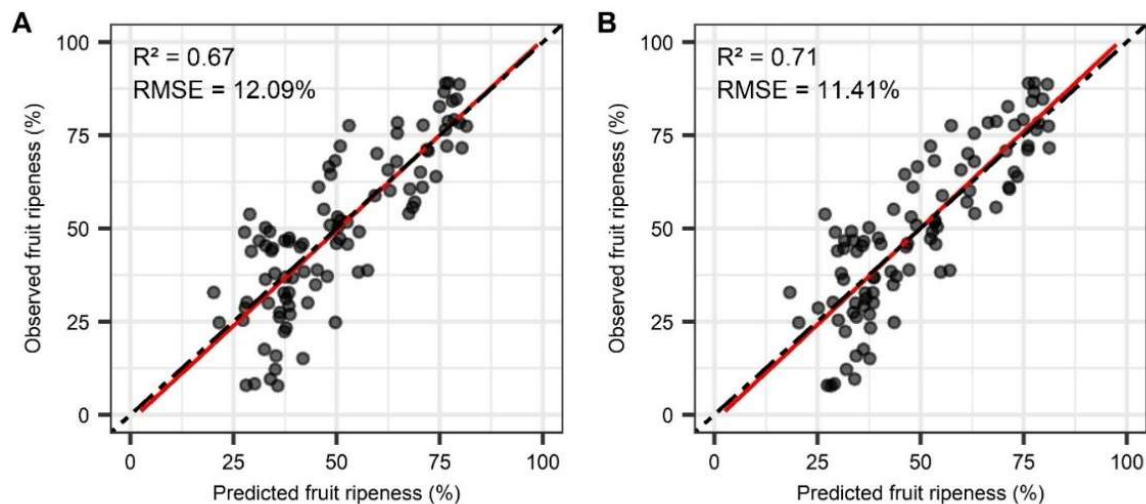


**Figure 7.** Scatterplots of the predicted versus observed values of fruit ripeness obtained using only the spectral variables (A) and the combination of spectral and textural variables (B) from both crop seasons. The 1:1 line (grey, dashed) is provided for reference. The red line represents the regression line.

Among the selected variables that were used as predictors, the spectral bands and VIs presented the highest importance (%) in the construction of the RF models. For both scenarios, the variables CRI, Red, MCARI1, and NIR were the ones that contributed most to the fruit ripeness prediction (Figure 8). These variables represented 61.01 and 44.50% of the total importance in scenarios 1 and 2, respectively. On the other hand, despite increasing the accuracy of the RF model when combined with the spectral variables, the textural variables showed a small contribution with the NDVI1 (5.31%) being the most important variable. The remaining variables, with the exception of the Gcorrel that showed the lowest importance, contributed similarly to other spectral variables whose importance varied from 3.54 to 4.61%.

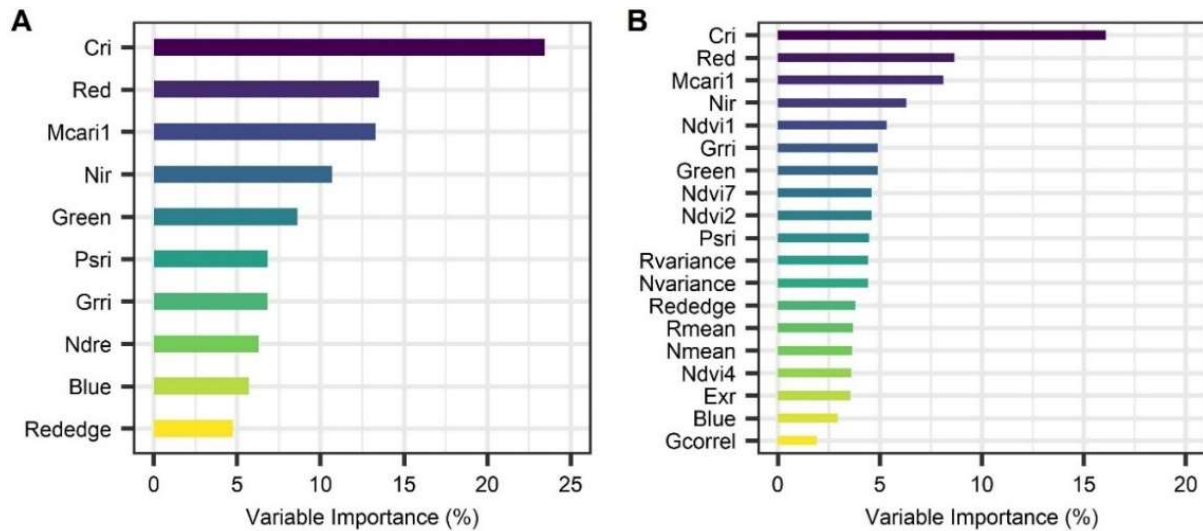


**Figure 8.** Variable importance attributed by the random forest algorithm for prediction of the fruit ripeness using only the spectral variables (A) and the combination of spectral and textural variables (B).

### 3.3.3 Spatiotemporal variability maps of the fruit ripeness

The spatiotemporal variations in the fruit ripeness are shown in the maps obtained with the best-performing RF models. Due to the higher availability of imagery, only the maps of fields A and F are presented (Figures 9 and 10). Predicted fruit ripeness (% unripe fruits) ranged from 17.65 to 85.34% within the sampling dates of both coffee fields. In addition, as observed in the field, the maps also presented a high spatial and temporal variability of fruit ripeness among trees as well as within a single tree. The spatiotemporal evolution of the fruit ripeness throughout the field samplings is highlighted on the maps through the dashed rectangles, which presents an amplified view of the crop rows. Regarding the visual difference in the maps from both scenarios, the maps obtained with spectral and textural variables, especially for field A, provided a better visual of the spatiotemporal variations in the fruit ripeness degree.

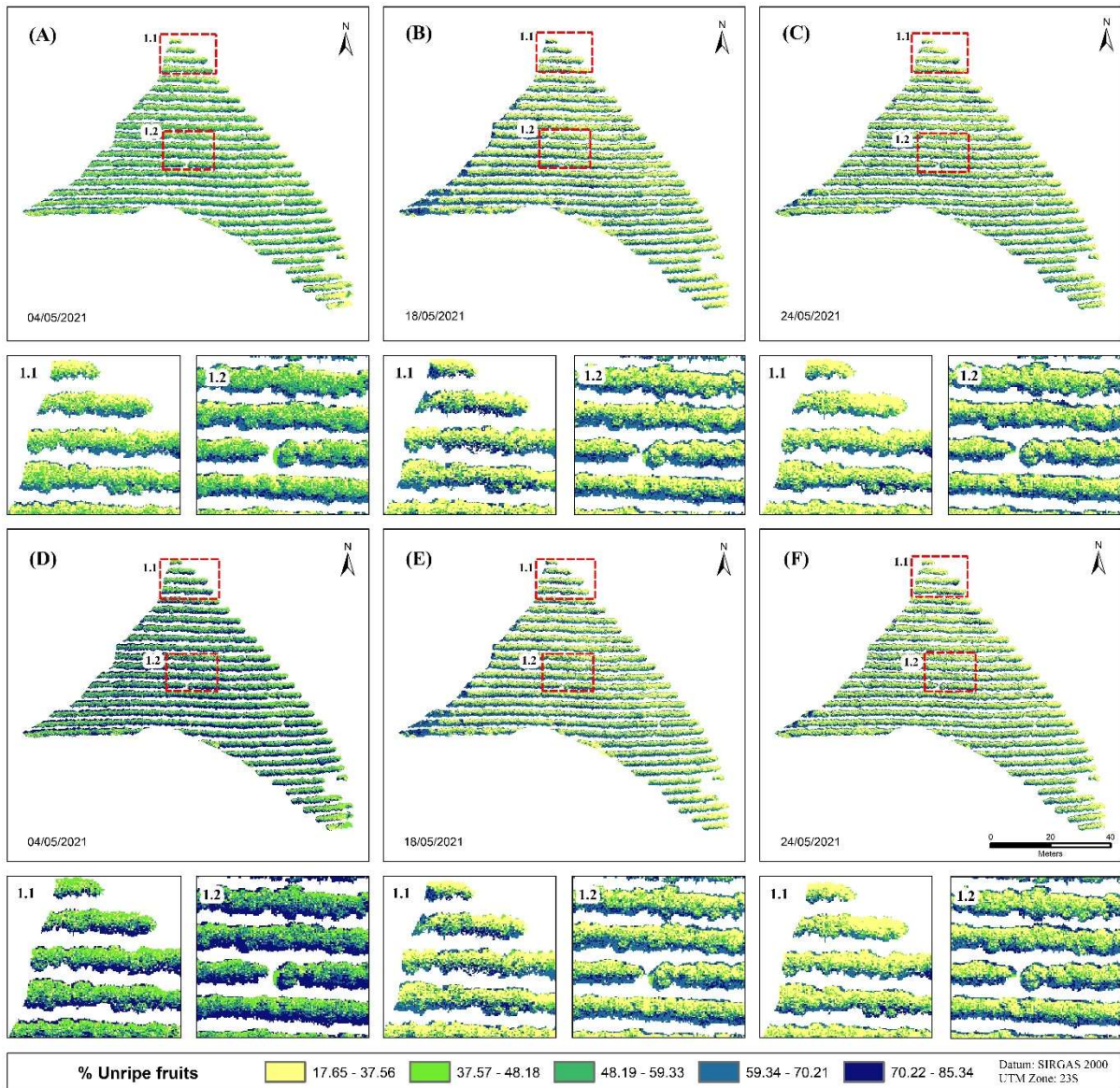


**Figure 9.** Spatial variability maps of the fruit ripeness (% unripe fruits) obtained with the random forest models using as predictors the spectral variables (A, B, and C) and the combination of spectral and textural variables (D, E, and H) from field A in 2021. The dashed rectangles identified as 1.1 and 1.2 on the maps represent an amplified view of the crop rows.

Overall, the spatiotemporal changes agreed with the expected reduction of the percentage of unripe fruits over time, as driven by the temporal evolution of the fruit ripeness. For field A, when looking at the fruit ripeness classes, the area of plants within the two first classes (17.65 – 48.18% of unripe fruits) increased from 44.66 to 55.29% and from 46.04 to 58.03% from May 04<sup>th</sup> to May 24<sup>th</sup>, 2021, respectively, for scenarios 1 and 2. Conversely, the area of plants with a higher percentage of unripe fruits decreased from 55.34 to 44.71% and from 53.96 to 41.97% respectively, for scenarios 1 and 2 (Table 5). In this field, major changes were observed between the two first sampling dates due to the higher interval of days.

**Table 5.** Temporal evolution of the fruit ripeness extracted from the maps of field A.

Spectral Variables										
Dates	04/05/2021		18/05/2021		24/05/2021		Difference between sampling dates			
Class	Area				18/05 – 05/05		24/05 – 18/05			
(% Unripe fruits)	m <sup>2</sup>	%	m <sup>2</sup>	%	m <sup>2</sup>	%	m <sup>2</sup>	%	m <sup>2</sup>	%
17.65 - 37.56	624.91	26.25	905.92	38.06	939.45	39.47	+281.01	+31.02	+33.53	+3.57
37.57 - 48.18	438.32	18.41	302.18	12.69	376.81	15.83	-136.14	-45.05	+74.64	+19.81
48.19 - 59.33	608.56	25.56	260.69	10.95	311.48	13.09	-347.87	-133.44	+50.80	+16.31
59.34 - 70.21	597.79	25.11	756.29	31.77	664.87	27.93	+158.50	+20.96	-91.42	-13.75
70.22 - 85.34	110.88	4.66	155.38	6.53	87.84	3.69	+44.50	+28.64	-67.54	-76.90
Spectral and Textural Variables										
% Unripe fruits	m <sup>2</sup>	%	m <sup>2</sup>	%	m <sup>2</sup>	%	m <sup>2</sup>	%	m <sup>2</sup>	%
17.65 - 37.56	563.49	23.67	940.45	39.51	934.90	39.27	376.96	+40.08	-5.55	-0.59
37.57 - 48.18	532.54	22.37	391.73	16.46	446.54	18.76	-140.81	-35.95	+54.81	+12.28
48.19 - 59.33	716.15	30.08	335.95	14.11	379.55	15.94	-380.20	-113.17	+43.60	+11.49
59.34 - 70.21	312.61	13.13	456.89	19.19	428.15	17.99	144.29	+31.58	-28.75	-6.71
70.22 - 85.34	255.67	10.74	255.44	10.73	191.33	8.04	-0.23	-0.09	-64.12	-33.51



Similarly, the temporal changes in the percentage of unripe fruits in the field F were detected on the maps as the fruit ripeness progressed (Figure 10 and Table 6). In this field, the area of plants included in the two first classes increased from 60.04 to 88.91% and from 54.2 to 87.87% from May 10<sup>th</sup> to May 31<sup>st</sup>, 2021, respectively, for scenarios 1 and 2. When compared to field A, it can be noted that field F presented a more accentuated change between the fruit ripeness classes.

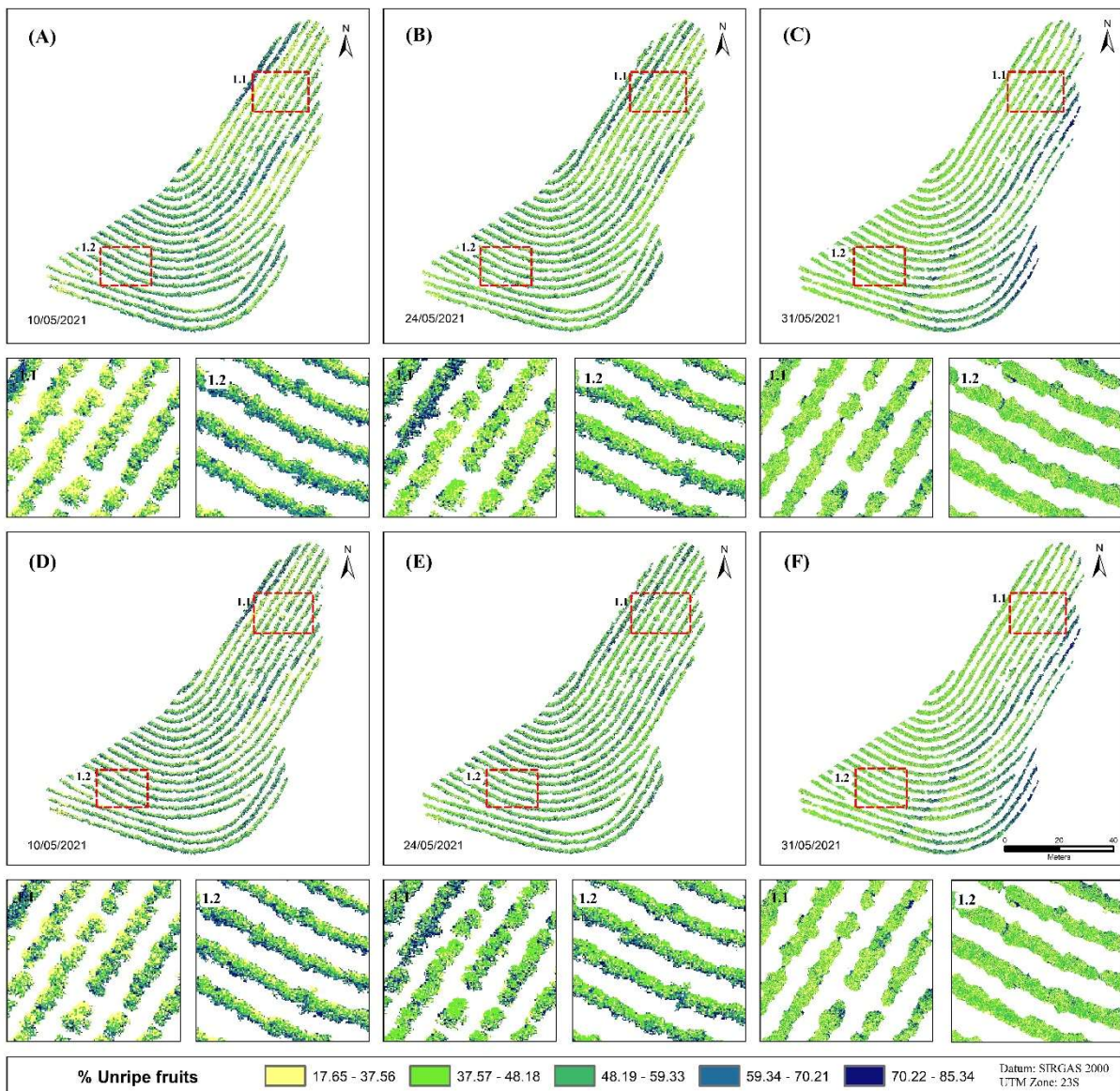


**Figure 10.** Spatial variability maps of the fruit ripeness (% unripe fruits) obtained with the random forest models using as predictors the spectral variables (A, B, and C) and the combination of spectral and textural variables (D, E, and F) from field F in 2021. The dashed rectangles identified as 1.1 and 1.2 on the maps represent an amplified view of the crop rows.

When looking at the maps, specifically for field A, it can be seen that the upper side of the plants presented a lower percentage of unripe fruits when compared to the lower side (Figure 9). This situation occurred due to the planting orientation of the coffee rows (from west to east), whose plant's upper side receives a higher incidence of solar radiation throughout the day. These differences in the fruit ripeness degree were also observed during the field campaigns.

Moreover, for both fields, the presence of shadows during the image acquisition ended up influencing the prediction and the spatial variability of the fruit ripeness in some maps. For field A, a higher percentage of unripe fruits can be observed on the left end of the field on May 18th, 2021 (Figures 9B and 9E). Differently, in field F these errors were mostly present throughout the left side of the field on May 31<sup>st</sup>, 2021 (Figures 10C and 10F). Despite the efforts, the presence of shadows on the imagery was unavoidable on some days since the coffee fields were surrounded by a eucalyptus plantation. Regardless, the spatiotemporal variability maps enabled the detection and quantification of the fruit ripeness changes over time, showing that this methodology can be used to replace the time-consuming fieldwork.

**Table 6.** Temporal evolution of the fruit ripeness extracted from the maps of field F.

Spectral Variables										
Dates	10/05/2021		24/05/2021		31/05/2021		Difference between sampling dates			
Class	Area						24/05 – 10/05		31/05 – 24/05	
(% Unripe fruits)	m <sup>2</sup>	%	m <sup>2</sup>	%	m <sup>2</sup>	%	m <sup>2</sup>	%	m <sup>2</sup>	%
17.65 - 37.56	995.63	34.45	1551.35	53.67	2139.77	74.03	+555.72	+35.82	+588.42	+27.50
37.57 - 48.18	739.85	25.60	596.42	20.63	430.18	14.88	-143.43	-24.05	-166.24	-38.64
48.19 - 59.33	828.07	28.65	484.71	16.77	201.69	6.98	-343.36	-70.84	-283.05	-140.36
59.34 - 70.21	203.71	7.05	142.09	4.92	28.74	0.99	-61.62	-43.37	-113.35	-394.46
70.22 - 85.34	123.11	4.26	115.80	4.01	90.02	3.11	-7.31	-6.31	-25.78	-28.64
Spectral and Textural Variables										
% Unripe fruits	m <sup>2</sup>	%	m <sup>2</sup>	%	m <sup>2</sup>	%	m <sup>2</sup>	%	m <sup>2</sup>	%
17.65 - 37.56	804.91	27.85	1437.34	49.73	2077.71	71.88	+632.43	+44.00	+640.37	+30.82
37.57 - 48.18	761.54	26.35	663.86	22.97	462.12	15.99	-97.67	-14.71	-201.75	-43.66
48.19 - 59.33	943.91	32.66	505.14	17.48	240.41	8.32	-438.77	-86.86	-264.72	-110.11
59.34 - 70.21	256.74	8.88	168.11	5.82	21.11	0.73	-88.64	-52.73	-146.99	-696.20
70.22 - 85.34	123.27	4.26	115.92	4.01	89.01	3.08	-7.35	-6.34	-26.90	-30.23

### 3.4 Discussion

In recent years, the use of multispectral cameras mounted on unmanned aerial vehicles (UAVs) has shown to be a feasible way for crop monitoring using remotely sensed data (ROSAS et al., 2020). Based on that, this study addressed the feasibility of using spectral and textural variables derived from UAV imagery to predict and map the spatiotemporal variability of the fruit ripeness in six coffee fields with distinct characteristics.

#### *3.4.1 Spectral and textural data fusion and its impact on model accuracy*

Previous studies focused on monitoring the coffee ripeness used only spectral variables (bands and VIs) leaving the inherent spatial information in the form of texture unexplored (HERWITZ et al., 2004; JOHNSON et al., 2004; NOGUEIRA MARTINS et al., 2021; ROSAS et al., 2021). Textural variables derived from high-resolution imagery enable a much better discrimination of vegetation structure (DOS REIS et al., 2020; SOLÓRZANO et al., 2018). Recent studies have shown that textural variables, not only increased the data dimensionality of UAV imagery with countable bands and VIs but improved the accuracy of prediction models for several crop parameters when combined with spectral data (LI et al., 2019; LIU et al., 2019; ZHENG et al., 2019; ZHOU et al., 2021). Accordingly, this study demonstrated that compared to the RF model based solely on spectral variables, the incorporation of textural variables increased the accuracy of the fruit ripeness prediction by reducing the RMSE from 12.09 to 11.41% and increasing the  $R^2$  from 0.67 to 0.71 (Figure 7). This indicates, to some extent, that textural variables aggregate valuable information for remote monitoring of the coffee crop.

Even though the prediction model that used spectral and textural variables presented superior accuracy, when looking at the variable importance metric of the RF algorithm, the most important texture variable ranked only as top-5 (NDVII). On the other hand, the spectral variables CRI, Red, MCARI1, and Nir presented the greatest contribution to the prediction model (Figure 8). This result can be explained by the way the spectral and textural values were obtained, and to what they represent.

While spectral variables detect the tonal variations at the pixel level, textural variables measure the heterogeneity in the tonal values of pixels within a defined area of an image (WOOD et al., 2012; ZHOU et al., 2021). Thus, since the textural variables were obtained using a GLCM window (3 x 3 pixels), the pixel values that contained information from leaves and fruits (crop canopy) were smoothed, which ended up reducing the sensitivity of these variables to detect the temporal changes of the fruit color. Conversely, the spectral variables

presented higher sensitivity to detect the changes on the crop canopy as they were extracted at the pixel level. Finally, the greater importance of the spectral variables is supported by the correlation analysis, in which these variables presented a higher association with the fruit ripeness than the textural variables (Figure 6).

When compared to previous studies, the RF model based on spectral variables outperformed the linear regression approach used by Nogueira Martins et al. (2021). These authors used different VIs in five coffee fields and obtained an  $R^2$  of 0.57 and RMSE of 14.60% when all fields were evaluated together. On the other hand, Herwitz et al. (2004) reported a higher correlation ( $R^2$ : 0.81; RMSE not available) in seven coffee fields. However, this analysis was carried determining the mean value of each field, which does not fully represent the spatiotemporal variability of the fruit ripeness. Therefore, these results highlights the suitability of the RF algorithm to be used as a baseline for the development of prediction models with UAV-derived data. Furthermore, this study filled a gap in the literature by developing the fruit ripeness spatial variability maps, which can be used as decision support tools for monitoring and identifying on a temporal scale the area of plants ready and not ready for harvest throughout the end of the season.

#### *3.4.2 Factors influencing the remote monitoring of coffee fruit ripeness*

The factors influencing the remote monitoring of the coffee crop are mainly related to the crop spectral response, which in turn is influenced by the crop characteristics (*e.g.*, canopy architecture and size, plant density, and yield), agrometeorological conditions, and the presence of biotic and abiotic stresses (BERNARDES et al., 2012; CHEMURA et al., 2018; CHEMURA; MUTANGA, 2017; CHQUILOFF VIEIRA et al., 2006; FERREIRA et al., 2014; JOHNSON et al., 2004; LOUZADA PEREIRA et al., 2018; MARIN et al., 2021; NOGUEIRA MARTINS et al., 2021; ROSAS et al., 2021). Regarding the fruit ripeness monitoring, the most limiting factors were the plant density, canopy volume, and crop yield as reported in previous studies.

Studies conducted by Johnson et al. (2004) and Herwitz et al. (2004) showed that the fruit ripeness was related to the spectral variables, but only in certain fields with significant fruit display on the crop canopy. More recently, Rosas et al. (2021) and Nogueira Martins et al. (2021) used different VIs for monitoring the fruit ripeness at the plant level in coffee fields with distinct characteristics of canopy volume, crop yield, cultivar, and plant density. The results showed that the interaction between crop yield and canopy volume were the main factors affecting the performance of the VIs. The combination of high crop yields with low canopy

volumes resulted in a greater amount of exposed coffee fruits, which caused a greater spectral change on the crop canopy and that were detected by the spectral variables during the ripening stage.

In this study, although the spectral and textural information from all fields were used together to build a global model, differences in the spatiotemporal variability maps from fields A and F were found when the fruit ripeness classes were discriminated. The field F presented a more accentuated change between the fruit ripeness classes when compared to field A. These differences are possibly associated with the lower crop canopy (Fields A and F: 2.91 and 2.78 m<sup>3</sup>) and the higher yield on this field (Fields A and F: 3850 and 4550 kg ha<sup>-1</sup>) (Figure 2).

In addition, another factor that influenced the fruit ripeness spatial variability was the unequal fruit ripening in different sides of the plants. Specifically for field A, it was observed during the field campaigns and, also, through the maps that the upper side of the plants presented a lower percentage of unripe fruits when compared to the lower side (Figure 9). This difference is possibly related to the planting orientation of the coffee rows (from west to east), in which the upper side of the plants are submitted to a higher incidence of solar radiation throughout the day. According to Cannell (1975), the initiation of the flower buds requires higher light intensities. In this sense, due to its greater insolation, the upper side of the plant may be receiving the “start” of the floral induction before the lower side, with an additional flowering beforehand. This may explain the occurrence of a higher percentage of ripe fruits on the upper side of the plants. The influence of solar radiation on coffee ripeness, and especially on the beverage quality has been discussed in previous studies (CAMARGO, 2010; FERREIRA et al., 2014; LOUZADA PEREIRA et al., 2018). Lastly, the visual quality of the image is also a limiting factor, especially when there is the presence of shadows and/or blur that can alter the reflectance values in the image. Here, the presence of shadows, which was unavoidable on some dates, ended up influencing the spatial variability of the fruit ripeness in specific areas of the maps.

#### *3.4.3 Limitations and directions for future studies*

The main limitations of this study are related to the crop characteristics, unequal fruit ripening, and image quality as discussed before. Since the coffee crop presents a complex spectral behavior that is highly influenced by the dense plant canopy, which in turn is composed of a mixture of green leaves, unripe, ripe, and overripe fruits; thus, spectral confusion and errors of underestimation or overestimation in the prediction models are unavoidable. In general, the

aerial monitoring of the fruit ripeness presents limitations, especially when the majority of the fruits are unripe, which results in high spectral confusion among fruits and leaves leading to underestimation of the fruit ripeness degree. On top of that, the unequal fruit ripeness among trees as well as within a single tree also ends up affecting the fruit ripeness mapping and the decision-making towards the definition of the ideal harvesting time.

Despite these limitations, the approach used in this study provides a framework for integrating field data and the spectral and textural variables derived from UAV imagery to map the fruit ripeness. In addition, the concepts presented here are expected to be consistent regardless of the multispectral sensor, provided that the spatial resolution of the imagery is able to capture the spatial variability of the fruit ripeness. Finally, future research needs to include data from more seasons as well as from several commercial fields to validate the methodology. More importantly, it should focus on developing an automated workflow for image acquisition, variable extraction, and better modeling of the fruit ripeness for practical uses in the future.

### 3.5 Conclusion

This study demonstrated that the combined use of spectral and textural variables derived from aerial imagery enhanced the prediction accuracy of the fruit ripeness models compared to the performance obtained using only spectral bands and vegetation indices.

Regarding the variable importance, the best spectral variables for predicting the fruit ripeness and developing the spatio-temporal variability maps were the VIs CRI and MCARI1 and the Red and NIR bands. As for the textural variables, only the NDVI1 was ranked among the top five most important variables.

Even though the fruit ripeness varies greatly among trees as well as within a single tree due to multiple coffee blossoms and environmental conditions, the random forest-based models were able to predict and quantify the spatiotemporal changes in fruit ripeness with moderate accuracies for both scenarios. Finally, despite the limitations, this study filled a gap in the literature by developing the fruit ripeness variability maps, which can be used as decision support tools for monitoring and identifying on a temporal scale the area of plants ready and not ready for harvest throughout the season.

### 3.6 References

ALVARES, C. A. et al. Köppen's climate classification map for Brazil. **Meteorologische Zeitschrift**, v. 22, n. 6, p. 711-728, 2013.

- BERNARDES, T. et al. Monitoring biennial bearing effect on coffee yield using MODIS remote sensing imagery. **Remote Sensing**, v. 4, n. 9, p. 2492-2509, 2012.
- BREIMAN, L. Random forests. **Machine Learning**, v. 45, n. 1, p. 1-32, 2001.
- CAMARGO, M. B. P. DE. The impact of climatic variability and climate change on arabic coffee crop in Brazil. **Bragantia**, v. 69, n. 1, p. 239–247, 2010.
- CANNELL, M. G. R. Crop physiological aspects of coffee bean yield: a review. **Journal of Coffee Research**, v. 1, 1975.
- CHEMURA, A. et al. Mapping spatial variability of foliar nitrogen in coffee (*Coffea arabica* L.) plantations with multispectral Sentinel-2 MSI data. **ISPRS Journal of Photogrammetry and Remote Sensing**, v. 138, p. 1–11, 2018.
- CHEMURA, A.; MUTANGA, O. Developing detailed age-specific thematic maps for coffee (*Coffea arabica* L.) in heterogeneous agricultural landscapes using random forests applied on Landsat 8 multispectral sensor. **Geocarto International**, v. 32, n. 7, p. 759–776, 2017.
- CHQUILOFF VIEIRA, T. G. et al. Crop parameters and spectral response of coffee (*Coffea arabica* L.) areas within the State of Minas Gerais, Brazil. **Coffee Science**, v. 1, n. 2, p. 111–118, 2006.
- DADRASJAVAN, F. et al. UAV-based multispectral imagery for fast Citrus Greening detection. **Journal of Plant Diseases and Protection**, v. 126, n. 4, p. 307-318, 2019.
- DAMATTA, F. M. et al. Ecophysiology of coffee growth and production. **Brazilian Journal of Plant Physiology**, v. 19, p. 485-510, 2007.
- DOS REIS, A. A. et al. Monitoring pasture aboveground biomass and canopy height in an integrated crop–livestock system using textural information from PlanetScope imagery. **Remote Sensing**, v. 12, n. 16, p. 1-21, 2020.
- DUBE, T.; MUTANGA, O. Investigating the robustness of the new Landsat-8 Operational Land Imager derived texture metrics in estimating plantation forest aboveground biomass in resource constrained areas. **ISPRS Journal of Photogrammetry and Remote Sensing**, v. 108, p. 12–32, 2015.
- FAGAN, E. B. et al. Efeito do tempo de formação do grão de café ( *coffea* sp ) na qualidade da bebida. **Bioscience Journal**, v. 27, n. 5, p. 729–738, 2011.



FERREIRA, W. P. M. et al. Influence of relief and global radiation on the quality of the coffee beverage. *In: American Society of Agricultural and Biological Engineers Annual International Meeting. ASABE. Annals [...]*, 2014, p. 1-10. Available online: <<https://elibrary.asabe.org/abstract.asp?aid=44604>>. Accessed on: 10/06/2021.

FITZGERALD, G. J. et al. Spectral and thermal sensing for nitrogen and water status in rainfed and irrigated wheat environments. **Precision Agriculture**, v. 7, n. 4, p. 233-248, 2006.

FU, Y. et al. Winter wheat nitrogen status estimation using uav-based rgb imagery and gaussian processes regression. **Remote Sensing**, v. 12, n. 22, p. 1–27, 2020.

FU, Y. et al. Improved estimation of winter wheat aboveground biomass using multiscale textures extracted from UAV-based digital images and hyperspectral feature analysis. **Remote Sensing**, v. 13, n. 4, p. 1–22, 2021.

GITELSON, A. A.; KAUFMAN, Y. J.; MERZLYAK, M. N. Use of a green channel in remote sensing of global vegetation from EOS- MODIS. **Remote Sensing of Environment**, v. 58, n. 3, p. 289-298, 1996.

HABOUDANE, D. et al. Hyperspectral vegetation indices and novel algorithms for predicting green LAI of crop canopies: Modeling and validation in the context of precision agriculture. **Remote Sensing of Environment**, v. 90, n. 3, p. 337-352, 2004.

HARALICK, R. M.; SHANMUGAM, K.; DINSTEN, I. Textural Features for Image Classification. **IEEE Transactions on Systems, Man, and Cybernetics**, v. 3, n. 6, p. 610–621, 1973.

HERWITZ, S. R. et al. Imaging from an unmanned aerial vehicle: Agricultural surveillance and decision support. **Computers and Electronics in Agriculture**, v. 44, n. 1, p. 49-61, 2004.

HIJMANS, R. et al. **raster: Geographic analysis and modeling with raster data**. Available online: <<http://CRAN.R-project.org/package=raster>>. Accessed on 08/06/2021.

JOHNSON, L. F. et al. Feasibility of monitoring coffee field ripeness with airborne multispectral imagery. **Applied Engineering in Agriculture**, v. 20, n. 6, p. 745-849, 2004.

KUHN, M. caret Package. **Journal of Statistical Software**, v. 5, p. 1-26, 2008.

LI, S. et al. Combining color indices and textures of UAV-based digital imagery for rice LAI

estimation. **Remote Sensing**, v. 11, n. 15, 2019.

LIAW, A.; WIENER, M. Classification and regression with Random Forest. **R News**, v. 2, p. 18-22, 2002.

LIU, Y. et al. Estimating biomass of winter oilseed rape using vegetation indices and texture metrics derived from UAV multispectral images. **Computers and Electronics in Agriculture**, v. 166, p. 1-10, 2019.

LOUZADA PEREIRA, L. et al. Influence of solar radiation and wet processing on the final quality of arabica coffee. **Journal of Food Quality**, 2018.

LU, D.; BATISTELLA, M. Exploring TM image texture and its relationships with biomass estimation in Rondônia, Brazilian Amazon. **Acta Amazonica**, v. 35, n. 2, p. 249–257, 2005.

MAIMAITIJANG, M. et al. Soybean yield prediction from UAV using multimodal data fusion and deep learning. **Remote Sensing of Environment**, v. 237, n. 12, p. 1-20, 2020.

MARIN, D. B. et al. Remotely Piloted Aircraft and Random Forest in the Evaluation of the Spatial Variability of Foliar Nitrogen in Coffee Crop. **Remote Sensing**, v. 13, n. 8, p. 1471, 10 abr. 2021.

MARTINEZ, H. E. P. et al. Zinc supplementation, production and quality of coffee beans. **Revista Ceres**, v. 60, n. 2, p. 293–299, 2013.

MERZLYAK, M. N. et al. Non-destructive optical detection of leaf senescence and fruit ripening. **Physiologia plantarum**, v. 106, n. 1, p. 135–141, 1999.

MEYER, G. E.; HINDMAN, T. Machine Vision Detection Parameters for Plant Species Identification. *In*: SPIE Conference on Precision Agriculture and Biological Quality. Boston. Massachusetts. **Annals** [...], 2014, v. 3543, p. 327-335. Available online: <<https://www.spiedigitallibrary.org/conference-proceedings-of-spie/3543/>>. Accessed on: 10/10/2021.

NOGUEIRA MARTINS, R. et al. A Novel Vegetation Index for Coffee Ripeness Monitoring Using Aerial Imagery. **Remote Sensing**, v. 13, n. 2, p. 1-16, 2021.

R CORE TEAM. R: A Language and Environment for Statistical Computing. **Vienna, Austria**, 2019.

ROSAS, J. T. F. et al. Low-cost system for radiometric calibration of UAV-based multispectral

imagery. **Journal of Spatial Science**, p. 1–15, 2020.

ROSAS, J. T. F. et al. Coffee ripeness monitoring using a UAV-mounted low-cost multispectral camera. **Precision Agriculture**, v. 23, n. 1, p. 300-318, 2021.

ROUSE, J. W. et al. Monitoring vegetation systems in the Great Plains with ERTS (Earth Resources Technology Satellite). *In: III Earth Resources Technology Satellite-1 Symposium; 1973, NASA. Washington, DC, USA. Annals [...]*, 1973, p. 301-317.

SCHUMACHER, P. et al. Do red edge and texture attributes from high-resolution satellite data improve wood volume estimation in a semi-arid mountainous region? **Remote Sensing**, v. 8, n. 7, p. 1–19, 2016.

SILVA, S. DE A. et al. Coffee quality and its relationship with Brix degree and colorimetric information of coffee cherries. **Precision Agriculture**, v. 15, n. 5, p. 543-554, 2014.

SILVA, T. V. et al. Potential of Laser Induced Breakdown Spectroscopy for analyzing the quality of unroasted and ground coffee. **Spectrochimica Acta - Part B Atomic Spectroscopy**, v. 135, p. 29–33, 2017.

SOARES, J. V. et al. An investigation of the selection of texture features for crop discrimination using SAR imagery. **Remote Sensing of Environment**, v. 59, n. 2, p. 234–247, 1997.

SOLÓRZANO, J. V. et al. Contrasting the potential of Fourier transformed ordination and gray level co-occurrence matrix textures to model a tropical swamp forest's structural and diversity attributes. **Journal of Applied Remote Sensing**, v. 12, n. 3, p. 1-19, 2018.

WANG, F. et al. Combining spectral and textural information in UAV hyperspectral images to estimate rice grain yield. **International Journal of Applied Earth Observation and Geoinformation**, v. 102, p. 1-10, 2021.

WOOD, E. M. et al. Image texture as a remotely sensed measure of vegetation structure. **Remote Sensing of Environment**, v. 121, p. 516–526, 2012.

ZHENG, H. et al. Evaluation of RGB, color-infrared and multispectral images acquired from unmanned aerial systems for the estimation of nitrogen accumulation in rice. **Remote Sensing**, v. 10, n. 6, 2018.

ZHENG, H. et al. Improved estimation of rice aboveground biomass combining textural and spectral analysis of UAV imagery. **Precision Agriculture**, v. 20, n. 3, p. 611–629, 2019.

ZHOU, Y. et al. Diagnosis of winter-wheat water stress based on UAV-borne multispectral

image texture and vegetation indices. **Agricultural Water Management**, v. 256, p. 1-12, 2021.

ZVOLEFF, A. **Glm: Calculate Textures from Grey-Level Co-Occurrence Matrices (GLCMs)**, 2020. Available online: <<https://cran.r-project.org/package=glcm>>. Accessed on: 07/2021.

## 4 Assessment of coffee cup quality using NIR spectroscopy and aerial remote sensing

### Abstract

Cup tasting is the main tool for the assessment of the coffee beverage quality. However, the use of sensory analysis can present some limitations and subjectivity due to its high-cost and the difficulty of setting up desirable limits for the different quality attributes. Therefore, this study aimed: (1) to predict the coffee beverage quality based on NIR spectra of roasted coffee; and (2) to classify the beverage quality using spectral, climate, and terrain variables obtained from UAV imagery. First, a field experiment was set up during the 2020-2021 season. At the end of the season, 13 flights were carried out using an unmanned aerial vehicle (UAV) equipped with an RGB camera. Then, different spectral, climate, and terrain variables were obtained from the UAV imagery. In the same period, the coffee was harvested, processed, and submitted to sensory analysis using the Specialty Coffee Association (SCA) protocol. After that, NIR spectra (1000-2450 nm) of 180 samples from five cultivars of Arabica coffee were analyzed. Next, partial least squares (PLS) and PLS-OPS (ordered predictors selection) regression models were developed to predict eight quality attributes. For the second objective, the UAV-based variables were used as input for machine learning algorithms for discriminating the beverage classes (Specialty and not Specialty). Overall, the best predictions were obtained for the aftertaste, overall perception, body, and balance quality attributes using the PLS-OPS models, whose coefficient of correlation ( $r_p$ ) and the root mean square error of the prediction ( $RMSEP$ ) ranged from 0.78 to 0.82 and from 0.15 to 0.13, respectively. Regarding the classification models, the random forest algorithm exhibited the highest accuracy, however it was still not satisfactory. Therefore, the use of UAV imagery for coffee quality assessment needs to be further explored.

**Keywords:** Near-infrared spectroscopy, Sensory analysis, UAV, Digital agriculture, *Coffea arabica* L.

### 4.1 Introduction

Coffee is one of the most valuable agricultural commodities, whose price setting and export potential are defined according to its beverage quality. The beverage quality is a result of complex interactions among the environment, plant genetics, crop management, harvest and post-harvesting practices (CHENG et al., 2016; LÄDERACH et al., 2011; SILVA NETO et al., 2018; SILVA et al., 2014). Specifically, the main factors influencing the coffee quality are the

fruit ripeness at harvest, planting altitude, edaphoclimatic conditions, the microbiome of plants and fruits, genotypes, soluble solids content (brix degree), and post-harvesting practices for selection and processing of the coffee fruits (DECAZY et al., 2003; OLIVEIRA APARECIDO et al., 2018; SILVA OLIVEIRA et al., 2021; SILVA et al., 2014; VELOSO et al., 2020; WORKU et al., 2018)

Currently, the beverage quality is assessed through sensory analysis (Cup tasting) performed by professional coffee tasters, also known as “Q-Graders”(DI DONFRANCESCO et al., 2014). These analyses are composed of different attributes (*e.g.*, aroma, acidity, flavor, and cup cleanness), that are distinguished by senses and can be assessed organoleptically by cuppers (SANTOS et al., 2012; TOLESSA et al., 2016). Then, the quality attributes are graded following specific protocols such as those of the Specialty Coffee Association (SCA) (SCA, 2021). However, this methodology is rather subjective, costly, time-consuming, requires trained cuppers, which hampers an efficient implementation of routine analysis, and is difficult to implement when many samples need to be processed during the peak of the coffee harvesting (CRAIG et al., 2018; FERIA-MORALES, 2002; TOLESSA et al., 2016). These issues encourage the search for faster, and reliable methodologies as an alternative to assess the beverage quality and, eventually, other attributes present in the coffee beans.

Spectroscopic methods in the near-infrared range (NIR) are good examples of fast, reliable, chemical-free, and low-cost techniques that have been widely used to assess food quality attributes (BARBIN et al., 2014; JING et al., 2010; SANTOS et al., 2012). Recent studies have demonstrated the potential of these techniques to predict coffee sensory attributes (BAQUETA et al., 2019; ESTEBAN-DÍEZ et al., 2004; TOLESSA et al., 2016), detect coffee adulteration (EBRAHIMI-NAJAFABADI et al., 2012), predict the roasting degree (ALESSANDRINI et al., 2008), assess coffee composition (PIZARRO et al., 2007; SHAN et al., 2017), and evaluate the presence of defects (CRAIG et al., 2015, 2014).

In general, these analyses are performed in laboratory after harvesting and processing the coffee fruits. However, the inherent information from the coffee fields (*e.g.*, terrain attributes, crop spectral response, and climatic variables) that also influences the beverage quality remains barely explored (FERREIRA et al., 2014; LOUZADA PEREIRA et al., 2018; TOLESSA et al., 2017). Based on that, the use of such attributes can be a key source for identification and management of fields with potential of producing specialty coffee.

In recent years, the advent of technology has led to the development of Unmanned Aerial Vehicles (UAV) using cost-effective multispectral sensors. These sensors have enabled

the acquisition of imagery with high spatial and temporal resolution at a low-cost, as well as providing detailed information on the crop canopy spectral patterns (LELONG et al., 2008; NOGUEIRA MARTINS et al., 2021). Previous studies have demonstrated the effectiveness of optical sensors onboard UAVs for discriminating ripe from unripe coffee fruits (NOGUEIRA MARTINS et al., 2021; ROSAS et al., 2021), mapping of foliar nitrogen content (MARIN et al., 2021a), detection of diseases (MARIN et al., 2021b), estimation of biophysical parameters (SANTOS et al., 2020a; SOUZA BARBOSA et al., 2021), and prediction of crop yield (BARBOSA et al., 2021).

In view of the aforementioned, the integration of NIR spectroscopy with the UAV imagery would be advantageous, not only to predict the coffee beverage quality, but also to identify coffee fields with potential of producing high-quality beverage. In addition, to the best of our knowledge, the integration of both proximal and aerial remote sensing for this matter has not yet been reported. Therefore, this study was aimed: (1) to predict the coffee cup quality based on NIR spectra of roasted coffee; and (2) to classify the beverage quality using spectral, climate, and terrain variables obtained from UAV imagery.

## **4.2 Material and Methods**

### *4.2.1 Study area*

This study was carried out in seven fields of arabica coffee (*Coffea arabica* L.) located in the municipalities of Paula Cândido and Araponga, Minas Gerais State, Southeastern Brazil (Figure 1). According to the Köppen-Geiger classification, the climate in the area is defined as humid subtropical with dry winter and hot summer (CWA) (Alvares et al., 2013).

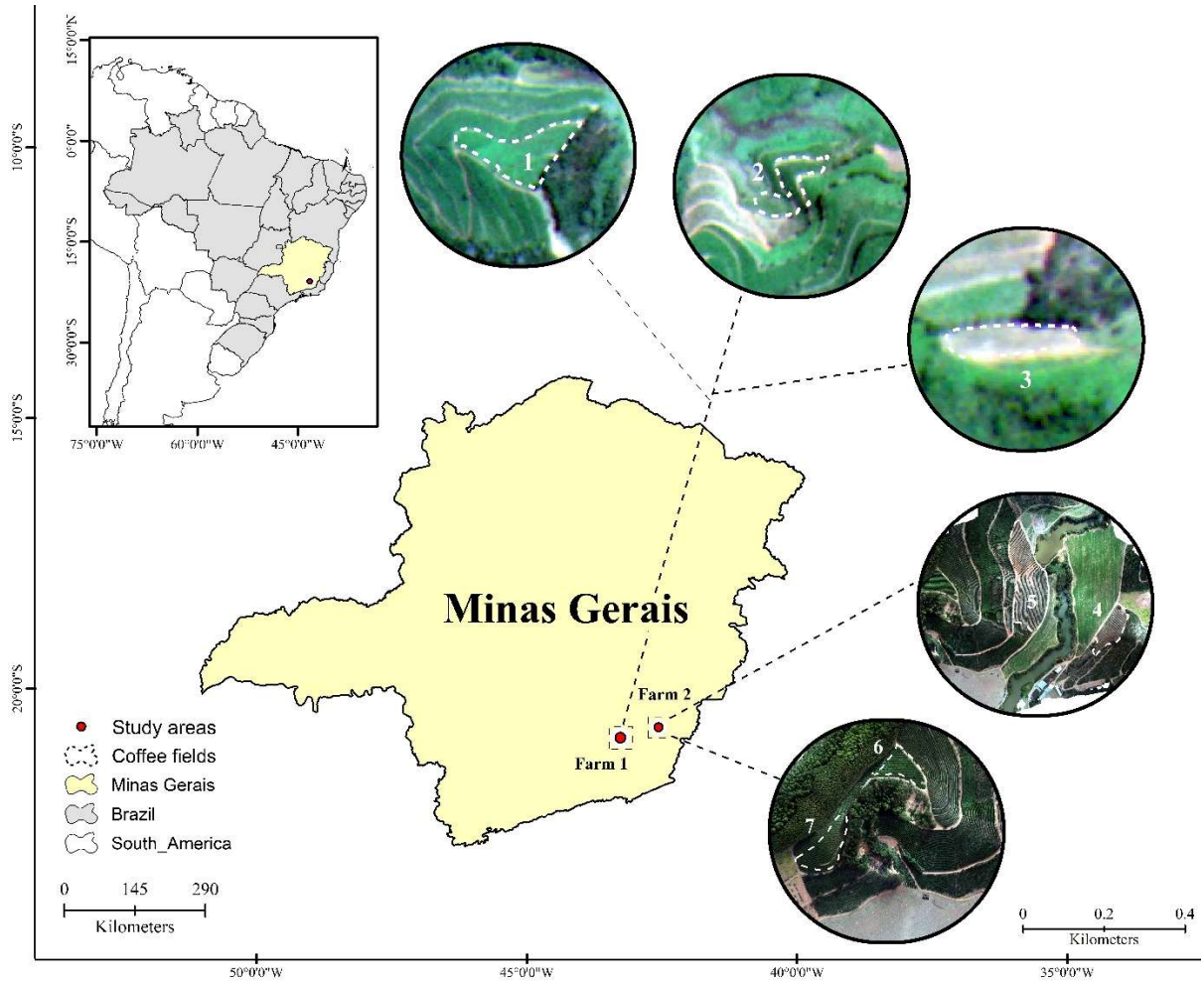


**Figure 1.** Location of the coffee fields in the *Zona da Mata* region of Minas Gerais State, Southeastern Brazil

The main characteristics of the seven coffee fields are presented in Table 1.

**Table 1.** Characteristics of the arabica coffee fields used in this study

Field	Area (ha)	Cultivar	Density (Plants ha <sup>-1</sup> )	Average Terrain Slope (%)	Average Altitude (m)
1	1.53	Catucai Saulo	8000	30.13 ± 10.10	863.39 ± 9.58
2	0.86	Catucai	8000	42.00 ± 19.47	838.74 ± 8.37
3	0.75	Geisha	3400	18.28 ± 6.02	923.58 ± 2.03
4	0.81	Catuai MG44	3800	23.53 ± 7.69	704.51 ± 3.96
5	2.57	Catuai MG44	3800	24.02 ± 8.78	703.59 ± 6.32
6	0.56	Red Catuai	4000	10.16 ± 5.65	772.29 ± 1.19
7	0.88	Red Catuai	4000	12.45 ± 5.15	762.81 ± 1.56



#### 4.2.2 UAV Imagery acquisition and processing

Imagery acquisition in the coffee fields was performed using a quadcopter (model: Phantom 4 Pro, DJI Innovations, Shenzhen, China) equipped with a RGB camera, which registers information in the following bandwidth:  $450 \pm 16$  nm (Blue),  $560 \pm 16$  nm (Green), and  $650 \pm 16$  nm (Red). The UAV flights were carried between 11:00 and 13:00 h local time under clear-sky conditions at 60 meters above ground level at  $9 \text{ m s}^{-1}$  speed with 80% front overlap and 75% side overlap between images. Thirteen UAV flights were conducted for the seven coffee fields from April 06<sup>th</sup> to May 31<sup>st</sup> always before harvesting the coffee samples. Prior to the flights, 20 ground control points (GCP) were distributed around the coffee fields for further geometric correction of the orthomosaics. These GCPs were georeferenced using a topographic GNSS (Global Navigation Satellite System) receiver (model: ProXT, Trimble Inc., Sunnyvale, CA, USA).

After the flights, all images were processed using the Agisoft™ MetaShape software, version 1.5.3 (Agisoft LLC, St. Petersburg, Russia) following the procedures detailed in Nogueira Martins et al. (2021). The final orthomosaics were georeferenced in the QGIS software, version 3.2 (QGIS Development Team, 2016) using the information from the GCPs. Finally, the empirical line method was used for the radiometric calibration of the orthomosaics (ROSAS et al., 2020). For that, four grayscale reflectance targets (85, 27, 12, and 7%) made of plywood and covered with synthetic nappa leather of polyvinyl chloride (PVC) were placed in the field during the UAV flights. The reflectance of the targets was obtained using a portable spectroradiometer (model: ASD Handheld 2, Analytical Spectral Devices, Inc., Boulder, CO, USA), which operates in the wavelength range from 325 nm to 1075 nm with a resolution of  $\pm 1$  nm. The spectroradiometer was calibrated using a white spectralon plate.

After processing the images, the orthomosaics and the digital elevation model (DEM) were used to obtain variables related to the crop spectral response, the field terrain, and climate. The spectral variables were composed of the bands Red, Green, and Blue and by the VIs Coffee ripeness index (CRI) (NOGUEIRA MARTINS et al., 2021), and the Green-red Ratio Ripeness Index (GRRI) (JOHNSON et al., 2004). As for the terrain and climate variables, the DEM was used as input to obtain the Altitude, Slope, Hillshade, Terrain Aspect (Orientation), and the Global Solar Radiation (Rg).

With the exception of the altitude that was extracted directly from the DEM, the remaining variables were obtained using the slope, hillshade, and aspect tools in the QGIS software. The Rg was obtained using the "Solar Radiation Area" tool (FU and RICH, 2002,

2000). This tool is based on the hemispheric scattering algorithm proposed by Rich et al. (1994) and derives the incoming solar radiation from a raster surface (DEM) (FU and RICH, 1999). The Rg was obtained for different periods, considering its accumulated value from the beginning of the full fruit formation phenological phase in January to the harvest date of each coffee field (Table 3). Then, the accumulated Rg was converted to the monthly daily average scale ( $\text{MJ m}^{-2} \text{ day}^{-1}$ ).

These variables were included in the analysis due to their influence on the coffee quality as reported in previous studies (AVELINO et al., 2005; FERREIRA et al., 2016, 2014). Finally, from the coordinates of the sampled points, polygonal masks considering three plants in a row (sampled point) were created and used to extract the average values of the spectral, terrain, and climatic variables using the zonal statistics tool.

#### 4.2.3 Field Data Collection and Processing

Coffee samples composed of three kilograms of cherry fruits were harvested on different dates from April to June in the 2020-2021 season (Table 2). For that, an irregular sampling grid was defined according to the fruit load on each coffee field in order to represent the entire area. The sampling points were represented by three plants located side by side in the same cultivation row. Then, for each plant, the fruits were manually harvested from eight plagiotropic branches, two per plant quadrant randomly chosen in the middle third of the plants. The sampling points were georeferenced using the same GNSS receiver as described before.

**Table 2.** Harvesting dates and the number of samples collected on each coffee field

Field	Date	Samples per Harvest				Total (n=180)
1	21/05/2021	7	-	-	-	7
2	21/05/2021	8	-	-	-	8
3	27/05/2021	22	-	-	-	22
4	06/04, 12/04, and 19/04/2021	6	14	11	-	31
5	08/04, 14/04, 21/04, and 27/04/2021	10	16	10	20	56
6	19/05 and 25/05/2021	22	8	-	-	30
7	01/06/2021	26	-	-	-	26

n, refers to the number of samples.

After the harvest, the coffee samples were pulped in a mechanical device (Model: DMMP - 04, Pinhalense, São Paulo, Brazil) in continuous water flow and dried in a mechanical dryer with a gas burner as detailed elsewhere (SILVEIRA et al., 2016). The temperature of the

drying air was kept between 35 and 40 °C until the coffee samples reached 12% moisture. The sample moisture content was monitored using a digital grain moisture meter (Model: G650, Gehaka, São Paulo, Brazil). After drying, the coffee samples remained with endocarp (parchment) and were packed in kraft paper bags, and stored until complete processing. Then, the samples were hulled using a portable device (Model: DRC-1 830, Pinhalense, São Paulo, Brazil), packed in plastic bags, and stored until sensory analysis.

#### *4.2.4 Sensory analysis using the SCA protocol*

Coffee cup quality was evaluated through the analysis of its sensory characteristics, following the protocol developed by the Specialty Coffee Association (SCA) (SCA, 2021). Three tasters, with Q-Grader certification, performed the sensory analysis. Initially, the coffee samples were roasted in a test roaster (Model: Probat Leogap TP2, Curitiba, Brazil) with an initial temperature of 190 °C and a roasting time ranging from 9 to 12 min. The final roasting temperature ranged between 200 and 210 °C. After the roasting process, the samples were ground using an electric grinder (Model: Bunn GVH-37, Springfield, Illinois, USA) with medium particle size. The tasting of the coffee was made with five cups per sample, in which each taster performed one determination per sample.

Based on the cupping protocol proposed by the SCA, the following attributes were evaluated: Fragrance/Aroma, Flavor, Aftertaste, Acidity, Body, Balance, Sweetness, Clean cup, Uniformity, and Overall cup perception. However, for this study, only the attributes Aroma, Flavor, Aftertaste, Acidity, Body, Balance, Overall cup perception, and the Final Score were used. The attributes Sweetness, Clean cup, and Uniformity were not included because all samples, regardless of the coffee cultivar, presented the same score.

These attributes are rated on a 16-point scale representing levels of quality in quarter point (0.25) increments between numeric values from 6 to 9. Theoretically, this scale ranges from 0 to 10 points. The lower end of the scale is below specialty grade (SCA, 2021). After assessing all attributes, the tasters assign a final score, in which 100 points is the maximum score that a coffee sample can receive. These scores represent the overall quality of the coffee beverage. Thus, if the coffee sample reaches a final score greater than or equal to 80 points, it is classified as specialty coffee (SCA, 2021).

#### *4.2.5 NIR spectra measurement*

Coffee spectra was recorded after processing and performing the sensory analysis. For that, the roasted coffee samples (20 g per sample) were conditioned in a black plastic lid, in

which the absorbance spectra was recorded using a spectroradiometer (model: ASD FieldSpec PRO 4, Analytical Spectral Devices, Inc., Boulder, Colorado, USA) with a spectral range of 350 to 2500 nm. The spectral resolution of this device was 3 nm for the region 350–1000 nm and 8 nm for the 1001–2500 nm. Despite that, the output resolution of the spectral data was 1 nm since the device automatically interpolates the data to a 1 nm resolution.

To acquire the absorbance spectra of the roasted coffee samples, a contact probe (also from Analytical Inc.) with a built-in light source (6.5 W halogen lamp) and a 2-cm-diameter circular viewing window was attached by a fiber-optic cable to the spectroradiometer (Figure 2). To ensure the positioning of the spectroradiometer in relation to the sample, the probe was fixed vertically to a black chamber, which had a hole on its top with the same diameter as the spectroradiometer probe, thus allowing it to fit into the chamber. The hole on the black chamber was sealed by the structure of the contact probe which had a rubber ring on its base, preventing the entry of light. Then, the probe was placed on top of the plastic lid with the coffee, and five measurements per sample were taken. The spectroradiometer was calibrated after every three samples using a white spectralon plate. Lastly, the average values of five readings was obtained to generate a representative spectral signature for each sample. For the purpose of this study, the spectra was reduced to the NIR region between 1000 and 2450 nm.

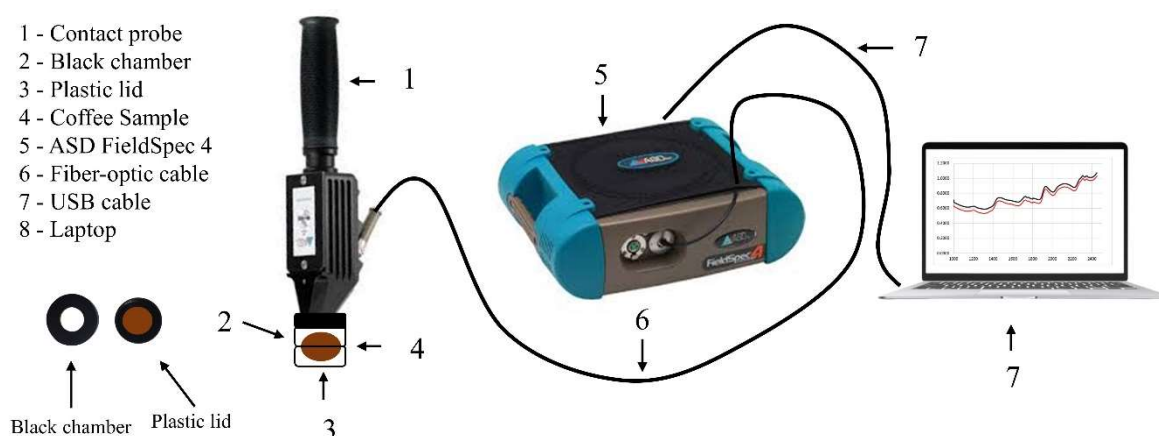


**Figure 2.** Laboratory experiment set up used to acquire the absorbance spectra of the roasted coffee samples.

#### 4.2.6 Data analysis

##### 4.2.6.1 Predicting coffee cup quality using NIR spectra

Initially, the spectra were arranged in a matrix of independent variables ( $X$ ), in which the lines were composed of the 180 spectra of the coffee samples, and the columns were composed of 1451 wavelengths (1000 to 2450 nm). The dependent variable vector ( $y$ ) was

composed of the results obtained in the cup quality analysis for each sensory attribute. Prior to the analysis, the data was split into calibration ( $n= 126$ , 70%) and validation ( $n = 54$ , 30%) datasets using the Kennard-Stone algorithm. The calibration dataset was used for preprocessing of data, selection of the number of latent variables (LVs), and selection of optimal wavelengths. The validation dataset was used with the final model for the prediction of the sensory attributes.

The training process was performed in two steps. First, different pre-processing techniques were applied to the raw spectra. This process aimed to transform data into useful information, remove unwanted information, such as spectral noise, and develop models with reliable performance for the subsequent multivariate analysis (CORRÊDO et al., 2021; OLIVERI et al., 2019). The pre-processing methods that provided the best performances in terms of model prediction were the following: Smoothing and mean center for aroma; Asymmetric least squares (AsLS) and autoscale for flavour; Robust normal variate (RNV) and normalization for aftertaste; Net analytical signal (NAS) and detrend for acidity; NAS and smoothing for body and balance; AsLS and NAS for overall perception; and Detrend and NAS for the final score.

In addition, a preliminary data overview was carried out using principal component analysis (PCA) to find outliers among the training and testing datasets. The combination of Q-residues and the Hotelling statistics ( $T^2$ ) ellipse at the significance level of 5% were used as parameters to identify and remove the outliers from the dataset (XU et al., 2018). Then, the PLS regression technique was used to select the number of LVs of the prediction models using the entire spectra (1000 to 2450 nm). The best pre-processing techniques and the number of LVs were chosen based on the lowest value of the root mean square error of cross-validation ( $RMSE_{CV}$ ), and the highest coefficient of correlation ( $r_{CV}$ ).

For the second step, the ordered predictors selection (OPS) method was used to select the wavelengths that presented the highest correlation with the sensory attributes. Then, the selected wavelengths were used to develop new prediction models. In this method, an informative vector containing information from the best independent variables for prediction is created. Then, the variables were selected according to the corresponding absolute values of the informative vector (TEÓFILO et al., 2009). Next, the original independent variables were arranged in decreasing order of magnitude, in which the higher the absolute value, the more important was the response variable.

Initially, the algorithm selected a subset of variables, which were then used to build, and evaluate the first model. Subsequently, new independent variables (windows) were added to

the first model, creating new models until all variables were considered. The performance of the models was obtained for each evaluation and stored for later comparison. Then, among the subsets of the chosen variables (initial window and its extensions), the one that presented the lowest  $RMSE_{CV}$  was chosen. For this study, a new version of the OPS that includes three approaches for variable selection (AutoOPS, feedOPS, and iOPS) was used. Specific details about the processes and the foundations of these OPS methods are presented elsewhere (ROQUE et al., 2019; TEÓFILO et al., 2009). Lastly, the performance of the PLS-OPS models was evaluated using the following statistical parameters: the root-mean-square-error of the prediction ( $RMSE_P$ ) and the coefficient of correlation of the prediction ( $r_P$ ). These analyses were carried out using the PLS Toolbox, version 9.0 (Eigenvector Research Inc., Wenatchee, WA, USA) and the Matlab, version 2015a software (Mathworks, Inc, Natick, Massachusetts, USA).

#### 4.2.6.2 Feasibility of UAV-based variables for the classification of coffee beverage quality

To evaluate the feasibility of using UAV imagery for the classification of the coffee beverage quality, two approaches were evaluated. First, the whole dataset was used as input for building the classification models. For that, the following machine learning (ML) algorithms were used: Random Forest (RF), Logistic Model Tree (LMT), and the Boosted Classification Trees (ADA). These algorithms were implemented using the R packages *Random Forest* (LIAW and WIENER, 2002), *Caret* (KUHNS, 2008), and ADA (CULP et al., 2006).

Second, a principal component analysis (PCA) was carried out to verify whether a smaller number of latent variables could be used as input for the same classification algorithms. Thus, the principal components (PCs) were chosen when they explained at least 70% of the accumulated variance and that each eigenvalue was above 1.0 (LI et al., 2007). The PCA analysis was performed using the “FactoMineR” package (LÉ et al., 2008). All modeling analyses and evaluations were performed using R the software, version 4.1 (R CORE TEAM, 2021).

Prior to data modeling, the dataset obtained from the images was arranged in an X matrix (predictors) and the final score attribute was arranged in the “y” vector (response variable). For the final score, the samples were reclassified as specialty coffee (Final Score  $\geq 80$  points) and not specialty coffee (Final Score  $< 80$ ). Then, the data was split into calibration ( $n = 126$ , 70%) and validation ( $n = 54$ , 30%) datasets. The hyperparameters from the ML models were fine-tuned using the *Caret* package and selected according to the accuracy estimation in the training

dataset. To do so, the models were trained using the k-fold cross-validation (5 folds) with 100 repeated experiments. Then, to evaluate the accuracy of the classification models, the following metrics were obtained: Overall Accuracy, Precision, Recall, F1 score, and the Area under the receiver operating characteristic curve (AUC-ROC).

### 4.3 Results

#### 4.3.1 Descriptive statistics of the coffee quality attributes

Results of the coffee quality attributes obtained through the sensory analysis with the SCA protocol are presented in Table 3. Among the 11 attributes initially evaluated, this study considered eight of them: aroma, flavour, aftertaste, acidity, body, balance, overall perception, and the final score. The minimum and maximum values from the individual quality attributes, ranged between 6 and 9 on the quality scale, therefore, being considered as specialty grade. As for the final score, the maximum value was 85, which was classified as excellent quality. On the other hand, the minimum value was below specialty quality (72.4 points). Despite that, when considering the average values, the coffee beverages were classified as very good quality since the final score was above 80 points, which is the threshold for this classification (SCA, 2021).

**Table 3.** Descriptive statistics of the coffee quality attributes

Quality Attribute	Average $\pm$ SD	Minimum	Maximum	CV (%)	Outliers	n
Aroma	7.44 $\pm$ 0.24	6.88	8.25	3.27	25	155
Flavour	7.34 $\pm$ 0.23	6.83	8.00	3.12	25	155
Aftertaste	7.06 $\pm$ 0.26	6.50	7.67	3.68	24	156
Acidity	7.29 $\pm$ 0.24	6.83	7.88	3.25	21	159
Body	7.17 $\pm$ 0.24	6.58	7.83	3.37	21	159
Balance	7.19 $\pm$ 0.24	6.58	7.83	3.45	23	157
Overall Perception	7.16 $\pm$ 0.27	6.50	7.88	3.79	20	160
Final Score	80.58 $\pm$ 1.77	72.40	85.00	2.20	21	159

SD, Standard deviation; CV, Coefficient of variation; n, Number of samples.

Despite the fact that five coffee cultivars were used in the sensory analysis, the variability (coefficient of variation) observed in the different quality attributes was low and ranged from 2.20 to 3.79%. Lastly, after preprocessing the spectra and applying the PCA and the combination of Q-residues versus leverage and the Hotelling statistics, different samples

for each quality attribute were identified as outliers and removed from the dataset (Table 3). Differences in the number of outliers occurred because the analysis was performed separately for each quality attribute.

#### 4.3.2 Spectral characterization of the coffee cultivars

The samples evaluated in this study presented a similar shape to the typical raw spectra of roasted coffee as observed in the literature (CRAIG et al., 2014; RIBEIRO et al., 2011). The spectra of the five cultivars showed notable similarity, being visually differentiated by a small variation in the absorbance ( $\log(1/R)$ ) intensity throughout the entire spectral range (Figure 3). The shape of the spectra was mostly dominated by water absorption bands in the regions from 1440 to 1460 nm (1<sup>st</sup> overtone of O–H stretching) and from 1920-1950 nm (combination bands of O–H stretching and O–H deformation) (CRAIG et al., 2014). Therefore, for both regions, the absorption of chemical compounds related to the coffee attributes was possibly reduced when compared with the water-related bands.

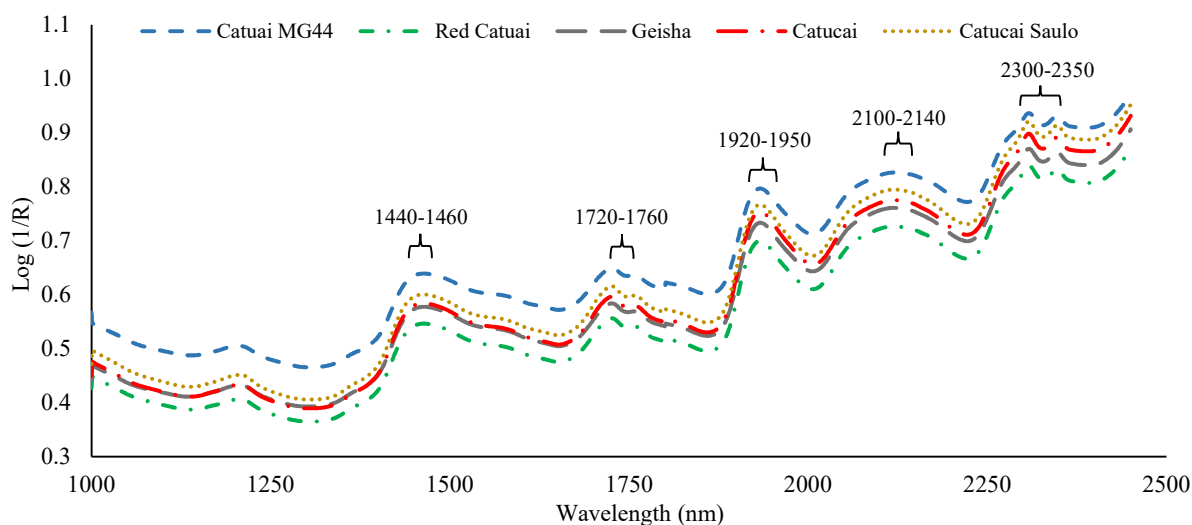


**Figure 3.** Average absorbance spectra in the NIR region obtained from the roasted coffee samples

The absorbance peaks in the regions between 1720-1760 nm (1<sup>st</sup> overtone of C–H and S–H) and from 2300 to 2350 nm (C–H + C–C combination bands) were previously associated with lipid content, whereas the region from 2100-2140 nm (N–H combination bands) was assigned to carbohydrates and/or chlorogenic acids and proteins (CRAIG et al., 2014; RIBEIRO et al., 2011). Despite that, these regions are represented by different bands that cannot be individually described due to the overlap of overtones and combination bands.



#### 4.3.3 Performance of the PLS and PLS-OPS regression models

The PLS and PLS-OPS models were calibrated and validated against the eight coffee quality attributes. The regression models were selected based on the lowest number of LV's and RMSE values, as well as in the highest coefficient of correlation ( $r$ ) between the observed and predicted data. The PLS-OPS models presented a slight improvement in the prediction performance for all quality attributes, with the exception of the aroma, which was best modelled using the PLS with the whole spectra (1000 to 2450 nm) (Table 4). Among the eight attributes studied, the aftertaste was the most accurately predicted by the PLS-OPS in the cross-validation ( $RMSE_{CV}$ : 0.15 and  $r_{CV}$ : 0.68) and prediction steps ( $RMSE_P$ : 0.13 and  $r_P$ : 0.82). Conversely, the lowest accuracy was obtained for the aroma ( $RMSE_{CV}$ : 0.15 and  $r_{CV}$ : 0.48;  $RMSE_P$ : 0.13 and  $r_P$ : 0.68).

**Table 4.** Results of the coffee quality attributes prediction using the PLS regression models with all variables (1000 to 2450 nm) and those selected by the PLS-OPS models

Attribute	Model	Variables	LV	RMSE <sub>C</sub>	r <sub>C</sub>	RMSE <sub>CV</sub>	r <sub>CV</sub>	RMSE <sub>P</sub>	r <sub>P</sub>
Aroma	PLS	1451	10	0.13	0.63	0.15	0.41	0.12	0.69
	PLS-OPS	260	10	0.13	0.64	0.15	0.48	0.13	0.68
Flavour	PLS	1451	15	0.06	0.95	0.15	0.65	0.15	0.72
	PLS-OPS	760	14	0.06	0.94	0.14	0.68	0.15	0.73
Aftertaste	PLS	1451	12	0.14	0.75	0.18	0.54	0.15	0.76
	PLS-OPS	100	12	0.12	0.80	0.15	0.68	0.13	0.82
Acidity	PLS	1451	10	0.13	0.74	0.17	0.51	0.15	0.70
	PLS-OPS	660	9	0.13	0.72	0.16	0.58	0.14	0.73
Body	PLS	1451	10	0.15	0.68	0.18	0.48	0.16	0.73
	PLS-OPS	180	10	0.15	0.67	0.17	0.54	0.15	0.79
Balance	PLS	1451	12	0.13	0.74	0.16	0.55	0.15	0.74
	PLS-OPS	1400	12	0.13	0.74	0.16	0.57	0.14	0.78
Overall	PLS	1451	8	0.14	0.76	0.19	0.55	0.16	0.74
	PLS-OPS	120	8	0.14	0.76	0.18	0.62	0.14	0.80
Final Score	PLS	1451	5	0.91	0.72	1.06	0.60	0.98	0.74
	PLS-OPS	580	5	0.90	0.72	1.00	0.64	0.95	0.75

LV, Number latent variables; RMSE<sub>C</sub>, RMSE<sub>CV</sub>, and RMSE<sub>P</sub> refer to the root mean square error in the calibration, cross-validation, and prediction steps; r<sub>C</sub>, r<sub>CV</sub>, and r<sub>P</sub> refer to the coefficient of correlation in the calibration, cross-validation, and prediction steps.

Regarding the number of variables, from the initial 1451 variables (1000-2450 nm) the OPS algorithm selected different subsets of wavelengths for each quality attribute (Table 4). Due to the large amount of data, which varied among the quality attributes, the selected variables were grouped in spectral regions and/or specific wavelengths and included in the supplementary material of this chapter (Appendix A). In summary, the number of regions selected by OPS was: 9 to build the aroma model, 9 for flavour, 26 for the aftertaste, 13 for acidity, 24 for body, 1 for balance, 25 for the overall perception, and 22 for the final score.

It should be mentioned that this study is not intended to provide a compilation of all spectral regions that could contribute to the prediction of each quality attribute. Instead, we aimed to show the general spectral regions that were selected and that were in accordance with the literature. In addition, the variable subset selection carried out by the OPS was based on

statistical criteria (*e.g.*, VIP values, correlation and regression coefficients, etc), as opposed to spectroscopy or chemical considerations. Therefore, there were some spectral regions that differed from those presented in the literature.

Nonetheless, for all quality attributes, the selected variables were distributed throughout the entire spectral range (1000-2450 nm). Particularly, the majority of the spectral regions and/or wavelengths (50 regions between all attributes) were in the range from 2000 to 2500 nm (combination bands region). This region is known to present absorption peaks for aromatic compounds, caffeine, chlorogenic acids, proteins, lipids and carbohydrates that are related to the studied quality attributes (BARBIN *et al.*, 2014; CRAIG *et al.*, 2014; RIBEIRO *et al.*, 2011).

When comparing the number of latent variables (LV) to build the regression models, both the PLS and PLS-OPS models resulted in the same number of LVs, with the exception of the flavour and acidity that presented different values among models. The results ranged from moderate (Aroma) to satisfactory (Aftertaste and Overall perception), when compared to previous studies that are presented in the discussion section. Lastly, the scatterplots of the predicted vs. measured sensory attributes are presented in Figure 4. Both calibration and validation sets were included to show that the samples were in the same range, regardless of the coffee cultivars, reinforcing the low variability (CV values) present in the dataset (Table 3).

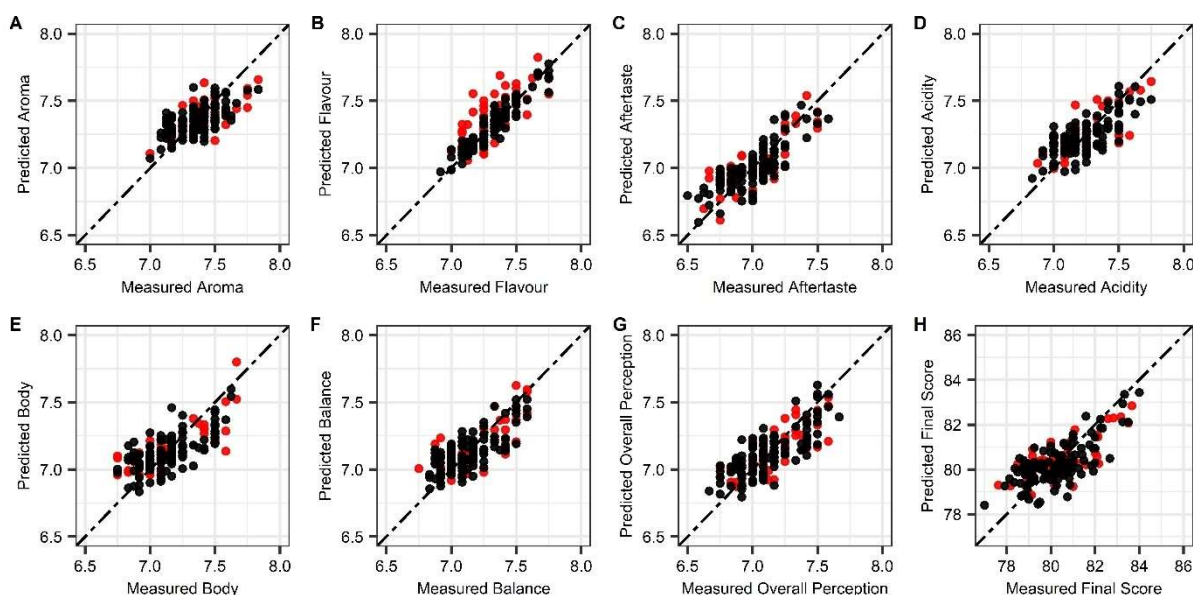


**Figure 4.** Scatter plots of the predicted versus measured values of the coffee quality attributes. A 1:1 line (grey, dashed) is provided for reference. Black and Red dots refer to the calibration and validation datasets.

#### 4.3.4 Feasibility of using UAV-based information for coffee quality classification

The second objective of this study was to perform a classification of the coffee beverage quality (Final Score) based on spectral, climate, and terrain variables obtained from UAV imagery. For that, two different approaches were evaluated. First, the whole dataset was used as input for the decision tree-based models. The results showed that all models exhibited low overall accuracy (RF: 0.61; LMT: 0.56; and ADA: 0.59) for discriminating the specialty coffee (Final Score  $\geq$  80 points) from non-specialty (Final Score  $<$  80 points). Still, among the three algorithms, the RF presented the best performance according to the majority of the metrics used. Conversely, the lowest performance was observed for the LMT model (Table 5).

**Table 5.** Average values of the classification metrics obtained with the test-set for the classification models

All variables					
Model	OA	Precision	Recall	F1 Score	AUC - ROC
RF	0.61	0.60	0.60	0.60	0.63
LMT	0.56	0.55	0.60	0.57	0.62
ADA	0.59	0.57	0.60	0.59	0.65
PCA – 3 Principal Components					
RF	0.58	0.56	0.75	0.64	0.63
LMT	0.59	0.57	0.60	0.59	0.65
ADA	0.54	0.52	0.65	0.58	0.60

RF, Random Forest; LMT, Logistic Model Tree; and ADA, Boosted Classification Trees; OA, Overall accuracy. AUC-ROC, Area under the receiver operating characteristic curve; PCA, Principal component analysis.

In the second analysis, a PCA was conducted before the classifications. As a result, the first three PCs were chosen for further analysis since they presented eigenvalues above 1.0 and explained 80.85% of the dataset variance. Then, new classification models were built using the PCs as input. Overall, there was not much change in the accuracy in relation to the first analysis. The LMT model showed some improvement for all metrics, whereas the ADA presented lower accuracy than before. As for the RF, some metrics improved (Recall and F1 score), while others decreased (OA and Precision).

Regarding the variable importance (%), there was not a consensus between the three ML models since different variables were ranked as most important for each model. However,

when compared among the type of variables (*e.g.*, terrain, climate, and spectral), the top-4 variables for each model were always the terrain-based ones (Figure 5). For all models, the variables Slope (RF: 27.68%; LMT: 18.34%; and ADA: 11.45%), Altitude (RF: 17.65%; LMT: 19.36%; and ADA: 15.36%), Hillshade (RF: 13.01%; LMT: 16.80%; and ADA: 18.56%), and Aspect (RF: 9.45%; LMT: 15.30%; and ADA: 18.77%) were the ones that most contributed to the classification models. On the other hand, the spectral variables exhibited the least importance, reinforcing the idea that the coffee beverage quality goes beyond the spectral response of a healthy crop canopy.

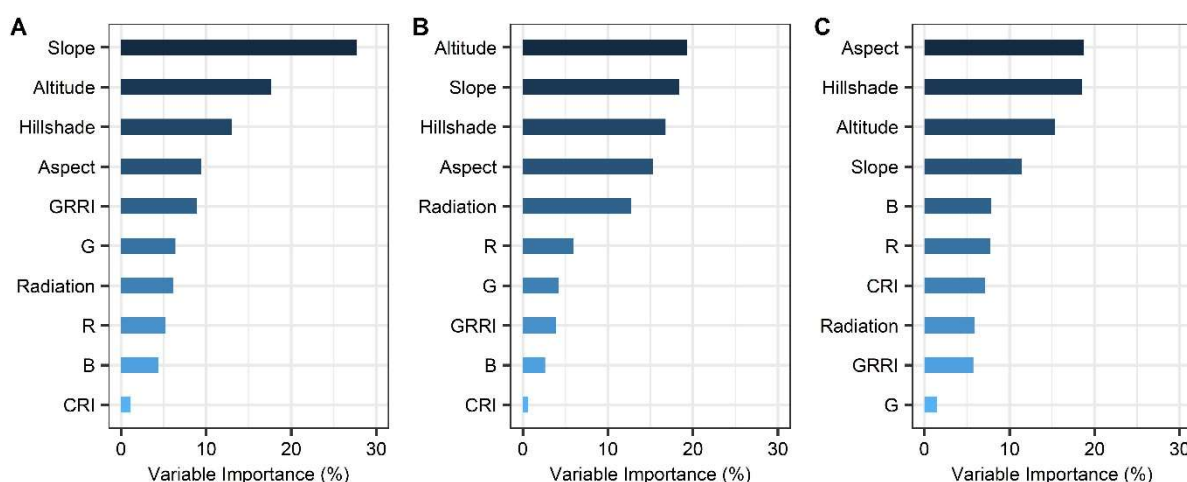


**Figure 5.** Variable importance attributed by the machine learning algorithms RF (A), LMT (B), and ADA (C) for classification of the coffee samples based on terrain, climate, and the crop canopy spectral characteristics

## 4.4 Discussion

### 4.4.1 Applicability of NIR spectroscopy for coffee beverage quality prediction

The coffee sensory analysis consists of a complex and subjective process, in which the quality attributes are distinguished by senses and can be assessed organoleptically by the Q-graders. Due to the influence of the individual preferences of the evaluators, there is a possibility of inconsistency in the results, since it is difficult to define the desirable limits for attributes such as acidity, flavor, sweetness, and body (AGNOLETTI et al., 2022; PEREIRA et al., 2020). Therefore, the use of instrumental methods coupled with statistical modeling to provide faster and unbiased results is encouraged. Based on that, for this study different coffee quality attributes were predicted based on the PLS and PLS-OPS regression models using the NIR spectra of roasted coffee samples as predictors.

Promising results were obtained for the final score and its individual quality attributes (aroma, flavour, aftertaste, acidity, body, balance, and overall perception) when compared to previous studies. Baqueta et al. (2019) when using NIR spectroscopy with PLS for the prediction of sensory attributes from commercial coffee varieties reported correlation coefficients ( $r_p$ ) and prediction errors ( $RMSEP$ ) of 0.75 and 0.16 for aroma, 0.77 and 0.13 for flavour, 0.80 and 0.28 for body, and 0.73 and 0.16 for overall quality. In the present study, the correlation values tended to be lower, especially for the aroma attribute ( $r_p$ : 0.69 and  $RMSEP$ : 0.12). However, the prediction errors were smaller, and the other attributes presented correlation values above 0.7, which can be considered satisfactory (SANTOS et al., 2019).

Tolessa et al. (2016) evaluated the same quality attributes of this study, with exception of the balance, and obtained higher performance for the overall perception ( $r_p$ : 0.90 and  $RMSEP$ : 0.22) and final score ( $r_p$ : 0.90 and  $RMSEP$ : 1.04). On the other hand, the attributes aroma ( $r_p$ : 0.01 and  $RMSEP$ : 0.40), flavour ( $r_p$ : 0.59 and  $RMSEP$ : 0.29), aftertaste ( $r_p$ : 0.72 and  $RMSEP$ : 0.27), and body ( $r_p$ : 0.72 and  $RMSEP$ : 0.24) presented lower performances than this study regardless of the model used here (PLS or PLS-OPS). In a more recent study, Agnoletti et al. (2022), used chemical data obtained by HS-SPME-GC/MS (solid-phase microextraction with headspace mode, combined with gas chromatography coupled to mass spectrometry) coupled with PLS and GA-SVR (Genetic algorithm with Support Vector Regression) to predict the scores of aroma, aftertaste, acidity, body, balance, and overall perception. The prediction performance varied among the quality attributes and was, in general, with the exception of the aroma and body, lower than those observed in this study.

Regardless of the analytical techniques used to obtain the chemical information to be used as predictors, the differences in the  $r_p$  and  $RMSEP$  values among these studies were small, reinforcing the applicability of PLS regression with chemometrics for the prediction of the coffee quality attributes. Such differences in model performance could be attributed to several causes, either relating to the number of samples used for model calibration and validation, the variable scanning procedures, multivariate methods, small range of values, and specially the low variability among the scores from different coffee samples. In this study, even though the spectra of the five cultivars differed in absorption intensity, the quality attributes presented low variability (Table 3 and Figure 4), and that affected the model performance.

Regarding the spectral regions and/or wavelengths selected, the PLS-OPS reduced the number of variables, as well as the computational cost, and increased the prediction accuracy when compared to the PLS models. For all attributes, the selected variables were distributed

along with the entire spectra range (1000-2450nm). This is due to the fact that the compounds that influence the coffee sensory attributes are absorbed throughout the whole spectrum (BELCHIOR et al., 2020). Here, since it was not the focus of the study to establish a relationship between the quality attributes and the spectra of chemical compounds present in the coffee samples, only a brief description of the relevant spectral regions and the quality attributes that presented similarities with previous studies is presented.

As an example, the spectral regions included in the range from 1552 to 1556 nm (1<sup>st</sup> overtone C-H), 1988 to 2082 nm (1<sup>st</sup> overtone of C=O and O-H combination bands), and from 2246 to 2394 nm (O-H and CH + CH combination bands) were assigned to organic and chlorogenic acids and used for beverage acidity prediction (RIBEIRO et al., 2011). The influence of these acids is justified by their decomposition during roasting and the influence of the resultant products on different compounds with sensory implications on acidity (ESTEBAN-DÍEZ et al., 2004). Here, for the acidity, the selected spectral regions were included throughout the whole spectrum, but the majority of the variables ranged from 2009 to 2084 and from 2138 to 2414 nm.

Coincident spectral regions between the aforementioned works and this study were also identified for flavour (1830-2060 and 2180-2250 nm), aftertaste (1722-1724 nm), and body (1721-1731, 1938-1939, 1966-1971, 2309-2314, and 2399-2401 nm) (Appendix A). Lastly, most of these spectral regions are closely related to the NIR spectra of trigonelline, chlorogenic acids, coffee lipids, pure caffeine, 5-caffeoylquinic acid, cellulose, sucrose, and casein that influence the scores of flavour, acidity, body, and overall perception (RIBEIRO et al., 2011).

Thus, since the selected spectral regions were distributed in the whole spectra, it becomes challenging to clearly specify and describe the chemical compounds that were related to and influenced each quality attribute, since their absorption peaks are close to each other. Besides that, as stated before, the PLS-OPS technique selects the variable subsets using a combination of statistical parameters, such as the VIP values and correlation coefficients (TEÓFILO et al., 2009), which do not always relate to the chemical compounds responsible for the quality attributes. Finally, as coffee is a complex matrix, which is susceptible to the influence of several variables in the production phases (*e.g.*, cultivation, harvesting, post-harvesting, and extraction of the sensory properties) (BELCHIOR et al., 2019), it is difficult to establish a linear relationship between the spectra and the sensory attributes. In this sense, future studies should include data from more coffee varieties and with a wider range of values for the quality attributes, as well as the use of other modeling techniques.

#### 4.4.2 *Applicability of UAV-based variables for coffee beverage quality classification*

In recent years, UAV imagery has been used for a variety of applications in several crops. For the coffee crop, the majority of the studies are relatively new and were mostly involved in the prediction of biophysical parameters (SANTOS et al., 2020b), disease detection (MARIN et al., 2021b), nitrogen spatial variability monitoring (MARIN et al., 2021a), yield prediction (BARBOSA et al., 2021), and the fruit ripeness monitoring and mapping (NOGUEIRA MARTINS et al., 2021; ROSAS et al., 2021). All of these studies used the crop canopy spectral information to obtain the characteristics of interest since in most situations they are visible (*e.g.*, foliar disease, leaf area, and fruit ripeness) and have a direct relationship with the variables derived from the UAV imagery.

However, when dealing with the beverage quality, this relationship goes beyond the visual aspect of the crop canopy or the fruit color since the coffee quality is a result of complex and multivariate interactions. In this sense, this study presented the first attempt, to the best of our knowledge, to classify the coffee beverage quality using spectral, climate, and terrain variables extracted from the UAV imagery. As shown in the results section, for both methodological approaches (All individual variables and PCA), the classification models exhibited poor accuracy for discrimination of coffee samples with specialty quality from non-specialty ones. Among the evaluated models, the RF presented higher accuracy in both analyses, which was still not satisfactory.

Regardless of the results, for all three classification models, the terrain-based variables (*e.g.*, Altitude, hillshade, slope, and aspect) were the most important, corroborating with previous studies, which showed that these variables have some influence on the beverage quality. The influence of altitude on the coffee quality is due to the presence of lower temperatures at higher altitudes, which delay the fruit ripeness and lead to a greater accumulation of aroma precursors (BERTRAND et al., 2006; WORKU et al., 2018). As for the shade (hillshade), it has been reported to improve the bean's physical and cup quality due to cool climates (BERTRAND et al., 2006; DECAZY et al., 2003; JOËT et al., 2010). The slope and aspect are related to the direction and duration of sun exposure, which influences air temperature and affects the length of the production cycle and the harvesting time, factors that are also important for the beverage quality (AVELINO et al., 2005; de SOUZA SILVEIRA et al., 2016).

Finally, the use of UAV imagery for the coffee quality assessment showed no satisfactory results and needs to be further explored. Recommendations for future studies



should include but are not limited to the integration of more robust multispectral and/or hyperspectral sensors for obtaining the UAV-based variables with soil fertility and plant nutrition attributes, crop yield, as well as with other climate variables, such as rainfall and photoperiod that together affects the coffee beverage quality.

#### 4.5 Conclusion

In this study, the potential of NIR spectroscopy and aerial remote sensing for the assessment of coffee quality attributes was evaluated under different analyses. First, PLS (partial least squares) and PLS-OPS (Ordered predictors selection) regression models were developed for the prediction of eight quality attributes. Overall, the best predictions were obtained using the PLS-OPS models that showed satisfactory performance for the aftertaste, overall perception, body, and balance. However, there is a need for improvement for aroma, flavor, and acidity. Hence the use of NIR spectra of roasted coffee with PLS-OPS is promising for fast and accurate prediction of beverage quality attributes.

In the second analysis, the RF algorithm exhibited the highest accuracy among the machine learning models for discriminating the beverage classes (Specialty and not specialty). Regardless, the classification models based on spectral, climate, and terrain variables obtained from UAV imagery showed no satisfactory results and need to be further explored.

#### 4.6 References

- AGNOLETTI, B. Z. et al. Multivariate calibration applied to study of volatile predictors of arabica coffee quality. **Food Chemistry**, v. 367, p. 1-8, 2022.
- ALESSANDRINI, L. et al. , Near infrared spectroscopy: An analytical tool to predict coffee roasting degree. **Analytica Chimica Acta**, n. 625, p. 95–102. 2008.
- ALVARES, C. A. et al. Köppen’s climate classification map for Brazil. **Meteorologische Zeitschrift**, v. 22, n. 6, p. 711-728, 2013.
- AVELINO, J. et al. Effects of slope exposure, altitude and yield on coffee quality in two altitude terroirs of Costa Rica, Orosi and Santa María de Dota. **Journal of the Science of Food and Agriculture**, n. 85, p. 1869-1876, 2005.
- BAQUETA, M. R.; COQUEIRO, A.; VALDERRAMA, P. Brazilian Coffee Blends: A simple and fast method by near-infrared spectroscopy for the determination of the sensory attributes elicited in professional coffee cupping. **Journal of Food Science**, v. 84, p. 1247–1255, 2019.

- BARBIN, D. F. et al. Application of infrared spectral techniques on quality and compositional attributes of coffee: An overview. **Food Research International**, v. 61, p. 23–32, 2014.
- BARBOSA, B. D. S. et al. UAV-based coffee yield prediction utilizing feature selection and deep learning. **Smart Agricultural Technology**, v. 1, p. 1-9, 2021.
- BELCHIOR, V. et al. FTIR and chemometrics as effective tools in predicting the quality of specialty coffees. **Food Analytical Methods**, v. 13, p. 275–283, 2020.
- BELCHIOR, V. et al. Attenuated total reflectance fourier transform spectroscopy (ATR-FTIR) and chemometrics for discrimination of espresso coffees with different sensory characteristics. **Food Chemistry**, v. 273, p. 178–185, 2019.
- Bertrand, B. et al. Comparison of bean biochemical composition and beverage quality of Arabica hybrids involving Sudanese-Ethiopian origins with traditional varieties at various elevations in Central America. **Tree Physiology**, v. 26, p. 1239–1248, 2006.
- CHENG, B. et al. Influence of genotype and environment on coffee quality. **Trends in Food Science & Technology**, v. 57, p. 20–30, 2016.
- CORRÊDO, L. P. et al. Near-infrared spectroscopy as a tool for monitoring the spatial variability of sugarcane quality in the fields. **Biosystems Engineering**, v. 206, p. 150–161, 2021.
- CRAIG, A. P. et al. Mid infrared spectroscopy and chemometrics as tools for the classification of roasted coffees by cup quality. **Food Chemistry**, v. 245, p. 1052–1061, 2018.
- CRAIG, A. P. et al. Fourier transform infrared spectroscopy and near infrared spectroscopy for the quantification of defects in roasted coffees. **Talanta**, v. 134, p. 379–386, 2015.
- CRAIG, A. P. et al. Application of elastic net and infrared spectroscopy in the discrimination between defective and non-defective roasted coffees. **Talanta**, v. 128, p. 393–400, 2014.
- CULP, M.; JOHNSON, K.; MICHAELIDIS, G. ada : An R package for stochastic boosting. **Journal of Statistical Software**, v. 17, p. 1–27. 2006.
- DE SOUZA SILVEIRA, A. et al. Sensory analysis of specialty coffee from different environmental conditions in the region of matas de minas, minas gerais, Brazil. **Revista Ceres**, v. 63, n. 4, p. 436-443, 2016.
- DECAZY, F. et al. Quality of different honduran coffees in relation to several environments. **Journal of Food Science**, v. 68, p. 2356–2361, 2003

DI DONFRANCESCO, B.; GUTIERREZ GUZMAN, N.; CHAMBERS, E. Comparison of results from cupping and descriptive sensory analysis of Colombian brewed coffee. **Journal of Sensory Studies**, v. 29, p. 301–311, 2014.

EBRAHIMI-NAJAFABADI, H. et al. Detection of addition of barley to coffee using near infrared spectroscopy and chemometric techniques. **Talanta**, v. 99, p. 175–179, 2012.

ESTEBAN-DÍEZ, I.; GONZÁLEZ-SÁIZ, J. M.; PIZARRO, C. Prediction of sensory properties of espresso from roasted coffee samples by near-infrared spectroscopy. **Analytica Chimica Acta**, v. 525, p. 171–182, 2004.

FERIA-MORALES, A. M. Examining the case of green coffee to illustrate the limitations of grading systems/expert tasters in sensory evaluation for quality control. **Food Quality and Preference**, v. 13, p. 355–367, 2002.

FERREIRA, W. P. M. et al. Effects of the orientation of the mountainside, altitude and varieties on the quality of the coffee beverage from the “Matas de Minas” region, Brazilian Southeast. **American Journal of Plant Science**, v. 7, p. 1291-1303, 2016.

FERREIRA, W. P. M. et al. Influence of relief and global radiation on the quality of the coffee beverage. *In: American Society of Agricultural and Biological Engineers Annual International Meeting. ASABE. Annals [...]*, 2014, p. 1-10. Available online: <<https://elibrary.asabe.org/abstract.asp?aid=44604>>. Accessed on: 10/06/2021.

FU, P.; RICH, P. M. A geometric solar radiation model with applications in agriculture and forestry. **Computers and Electronics in Agriculture**, v. 37, p. 25–35, 2002.

FU, P.; RICH, P. M. **The Solar Analyst, version 1.0** - User Manual, 2000. 53p.

FU, P., RICH, P. M. Design and implementation of the solar analyst: an ArcView extension for Modeling solar radiation at landscape scales. *In: 19th Annual ESRI User Conference, 1999. Annals [...]*, 2014, v. 1, p. 1-31. Available online: <<https://proceedings.esri.com/library/userconf/proc99/proceed/papers/pap867/p867.htm>>. Accessed on: 10/11/2021.

JING, M.; CAI, W.; SHAO, X. Quantitative determination of the components in corn and tobacco samples by using near-infrared spectroscopy and multiblock partial least squares. **Analytical Letters**, v. 43, p. 1910–1921, 2010.

JOËT, T. et al. 2010. Use of the growing environment as a source of variation to identify the

- quantitative trait transcripts and modules of co-expressed genes that determine chlorogenic acid accumulation. **Plant, Cell & Environment**, v. 33, n. 7, p. 1220-1233, 2010
- JOHNSON, L. F. et al. Feasibility of monitoring coffee field ripeness with airborne multispectral imagery. **Applied Engineering in Agriculture**, v. 20, n. 6, p. 745-849, 2004.
- KUHN, M. caret Package. **Journal of Statistical Software**, v. 5, p. 1-26, 2008.
- LÄDERACH, P. et al. Systematic agronomic farm management for improved coffee quality. **Field Crops Research**, v. 120, n. 3, p. 321-329, 2011.
- LÊ, S.; JOSSE, J.; HUSSON, F. FactoMineR: An R package for multivariate analysis. **Journal of Statistical Software**, v. 25, n. 1, p. 1-18, 2008
- LELONG, C. C. D. et al. Assessment of unmanned aerial vehicles imagery for quantitative monitoring of wheat crop in small plots. **Sensors**, v. 8, n. 5, p. 3557-3585, 2008.
- LI, Y. et al. Delineation of site-specific management zones using fuzzy clustering analysis in a coastal saline land. **Computers and Electronics in Agriculture**, v. 56, n. 2, p. 174-186, 2007.
- LIAW, A.; WIENER, M. Classification and regression with Random Forest. **R News**, v. 2, p. 18-22, 2002.
- LOUZADA PEREIRA, L. et al. Influence of solar radiation and wet processing on the final quality of arabica coffee. **Journal of Food Quality**, v. 1, p. 1-9, 2018.
- MARIN, D. B. et al. Remotely piloted aircraft and random forest in the evaluation of the spatial variability of foliar nitrogen in coffee crop. **Remote Sensing**, v. 13, p. 1471-1485, 2021a.
- MARIN, D. B. et al. Detecting coffee leaf rust with UAV-based vegetation indices and decision tree machine learning models. **Computers and Electronics in Agriculture**, v. 190, p. 1-10, 2021b.
- NOGUEIRA MARTINS, R. et al. A Novel Vegetation Index for Coffee Ripeness Monitoring Using Aerial Imagery. **Remote Sensing**, v. 13, n. 2, p. 1-16, 2021.
- OLIVEIRA APARECIDO, L. E. et al. Maturation periods for Coffea arabica cultivars and their implications for yield and quality in Brazil. **Journal of the Science of Food and Agriculture**, v. 98, n. 10, p. 3880-3891, 2018.
- OLIVERI, P. et al. The impact of signal pre-processing on the final interpretation of analytical

outcomes – A tutorial. **Analytica Chimica Acta**, v. 1058, p. 9–17, 2019.

PEREIRA, L. L. et al. New propositions about coffee wet processing: Chemical and sensory perspectives. **Food Chemistry**, v. 310, p. 1-10, 2020.

PIZARRO, C. et al. Use of near-infrared spectroscopy and feature selection techniques for predicting the caffeine content and roasting color in roasted coffees. **Journal of Agricultural and Food Chemistry**, v. 55, p. 7477–7488, 2007.

R CORE TEAM. **R: A Language and Environment for Statistical Computing**. Vienna, Austria, 2021.

RIBEIRO, J. S.; FERREIRA, M. M. C.; SALVA, T. J. G. Chemometric models for the quantitative descriptive sensory analysis of Arabica coffee beverages using near infrared spectroscopy. **Talanta**, v. 83, p. 1352–1358, 2011.

RICH, P. M. et al. Using viewshed models to calculate intercepted solar radiation: Applications in ecology. **American Society for Photogrammetry and Remote Sensing**, p. 524–529, 1994

ROQUE, J. V. et al. Comprehensive new approaches for variable selection using ordered predictors selection. **Analytica Chimica Acta**, v. 1075, p. 57–70, 2019.

ROSAS, J. T. F. et al. Low-cost system for radiometric calibration of UAV-based multispectral imagery. **Journal of Spatial Science**, p. 1–15, 2020.

ROSAS, J. T. F. et al. Coffee ripeness monitoring using a UAV-mounted low-cost multispectral camera. **Precision Agriculture**, v. 23, n. 1, p. 300-318, 2021.

SANTOS, D. A. et al. Multi-product multivariate calibration: determination of quality parameters in soybean industrialized juices. **Acta Scientiarum Technology**, v. 41, p. 1-11, 2019.

SANTOS, J. R. et al. Evaluation of green coffee beans quality using near infrared spectroscopy: A quantitative approach. **Food Chemistry**, v. 135, p. 1828–1835, 2012.

SANTOS, K. M. et al. Classification of Brazilian coffee using near-infrared spectroscopy and multivariate calibration. **Analytical Letters**, v. 45, p. 774–781, 2012.

SANTOS, L. M. et al. Biophysical parameters of coffee crop estimated by UAV RGB images. **Precision Agriculture**, v. 21, n. 16, p. 1227-1241, 2020a.

SANTOS, L. M. et al. Determining the leaf area index and percentage of area covered by coffee

crops using UAV RGB images. **IEEE Journal of Selected Topics in Applied Earth Observations and Remote Sensing**, v. 13, p. 6401–6409, 2020b.

SHAN, J. et al. Application of curve fitting and wavelength selection methods for determination of chlorogenic acid concentration in coffee aqueous solution by vis/NIR Spectroscopy. **Food Analytical Methods**, v. 10, p. 999–1006, 2017.

SILVA NETO, F. J et al. Shade trees spatial distribution and its effect on grains and beverage quality of shaded coffee trees. **Journal of Food Quality**, p. 1–8, 2018.

SILVA OLIVEIRA, E. C. et al. Chemical and sensory discrimination of coffee: impacts of the planting altitude and fermentation. **European Food Research and Technology**, v. 248, p. 659–669, 2021.

SILVA, S. de A. et al. Coffee quality and its relationship with Brix degree and colorimetric information of coffee cherries. **Precision Agriculture**, v. 15, n. 5, p. 543–554, 2014.

SILVEIRA, A. de S. et al. Sensory analysis of specialty coffee from different environmental conditions in the region of Matas de Minas, Minas Gerais, Brazil. **Revista Ceres**, v. 63, p. 436–443, 2016.

SOUZA BARBOSA, B. D. et al. Application of RGB images obtained by UAV in coffee farming. **Remote Sensing**, v. 13, p. 1–19, 2021.

SPECIALTY COFFEE ASSOCIATION - SCA. **Protocols and Best Practices**, 2021. Available in: <<https://sca.coffee/research/protocols-best-practices>>. Accessed on: 07/2021.

TEÓFILO, R. F. et al. Sorting variables by using informative vectors as a strategy for feature selection in multivariate regression. **Journal of Chemometrics**. v. 23, p. 32–48, 2009.

TOLESSA, K. et al. Influence of growing altitude, shade and harvest period on quality and biochemical composition of Ethiopian specialty coffee. **Journal of the Science of Food and Agriculture**, v. 97, p. 2849–2857, 2017.

TOLESSA, K. et al. Prediction of specialty coffee cup quality based on near infrared spectra of green coffee beans. **Talanta**, v. 150, p. 367–374, 2016.

VELOSO, T. G. R. et al. Effects of environmental factors on microbiota of fruits and soil of *Coffea arabica* in Brazil. **Scientific Reports**, v. 10, p. 1–11, 2020.

WORKU, M. et al. Effect of altitude on biochemical composition and quality of green arabica coffee beans can be affected by shade and postharvest processing method. **Food Research**

**International**, v. 105, p. 278–285, 2018.

XU, S. et al. Comparison of multivariate methods for estimating selected soil properties from intact soil cores of paddy fields by Vis–NIR spectroscopy. **Geoderma**, v. 310, p. 29–43, 2018.

## 5 General Conclusions

The vegetation index CRI (Coffee ripeness index) proposed for estimation of the coffee ripeness using aerial images showed higher sensitivity among all VIs (MCARI1, NDVI, NDRE, GNDVI, and GRRI) to discriminate coffee plants suitable for harvest from those not suitable, as well as for the estimation of the percentage of fruit ripeness. Regarding the two cameras evaluated, the RGB camera can be a viable alternative for obtaining the CRI to monitor the coffee ripeness, especially in small properties due to its lower cost compared to the multispectral camera.

In the third chapter, it was demonstrated that the combined use of spectral and textural variables obtained using aerial images resulted in better performance of the fruit ripeness prediction models when compared to the model obtained using only spectral bands and vegetation indices. Furthermore, despite the high variability in the fruit ripeness, the prediction models based on the Random Forest algorithm were able to predict and quantify the spatio-temporal changes in fruit ripeness with moderate accuracy for both scenarios.

Furthermore, in the fourth chapter, different approaches for predicting and classifying the coffee beverage quality were evaluated. Initially, prediction models using Partial Least Squares (PLS) regression and the Ordered Predictors Selection (OPS) algorithm were created for modeling eight coffee quality attributes based on NIR spectroscopy of roasted coffee samples. Overall, the best results were obtained using the PLS-OPS models for the attributes of aftertaste, overall perception, body, and balance. On the other hand, there is still a need for improvement in the prediction models for aroma, flavor, and acidity.

In the second analysis, spectral, weather, and terrain variables extracted from aerial images were used for the classification of the beverage final quality (Special and not special). The results were not satisfactory, although it was observed in all classification models a greater influence from the terrain variables that are related to beverage quality. Finally, the use of UAV images for beverage quality classification still needs to be further explored in future studies.

Finally, this thesis made it possible to demonstrate that the manual monitoring of coffee fruit ripeness can be replaced by the methodology based on aerial remote sensing, especially through the use of spatio-temporal variability maps of the fruit ripeness. Regarding the coffee beverage quality, the use of NIR spectroscopy with PLS-OPS showed to be a promising approach for fast and accurate prediction of the quality attributes. However, there is still a need for improvements in modeling and validation prior to its implementation in the beverage quality analysis.



## Appendix

### Appendix A

**Table 1.** Regions and specific wavelengths selected by the OPS algorithm for construction of the PLS regression models

Attribute	Wavelength range (nm)
Aroma	1020-1030, 1135-1190, 1310-1350, 1420-1500, 1520-1580, 1730-1740, 1850-1880, 1920-1950, 1980-2010
Flavour	1000-1180, 1240-1420, 1510-1560, 1590-1680, 1790-1800, 1830-2060, 2180-2250, 2335-2350, 2360-2450
Aftertaste	1000, 1035-1036, 1088, 1112-1113, 1120-1130, 1162-1163, 1180-1190, 1308-1318, 1494-1500, 1560-1565, 1587-1591, 1701-1702, 1722-1724, 1767, 1777-1785, 1867-1881, 1950-1952, 1983-1988, 2217-2221, 2268, 2286-2287, 2322-2335, 2349-2350, 2356-2362, 2402
Acidity	1023-1032, 1042-1050, 1110-1286, 1354, 1401-1491, 1564-1654, 1776-1831, 2009-2015, 2037-2084, 2138-2369, 2383-2385, 2391-2407, 2413-2414
Body	1002-1013, 1270-1272, 1278-1282, 1313-1346, 1721-1731, 1742-1750, 1786-1792, 1836-1837, 1853-1871, 1878-1885, 1904-1925, 1938-1939, 1943-1952, 1966-1971, 2000-2001, 2010-2016, 2220-2222, 2267-2269, 2282, 2287-2289, 2295-2304, 2309-2314, 2392-2395, 2399-2401
Balance	1000-2417
Overall	1088, 1097, 1110, 1105-1115, 1119-1134, 1143-1151, 1157-1160, 1165, 1264-1269, 1555-1556, 1854-1866, 1877-1882, 2152-2158, 2219-2222, 2228-2231, 2236-2238, 2242-2246, 2252-2256, 2335-2340, 2351-2352, 2370-2371, 2377, 2386-2388, 2401-2408, 2415-2416
Final score	1045-1074, 1090-1155, 1175-1178, 1184-1185, 1190-1195, 1218-1255, 1301-1381, 1455-1490, 1693-1733, 1770-1851, 1930-1934, 1996-2006, 2050-2072, 2096-2155, 2215-2217, 2223-2248, 2264-2288, 2322-2339, 2362-2367, 2383-2406, 2413-2420, 2426-2430